SSC-SR-1017

The Superconducting Super Collider

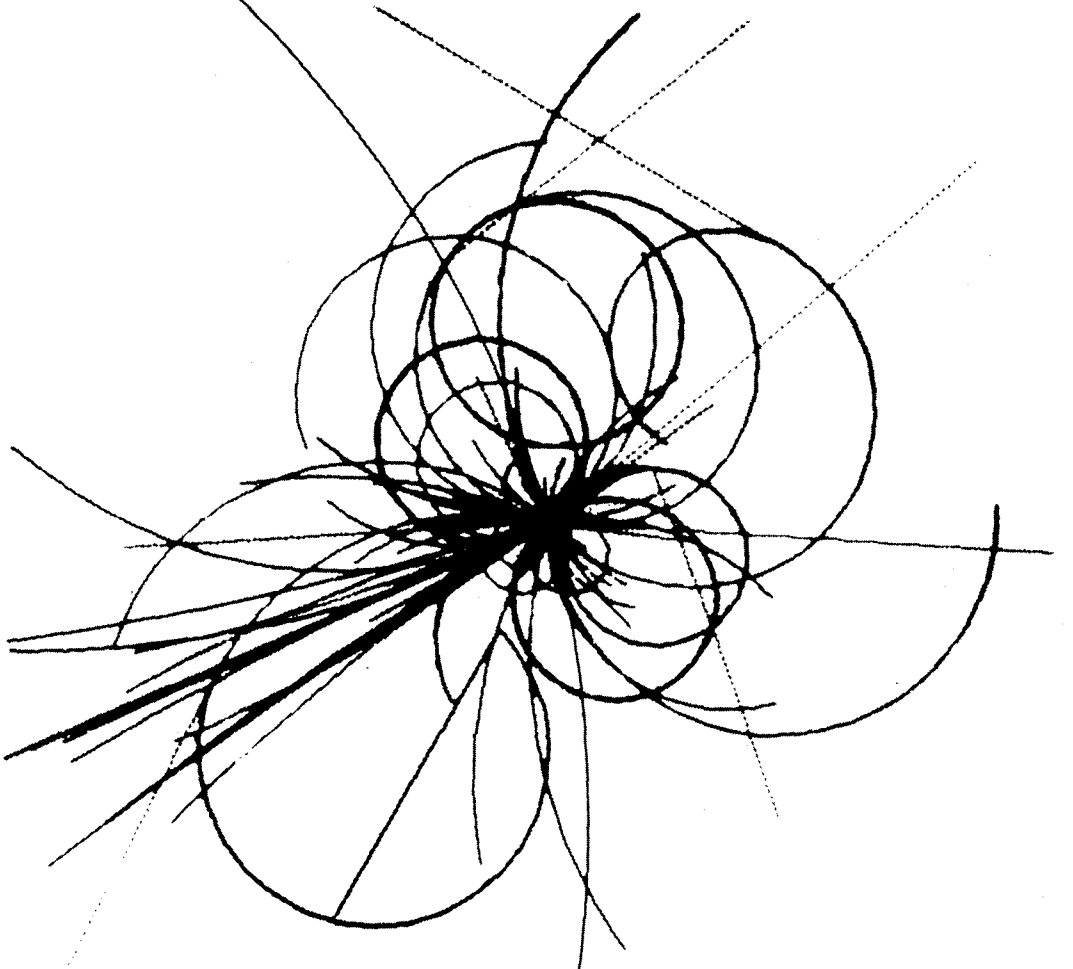

Report of the SSC Impedance Workshop

October 28, 1985

SSC IMPEDANCE WORKSHOP

June 26 and 27, 1985

Lawrence Berkeley Laboratory

Building 90

SSC/CDG Conference Room A

Participants

Bane, K.	SLAC
Bisognano, Joe	SSC/CDG, Chairman
Chao, Alex	SSC/CDG
Chattopadhyay, S.	LBL
Forest, Etienne	SSC/CDG
Giordano, S.	LASL
Lambertson, Glen	LBL
Neuffer, D.	TAC
Ng, Bill	FNAL
Ruth, Ron	SLAC
Schachinger, Lindsay	SSC/CDG
Shafer, R.	FNAL
Simpson, J.	ANL
Wang, T.S.	LASL
Wang, J.M.	BNL
Wilson, P.	SLAC

SSC IMPEDANCE WORKSHOP
June 26 and 27, 1985
Lawrence Berkeley Laboratory
Building 90
SSC/CDG Conference Room A

Agenda

Wednesday Morning, June 26, 9:00 A.M.

J.Bisognano	Introductory Remarks	(45 min)
K.Bane and R.Ruth	Results on Coupled-mode Instability Threshold	(45 min)
[Coffee Break]		(20 min)
R.Shafer	Pickup Requirements for SSC Wall Resistance	(30 min)
T.S.Wang	Estimates of Kicker Impedance	(15 min)
J.Simpson	Impedance Measuring Facility at ANL	(30 min)
[Lunch Break]		

Wednesday Afternoon 1:30 P.M. and Thursday Morning 9:00 A.M.

[Wednesday Evening Dinner 7:00 P.M.]

Open Discussion of Issues

1. Single-bunch Stability: Island Structure, Impact of Impedance Spectrum, Couple-mode vs Fast Blow

2. Shielded vs Unshielded vs Inner Bellows

3. Wire and Beam Measurements of Component Impedance

4. Scaling of Impedance and Instability with Machine Size and Component Mix.

5. Kicker Impedances and Conductor Shields

6. Pickup Impedances

7. Resistive Wall Impedance

8. Coupled-bunch Instabilities

Thursday Afternoon 1:30 P.M.

Summaries of Workshop Discussions

Planning Future Efforts

TABLE OF CONTENTS

Page

Impedance Issues for the SSC. 1
J. J. Bisognano

Bellows Wake Fields and Transverse Single Bunch Instabilities in the SSC. 10
K. L. F. Bane and R. D. Ruth

An Estimate of the Contributions of Bellows to the Impedances and Beam Instabilities of the SSC 45
J. Bisognano and K. Y. Ng

Impedances of the Shielded Bellows in the SSC and the Effects on Beam Stability 61
K. Y. Ng

An Investigation of the Skin Depth Effect of a Metallic Coating on a Ceramic Beam Pipe Inside a Kicker. 99
K. Y. Ng

Impedance Measruement Group Report. 95
J. Simpson, S. Giordino, F. Voelker, J. Hinkson, and G. Spalek

A Better Estimate of Expected Beam Wake Test Sensitivity. 103
J. Simpson

Experience with Wire Impedance Measurements 107
S. Giordano

SSC Kicker Impedances 119
E. Colton and T. F. Wang

Longitudinal and Transverse Coupling Impedances of Beam Position Monitors 127
R. Shafer

On Shielding the Beam from Kicker Magnets at High Frequencies 133
R. Shafer

IMPEDANCE ISSUES FOR THE SSC

Joseph J. Bisognano

SSC/CDG

Single-bunch and coupled-bunch instabilities have limited achievable current and phase space density in both electron and proton storage rings. For the modest bunch spacing of the SSC, feedback systems with bandwidths of tens of megahertz appear capable of damping coupled-bunch instabilities. Of course, detailed designs need to be pursued to optimize costs and power requirements of the hardware. On the other hand, single-bunch instabilities and tune shifts remain best-treated by impedance control although broadband feedback systems offer considerable promise. The Reference Designs Study identified the transverse, single-bunch, coupled-mode instability as the primary current limit in the SSC. Bellows, pickups, and kickers appeared to be the major contributors to the machine impedance, and it was recommended that

bellows have sliding contact shields. With the modest synchrotron radiation energy loss encountered in the SCC, the RF system is a relatively small part of the impedance inventory. Later work indicated that with momentum spreads at the 10^{-4} level unshielded bellows alone would contribute enough coupling to be within a factor of two of driving beam instability.

In light of these previous studies, this first SSC Impedance Workshop focused attention on the transverse, single-bunch instability and the detailed analysis of the broadband impedance which would drive it. Issues which were discussed included:

1) Single-bunch stability: impact of impedance frequency shape, coupled-mode vs. fast blowup regimes, possible stopband structure

2) Numerical estimates of transverse impedance of inner bellows (PEP-like) and sliding contact shielded bellows

3) Analytic estimates of pickup and kicker impedance contributions

4) Feasibility studies of wire and beam measurements of component impedance

Following this section are the participants' contributions, which describe in detail the stability limits in the SSC, the impact of a variety of hardware designs on machine impedance and energy loss, and the prospect for measurements of component impedance. The remainder of this section is devoted to an overview of beam stability in the SSC which highlights some of the workshop efforts.

At low frequencies the threshold condition of transverse mode coupling due to coherent tune shifts is of the form

$$N_B(\text{m-c}) = \frac{8\pi^{3/2}}{ec} \frac{E}{e} \frac{R\eta}{\beta Z_{t,reac}} \frac{\sigma_E}{E} F_1 \qquad (1)$$

where N_B is the number of particles/bunch and $F_1 \simeq 1.5$ in the long bunch limit. At high frequencies, the fast-blowup condition yields

$$N_B(\text{f-b}) = N_B(\text{m-c}) \; (Z_{t,reac}/Z_{t,res}) \; [n_c\sigma_l/(R\pi^{1/2})]/ \; F_1 \qquad (2)$$

where $f_c = n_c f_o$ is the "resonant" frequency of the broadband impedance. For a $Q = 1$ resonator the reactive part of Z_t at low frequency is equal in magnitude to the resistive transverse impedance at resonance. For a 3 cm diameter beam pipe $f_c \simeq 5$GHz, the bracketed factor is about 4, and it would appear that the low frequency coupled-mode instability would

dominate. However, discontinuities such as bellows and bellow shields can exhibit behaviour typified by a higher Q, which would result in the peak resistive part of Z_t being substantially larger than the low frequency reactive part of Z_t. This effect would compensate for the enhanced Landau damping described by the bracketed term and bring the fast-blowup threshold closer to the coupled-mode threshold. Studies indicate that PEP-like inner shields (see papers of Ruth and Bane, and Ng and Bisognano) behave approximately as a Q=4 resonator with a cutoff frequency of 12GHz (which sets the bracketed term to 10). Thus it appears that the fast blowup threshold current is only a factor of 1.7 (10/4/1.5) higher than the mode-coupling value. Increasing the bunch length (and lowering the peak current) can improve the fast-blowup threshold, however.

Experimental tests of the transverse mode-coupling instability have been confined to electron rings with short bunches. In this regime coupling occurs near the "resonant" frequency of the machine impedance where neighboring modes are shifted in opposite directions (since the sign of the reactive impedance is changing) and where there is substantial resistive impedance to cause growth. The transverse instability has yet to be observed in existing proton rings where the issue is clouded both by space charge tune spreads at injection and the onset of longitudinal instability. Figure 1 shows the results of two runs of a transverse mode-coupling code (authored by Ruth) for a Q = 1 resonator with f_c = 1.6GHz and 6.4GHz ($\omega_c = 2\pi f_c$). With the lower frequency cutoff, mode-

coupling yields persistent growth as a function of current. The higher cutoff, on the other hand, indicates a stopband structure with small growth rates. Work of Ruth and Bane indicates that a bellows alone, since it has even less resistance at low frequencies, offers an even broader passband structure. However, other sources of impedance from, for example, pickups and kickers, can provide the low frequency resistance necessary for instability. This appears to be borne out in the studies of Ruth and Bane with pickup impedance as determined by work of Shafer. Several comments are in order. First, the fast-blowup instability is only a factor of 1.7 higher in threshold, and any easing of the coupled-mode criterion can at best yield this factor. Secondly, it is doubtful that the injection process can be so well controlled as to always miss the stopbands. Beam loss may occur in reaching an equilibrium in a passband which would not be tolerable in a superconducting environment. On the other hand, equilibrium may be reached by redistribution of the bunch current to a shape which produces less differential mode frequency shift. Also, pickup and kickers may be shielded at high frequencies, and this will limit the resistance offered. Given these uncertainties, the prudent approach remains to design with the no-coupling condition of equation (1) satisfied.

Estimates of the contributions of PEP-like inner bellows were performed by Ng and Bisognano, and Bane and Ruth. The code TBCI of Weiland was used with the frequency dependent impedance determined by fast Fourier transforms of the wakefields. For a 90Km machine,

bellows impedance of about 70MΩ/m was obtained. The coupled-mode criterion indicates that for the Reference Designs study lattice 180MΩ/m is tolerable at rms fractional momentum spread of 1.5 10^{-4}. For CDG lattices:

60° 6T implies limit of 188 MΩ/m

90° 6T implies limit of 119 MΩ/m

The contribution of bellows is significant. The threshold current limit can be eased by increasing momentum spread at the expense of RF. Assuming a 4σ bucket height, an increase from 1.5 10^{-4} to 3.0 10^{-4} in energy spread is consistent with the dynamic and physical aperture of the machine. However, the best solution appears to be sliding contact shielding of bellows which studies of Ng and Bane and Ruth indicate can reduce the bellows contributions by an order of magnitude.

The impedance contributions of beam position monitors and abort and injection kickers were reviewed during the workshop (Shafer, Lambertson, Wang, et al.). Both impedance sources were estimated to contribute transverse impedances of several megohms/meter. These components distinguish themselves from bellows in being resistive at much lower frequencies (in the 10-100 MHz) range. Since neither class of devices requires broad bandwidth, disigns which can be compensated by narrow band feedback should be considered.

The Impedance Measurement Group concluded that wire measurement up to 3 GHz would yield meaningful results, and that there would be sufficient sensitivity to measure transverse impedances in the 100 Ω/m range. This would be sufficient to measure a bellows assembly or a shielded bellows structure, although a PEP-like bellows assembly would not be significantly resistive at these frequencies. The greatest uncertainties in impedance estimate remains with kicker structures and, to a lesser extent, with beam position monitors. Since these structures are relatively low frequency in character and not amenable to existing numerical codes, wire measurements offer a good choice for impedance determination. The work of Bane and Ruth indicates that shielded bellows can produce significant longitudinal power loss if sufficient sliding element contact is not provided. Since the bunch spectrum (bunch length $\sigma_l \simeq 7$ cm) falls off rapidly above 1GHz, wire measurement again appear useful in sorting out various designs.

Beam measurements of impedance were also discussed during the workshop. The "witness pulse" method offers the possibility of impedance measurements above the 3GHz limit of wires, and would provide information on the resistive impedance offered by bellows convolutions (≃12GHz). Sensitivity with respect to transverse impedance remains a concern.

Several future efforts suggest themselves:

1) The cataloging of impedance is of necessity incomplete. Although the goals set for the SSC appear reasonable in view of what has been achieved in electron storage rings, measurement of the impedance of a superconducting proton accelerator, namely, the Tevatron, would be enlightening. The Tevatron was designed with unshielded bellows which may produce a few ohms of longitudinal impedance. Measured values above this level would indicate other important sources which need itemization.

2) Wire measurements of abort and injection kicker impedances should be pursued at the earliest opportunity. Their contribution to beam stability is enhanced by the high β-functions in abort sections.

3) Mechanical design of shielded bellows structures and subsequent measurement of transverse impedance and longitudinal energy loss is needed. The success and costs of these designs will determine whether the enhanced thresholds and design safety margins apparently offered by shielded bellows can in fact be realized.

Figure 1. Structure of Coupled Mode Instability

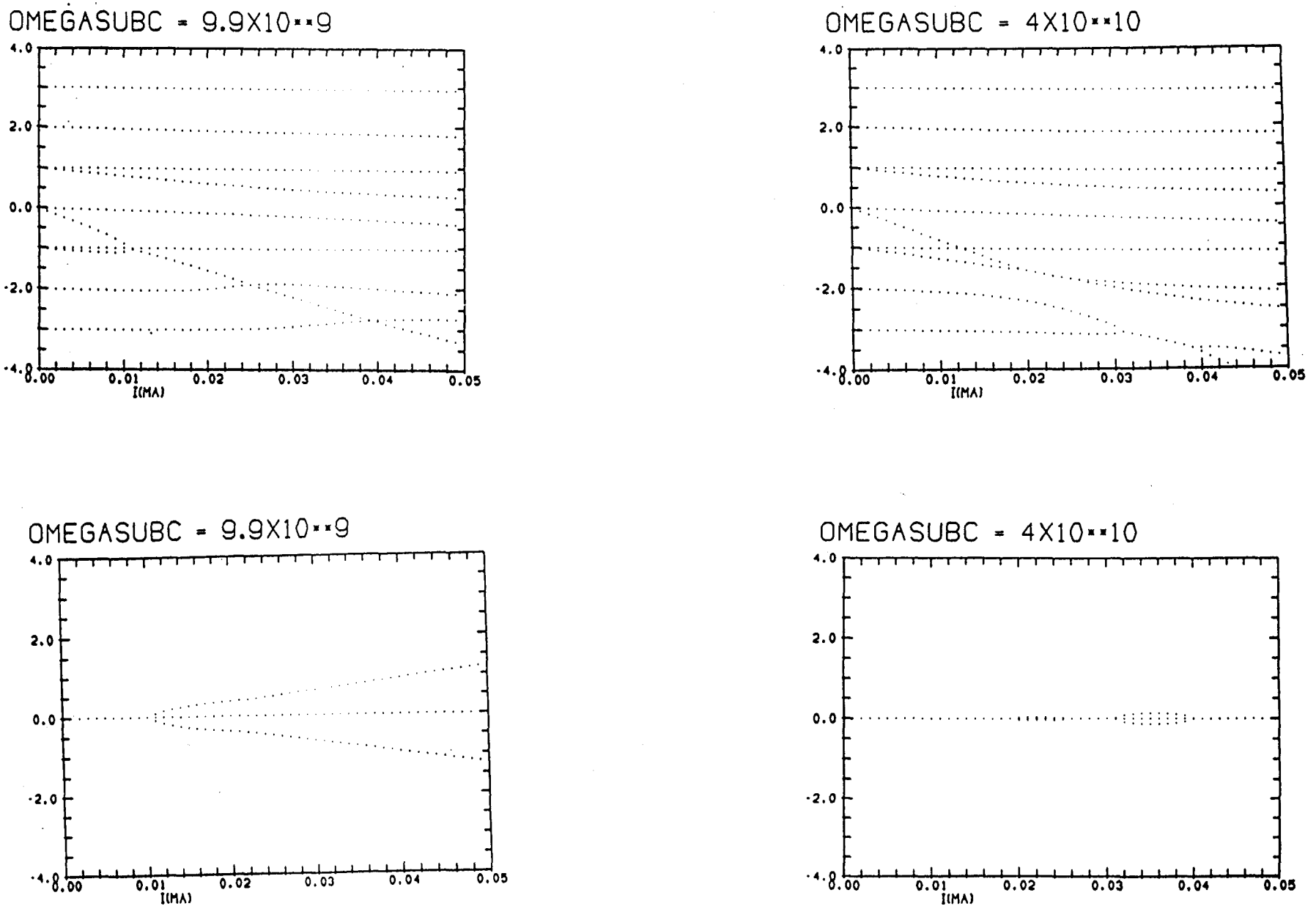

SLAC – AP – 45
October 1985
(AP)

BELLOWS WAKE FIELDS AND TRANSVERSE SINGLE BUNCH INSTABILITIES IN THE SSC*

K. L. F. BANE AND R. D. RUTH

Stanford Linear Accelerator Center
Stanford University, Stanford, California, 94305

Presented at the SSC Impedance Workshop, June 26-27, 1985

* Work supported by the Department of Energy, contract DE-AC03-76SF00515

1. Introduction

In this paper we study the transverse wake field due to the bellows in the SSC and its effect on the transverse mode coupling instability. For long bunches this instability has a small growth rate which depends critically on the real part of the transverse impedance at $\omega \leq 1/\sigma_\tau$ where σ_τ is the bunchlength in seconds. The instability is caused by the coupling of mode 0, the rigid dipole mode, and mode '-1' , the mode shifted by $-\nu_s$ from the betatron tune. Thus, the instability needs a large frequency shift as well as a large 'off diagonal' element to couple the modes. The frequency shift is induced by the imaginary part of the transverse impedance at $\omega \leq 1/\sigma_\tau$ while the off diagonal element is related to the real part of the impedance at $\omega \simeq 1/\sigma_\tau$. In addition, if the beam current is large enough, there can be a coasting-beam-like instability with a growth rate larger than the synchrotron frequency. By comparing the transverse and longitudinal instability thresholds, it is straightforward to see that the single bunch transverse instability is more restrictive than the single bunch longitudinal instability in the SSC.[1]

There have been calculations which suggest that bellows can be a large source of transverse impedance, and thus can drive transverse instabilities.[2,3] Therefore, in this paper we will emphasize the bellows impedance but also include the beam position monitor impedance. There are certainly other sources of transverse impedance which will be omitted here.

In the following sections we first discuss the instability thresholds and then show calculations of the bellows wake fields. To reduce the wake field effects, another design with shielded bellows is then considered. Next we discuss briefly the impedance of the beam position monitors. Finally, we show the effect of the bellows and beam position monitors on transverse mode coupling.

2. Thresholds for Transverse Instabilities

There are two 'types' of transverse instabilities considered here. The first is the transverse mode coupling instability in which two low-order modes couple to cause an instability. The second is the 'transverse microwave' instability which is the coasting-beam-like instability mentioned above. The second of these involves the cooperation of an infinity of the so called head-tail modes and is better analyzed with different techniques.[4,5] It is important to note that in essence these two 'types' of transverse instabilities involve the same physics. The division is made for the purposes of calculation only.

2.1 THRESHOLD FOR FAST BLOW-UP $[\Im m(\omega) \gg \omega_s]$

Consider an impedance which is somewhat broad band and large in the neighborhood of some frequency ω_r. The impedance should vary slowly in a frequency range of $1/\sigma_\tau$. Then the *sufficient condition for no fast blow-up* for a Gaussian bunch is given by[4,5]

$$\frac{eI \mid Z_\perp(\omega_r) \mid \beta_{ave}}{4E\eta\sigma_\epsilon\sigma_\tau\omega_r} \leq 1 \quad , \tag{1}$$

where

$$\sigma_\epsilon = \Delta p/p \text{ rms}$$

$$I = \text{bunch current}$$

$$E = \text{energy}$$

$$\eta = \text{frequency slip factor}$$

$$Z_\perp = \text{transverse impedance}$$

$$\beta_{ave} = \text{average beta function} \quad .$$

The chromaticity is assumed to be zero so that the spread in frequency above is entirely due to the spread in revolution frequency.

Equation (1) can be thought of as the 'threshold' for fast blow-up; however, since it is actually a sufficient condition for *no* fast blow-up, it may be somewhat pessimistic. That is, the actual instability may occur at a current as much as a factor of 2 or 3 more than the current which satisfies the equality in Eq. (1), but the instability will not occur at lower values. We will use the term threshold to refer to the equality in Eq. (1) while keeping in mind this caveat.

2.2 THRESHOLD FOR THE TRANSVERSE MODE COUPLING INSTABILITY[5,6]

This instability has been seen both in PETRA and PEP and is due to the coupling of low order head-tail modes. To estimate the threshold consider the shift of mode 0. For a Gaussian bunch the shift of the rigid dipole mode for small currents is given by

$$\frac{\Delta\nu}{\nu_s} = \frac{-ieI\beta_{ave}}{4\pi E\nu_s} \int_{-\infty}^{\infty} Z_\perp(p\omega_0) e^{-p^2\omega_0^2\sigma_\tau^2} dp \quad . \tag{2}$$

If we assume that there is sufficient resistive impedance at $\omega < 1/\sigma_\tau$ to couple modes 0 and -1, then the threshold typically occurs when mode 0 has shifted by about ν_s. For long bunches, however, mode -1 moves down also with a slope which is 1/4 of the slope for mode 0. Thus, a simple extrapolation would yield mode coupling if mode 0 is shifted by about $4\nu_s/3$. This yields a formula for the threshold,

$$\frac{4}{3} \simeq \frac{ieI\beta_{ave}}{4\pi E\nu_s} \int_{-\infty}^{\infty} Z_\perp(p\omega_0) e^{-p^2\omega_0^2\sigma_\tau^2} dp \quad . \tag{3}$$

If the bunch is sufficiently long, and the imaginary part of the transverse impedance

varies little from 0 to about $1/\sigma_\tau$, the threshold is given approximately by

$$\frac{4}{3} \simeq \frac{eI\Im m[Z_\perp(1/\sigma_\tau)]\beta_{ave}}{4\pi E\nu_s}\frac{\sqrt{\pi}}{\sigma_\tau\omega_0} \quad . \tag{4}$$

If we compare the two thresholds and note that $\nu_s\sigma_\tau\omega_0 = \eta\sigma_\epsilon$, we find

$$\frac{I_{th}(\text{Fast Blow Up})}{I_{th}(\text{Mode Coupling})} = \frac{3\sigma_\tau\omega_r}{4\sqrt{\pi}}\frac{\Im m[Z_\perp(1/\sigma_\tau)]}{\mid Z_\perp(\omega_r)\mid} \quad . \tag{5}$$

3. Bellows Wake Fields/Impedances

The computer code TBCI[7] can be used to calculate the dipole wake field due to a bellows. Ideally we would like the wake field due to a point charge (the δ-function wake) $W_\perp(t)$, from which we get the transverse impedance $Z_\perp(\omega)$ by

$$iZ_\perp(\omega) = \int_0^\infty W_\perp(t)e^{i\omega t}\,dt \quad . \tag{6}$$

The code, however, solves for the wake field of a smooth finite-length bunch, which we will denote by $\bar{W}_\perp(t)$. $\bar{W}_\perp(t)$ is simply the convolution of $W_\perp(t)$ with the current distribution. If a short enough bunch length is chosen, $\bar{W}_\perp$ is very similar to $W_\perp$. For a Gaussian current distribution with rms bunch length σ_τ, the Fourier transform of the bunch wake $\bar{Z}_\perp(\omega)$ is related to the impedance by

$$\bar{Z}_\perp(\omega) = Z_\perp(\omega)e^{-\omega^2\sigma_\tau^2/2} \quad . \tag{7}$$

Given $\bar{Z}_\perp$, Eq. (7) can be used to find $Z_\perp$.

In practice $Z_\perp$ can be found only up to some limiting frequency due to numerical inaccuracies. One such source of inaccuracy is the finite mesh size used in TBCI to calculate $\bar{W}_\perp$. Another source is the Gaussian driving bunch; for $\omega\sigma_\tau$ large enough the Gaussian factor of Eq. (7) destroys all meaningful information in $\bar{Z}_\perp$. In all examples presented here short driving bunches were used with $c\sigma_\tau$ of 1 or 2 mm. The mesh size was taken to equal $c\sigma_\tau/4$. For this situation meaningful information appears to be limited to $\omega/2\pi \simeq 1/2\sigma_\tau$ which for the cases above is 75 or 150 GHz.

For single bunch instability studies it is only necessary to calculate the wake field over a distance equal to the total design bunch length. Since the SSC rms bunch length is 7 cm, it was deemed sufficient to calculate the wake field out to 20 cm. The resolution due to this limited sampling range is $\Delta f = c/20\,\mathrm{cm} = 1.5$ GHz.

3.1 Simple Bellows

Calculation:

The first example is that of a simple rectangular bellows (See Fig. 1a). The actual bellows used may have rounded corners or be triangular in shape, but the rectangular approximation with appropriately chosen dimensions should give the same basic behavior. For the TBCI calculation we have chosen a beam tube radius $b = 1.65$ cm, a bellows period $p = 0.22$ cm and a depth of corrugation $\Delta = 0.35$ cm. These bellows are directly scaled from the PEP inner bellows. Forty cells were used in the computation. The mesh spacing was 1/10 of a period. Fig. 2 gives $\bar{W}_\perp$ in units of V/pC/cell due to a Gaussian bunch with $c\sigma_\tau = 1.0$ mm, centered at $ct = 0$ and with its head at $ct < 0$. Note that the

wake has a maximum value of 5.6 V/pC per cell. By taking the Fast Fourier Transform of $\bar{W}_\perp$ and then using Eq. (7), we get the impedance $Z_\perp$ (See Fig. 2). The units are in kΩ/m/cell.

From the plots we see that the bellows impedance is dominated by what appears to be a damped resonance peaked at 13.5 GHz. The peak is above the first TM1 cut-off of the tube, $f_c = (c/2\pi)(3.83/0.0165\text{m}) \approx 11$ GHz. The peak value of $\Re e(Z_\perp)$ is about 370 Ω/m per cell. If we let the quality factor Q be the resonant frequency divided by the full width at half maximum we get $Q \approx 5$. Note that the ratio of the first peak of $\Re e(Z_\perp)$ to the magnitude of $\Im m(Z_\perp)$ near zero also appears to be about 5. (This is consistant with the isolated resonance picture discussed below.) In addition, a second much weaker peak can be seen at 50 GHz.

The SSC bunch samples the impedance up to $\omega/2\pi \sim 0.7$ GHz since the bunch length is 7 cm. Over this frequency range $\Im m(Z_\perp) = -79$ Ω/m per cell. If 1.2 km of bellows are needed, which corresponds to 550,000 of these cells, then $\Im m(Z_\perp) = -43$ MΩ/m for the entire SSC ring. Although this is a large value, the real part of the impedance over this frequency range is very small.

Discussion and Scaling:

The computer code TRANSVRS[8] can be used to calculate the transverse frequencies of infinitely repeating, rectangular bellows. According to this code the first two dipole modes excited by an ultra-relativistic charge traversing the simple bellows described above are at 12.2 GHz and 47.7 GHz. It is this result that leads us to describe the two peaks of $\Re e(Z_\perp)$ as isolated resonances. The frequencies calculated by the two codes compare reasonably well. Further TBCI computations of this bellows, but with a varied number of cells, show an increase

in the fundamental frequency ω_0 with a decrease in the number of cells. For the bellows example described above $\omega_0/2\pi = 18$ GHz when only one cell is used. Therefore, the agreement of the two codes for the resonant frequencies of bellows with very many periods may be even better than is apparent here.

In addition, TRANSVRS was used to calculate the fundamental frequency for rectangular bellows with various dimensions. The results can be summarized by the scaling relation

$$\frac{\omega_0 b}{c} = 1.79 \left(\frac{\Delta}{b}\right)^{-0.55} \quad . \tag{8}$$

The above relation gives the TRANSVRS results to within 5% for $0.05 < \Delta/b < 0.30$ and $0.05 < p/b < 0.20$. The discrepancy is largest for Δ/p small. We know that this scaling cannot be valid for structures with $\Delta/p \ll 1$, since for these structures (assuming p/b is small) $\omega_0 p/c \approx \pi$.[9] Such a structure, however, would make a poor bellows!

Since the bellows impedance is dominated by a single mode, its wake field can be written as[10]

$$W_\perp \approx \frac{2c\,k_{\perp 0}}{b^2\omega_0} \sin\omega_0 t \, \exp\left(-\frac{\omega_0 t}{2Q_0}\right) \qquad \text{for } t > 0 \quad , \tag{9}$$

where ω_0, $k_{\perp 0}$ and Q_0 are respectively the frequency, the strength factor (or loss factor) and the quality factor of the first dipole mode, and ct is the distance that the test charge is behind the driving charge. From Eq. (6) we see immediately that the strength factor is related to the value of $\Im m(Z_\perp(0))$ by

$$\Im m(Z_\perp(0)) \approx -\frac{2c\,k_{\perp 0}}{b^2\omega_0^2} \quad , \tag{10}$$

when $1/4Q_0^2$ is small. Furthermore, when $1/Q_0$ is small, we have

$$\hat{W}_\perp \approx -\omega_0 \Im m(Z_\perp(0)) \quad , \tag{11}$$

where $\hat{W}_\perp$ is the maximum of $W_\perp$. Neither $\Im m(Z_\perp(0))$ nor $\hat{W}_\perp$ depend on Q_0 for $1/Q_0$ small.

The value of $\Im m(Z_\perp(0))$ can also be approximated by[11]

$$\Im m(Z_\perp(0)) = -\frac{Z_0 p}{2\pi b^2}\frac{s^2-1}{s^2+1} \quad , \tag{12}$$

where $Z_0 = 377\ \Omega$ is the impedance of free space and $s = 1 + \Delta/b$. With the help of Eqs. (8), (10), (11)and (12) the values of ω_0, $k_{\perp 0}$, $\hat{W}_\perp$ and $\Im m(Z_\perp(0))$ can be approximated for most practical simple bellows. For the above example these relations yield $\omega_0/2\pi = 12.2$ GHz, $k_{\perp 0} = 0.25$ V/pC/cell, $\hat{W}_\perp = 7.1$ V/pC/cell and $\Im m(Z_\perp(0)) = -92\,\Omega$/m/cell. These values compare reasonably well with the Fourier transforms of the TBCI calculations.

The Finite Q:

The TBCI computations assume perfectly conducting walls. Under this assumption any trapped mode would have an infinite Q: there would be no energy loss. For a mode above cut-off, however, energy can leak down the beam tube yielding a resonance peak in $\Re e(Z_\perp)$ with a finite width. We can therefore speak of such a mode as having a finite Q. But as the number of periods in our bellows approaches infinity, we expect the Q of this mode also to approach infinity. For a sufficiently large number of bellows periods

$$Q_0 = \frac{\omega_0 U_0}{P_0} = \frac{\omega_0 p}{v_{g0}} N_p \quad , \tag{13}$$

where U_0, P_0, v_{g0} are respectively the total energy stored in the bellows, the

power loss and the group velocity of the mode; p is the period of the structure and N_p is the number of bellows periods. In practice for a very large number of periods, the Q will be limited by the finite resistivity of the metal walls. For copper, at these frequencies, the Q will be limited to a value of some thousands. If the cells differ slightly, the effective Q will also be reduced.

For the bellows above, where the wavelength $2\pi c/\omega_0 = 2.2$ cm $=10p$, one would presumably need some tens of periods for the above approximation to be valid. For this example TRANSVRS calculates $v_{g0} = 0.4c$. Therefore, for forty cells, the above approximation yields $Q_0 = 60$.

The code TBCI, however, yields a result of $Q_0 \approx 5$ for 40 cells, which is approximately the same value it gets when only 20 cells are used in the calculation. Numerical errors caused by the finite mesh size used in the TBCI calculation will contribute to field and frequency inaccuracies and therefore to a resonance widening. We have seen indications that this is the cause of the unexpectedly low value of Q_0 computed by TBCI. Unfortunately, it is difficult to use a mesh which is fine enough to investigate this question further. In any case a real bellows has an effective Q_0 limited by the construction imperfections as discussed above. In the subsequent calculations we will assume the Q_0 given by TBCI.

3.2 Shielded Bellows

Calculations:

An example of a shielded bellows in the expanded position is shown schematically in Fig. 1b. The wiggles at the top of the figure represent the simple bellows that is being shielded. The shielding cylinders which have a thickness of 2 mm overlap by 11 cm when expanded. For this example we choose a gap g of 10

cm and a depth d of 5.5 mm. In order to reduce the number of mesh points required, the actual calculations are done for the structure shown in Fig. 1c. For a wake field reaching only to 20 cm behind the bunch head, the results for the two configurations are the same: no wave launched by the head of the bunch can travel to point P in Fig. 1b and return to a test particle located 20 cm behind the head.

Fig. 3 gives the wake field calculated by TBCI for a bunch with $c\sigma_\tau = 2$ mm. The first peak has a value of 46.3 V/pC/m per shielded bellows. Note that the wake does not exhibit such a clear resonance as before. The period for such a resonant behavior must be about the time for information from the rest of the cavity to return back to the axis. The resultant low frequency resonance will affect only the multi-bunch beam behavior. The value of $\Im m(Z_\perp(0))$ is -2 kΩ/m per shielding unit. Although $\Re e(Z_\perp)$ is again small at low frequencies, it rises much sooner than in the simple bellows case. We see peaks at 3.3 GHz and 9.8 GHz with values of 1.4 $k\Omega$/m and 1.5 $k\Omega$/m respectively.

The impedance of this shielded bellows should be compared to the number of simple bellows it can shield. Let us assume that each unit shields 30 cm of simple bellows, or 136 periods of the simple bellows presented in the previous section. Then 1.2 km of bellows corresponds to 4000 of these shielding units. For the whole machine $\Im m(Z_\perp(0)) = -8.0$ MΩ/m.

Variations and Scaling:

Running the shielded bellows again (with $c\sigma_\tau = 2$ mm) but with $d = 4$ mm results in the wake field of Fig. 4. The wake field looks very similar to that of the previous example. The first peak has a value of 33.6 V/pC/m. The impedance looks similar, though the strong resonance at 9.8 GHz is missing. $\Im m(Z_\perp(0))$ is

-1.1 kΩ/m.

We see that the value of the first peak of the wake scales almost exactly by the ratios of d used in the two cases, *i.e.* 4.0/5.5= 0.73. To test the scaling with g, we have run with g set to 7 cm and 13 cm. Neither case yields a significant change in the peak of the wake field. Therefore, the peak of the wake field is roughly independent of the gap g as long as it is not too small. In summary, for a shielded bellows the peak of the wake field scales as

$$\hat{W}_\perp = \hat{W}_{\perp 0} \left(\frac{b}{b_0}\right)^{-3} \left(\frac{d}{d_0}\right) \quad , \tag{14}$$

where $W_\perp$ is the wake field per shielding unit. The value of $\Im m(Z_\perp(0))$ also follows this scaling approximately.

Finally, the cell of Fig. 1d was used to model the shielded bellows of Fig. 1b but with the space between the two shielding cylinders perfectly closed by something like a metallic washer at position Q. The depth d was set to 4 mm. In this case 136 small corrugations of the simple bellows are replaced by one larger corrugation. Fig. 5 gives the resultant transverse wake field and impedance. The first peak of $\bar{W}_\perp$ has a value of 32.3 V/pC/m. Although the value of the peak of the wake field is approximately the same as in the previous example, in this case the total area under this peak is much less; thus, the impedance is significantly reduced. The value of $\Im m(Z_\perp)$ at 1.5 GHz is -620Ω/m, about half the value without the washer in place. In addition, the resonance peak near 2 GHz has been eliminated. In fact $\Re e(Z_\perp)$ is essentially zero up to about 4 GHz.

3.3 THE LONGITUDINAL IMPEDANCE OF BELLOWS

Simple Bellows:

TBCI can also be used to calculate the longitudinal wake field $\bar{W}_{\|}$ of a bunch traversing a bellows, from which we can get the longitudinal impedance $Z_{\|}$ just as in the transverse case. The longitudinal wake was calculated for forty periods of the simple bellows introduced in Section 3.1 for a bunch with $c\sigma_\tau = 1$ mm (See Fig. 6.) As in the transverse case, the longitudinal impedance is dominated by what appears to be a damped resonance. The resonant frequency is at 12.3 GHz, which is above the first TM0 cut-off frequency. A second resonance can be seen at 49 GHz. The computer code KN7C,[12] the longitudinal counterpart of TRANSVRS, yields frequency values of 11.6 GHz and 47.7 GHz for the first two longitudinal modes. It is interesting to note that the first two longitudinal modes are almost at the same frequency as the first two dipole modes.

For the SSC, the heating of the walls is the only effect of the longitudinal wake which we need to consider. Given the total loss factor $k_{\|tot}$, the power lost per turn is given by

$$P = k_{\|tot}\, e^2 N^2 n_b f_{rev} \quad , \tag{15}$$

where N is the number of particles per bunch, n_b is the number of bunches and f_{rev} is the revolution frequency. For a Gaussian bunch $k_{\|tot}$ is given by

$$k_{\|tot} = \frac{1}{\pi} \int_0^\infty \Re e(Z_{\|}) e^{-\omega^2 \sigma_\tau^2}\, d\omega \quad . \tag{16}$$

For the simple bellows $\Re e(Z_{\|})$ is so small over the bunch spectrum that $k_{\|tot}$ is completely negligible. For example, at 8 GHz, where $\Re e(Z_{\|})$ begins to grow, the exponential factor in the above equation is $-\omega^2\sigma_\tau^2 = -140$.

Shielded Bellows:

For the shielded bellows with $d = 5.5$ mm TBCI computes $k_{\|tot} = 0.010$ V/pC per shielded bellows. Inserting the SSC parameters into Eq. (15) yields 1.5 W of power lost in each shielding unit. Assuming the ring needs 4000 such units, the total power loss is 6 kW. This is quite a large value for the SSC.

The shielded bellows with $d = 4.0$ mm loses 0.9 W per shielding unit. For the shielded, shorted bellows with $d = 4.0$ mm the power loss again becomes negligible as in the simple bellows case. As we saw in the transverse case, shorting the shielded bellows pushes the first rise of $\Re e(Z_{\|})$ to higher frequencies. In the time domain we can say that with the shorting washer in place all the energy lost by the front half of the bunch is picked up by the back half. Without it, ten times as much energy is radiated by the head. In addition, most of the energy lost by the head is radiated between the two shielding tubes and doesn't return to the tail (See Fig. 7).

The lesson from these longitudinal computations is that if one wants to shield the bellows, then either the depth d must be made very small or the gap between the shielding tubes should be closed. Alternatively, one could design a shielding structure with only gradual discontinuities, such as those planned for LEP.[13] To conclude this section we summarize some key features of the bellows impedance calculations in Table 1.

Table 1. Bellows Contribution to the SSC Impedance and Power Loss

Bellows Type	$\Im m(Z_\perp(0))$	Power
simple bellows	-43.0 MΩ/m	0.0 kW
shielded ($d = 5.5$ mm)	-8.0 MΩ/m	6.0 kW
shielded ($d = 4.0$ mm)	-4.4 MΩ/m	3.6 kW
shorted ($d = 4.0$ mm)	-2.5 MΩ/m	0.0 kW

4. The Impedance of the Beam Position Monitors

There are many other contributions to the total impedance of the SSC vacuum chamber. One of the most important is the contribution from beam position monitors. The impedance of the position monitors has been discussed in Refs. 14 and 15; we quote the results here for completeness.

The BPM's discussed in Ref. 15 consist of 4 striplines positioned at 45° from the median plane so as not to intercept synchrotron radiation. The x or y position can be obtained by an appropriate linear combination of the signals from the 4 striplines. These would be placed at each quadrupole in the SSC.

The transverse impedance due to the stripline position monitors described above is given by

$$Z_\perp(\omega) = \frac{16 P Z_p c \sin^2(\phi_0/2)}{\pi^2 b^2 \omega}[\sin^2(\omega\ell/c) + i\sin(\omega\ell/c)\cos(\omega\ell/c)] \qquad (17)$$

where

$P = 880 =$ the number of pickups

$Z_p = 50\,\Omega =$ pickup impedance

$b = 1.65\,\text{cm} =$ chamber radius

$\ell = 20\,\text{cm} =$ length of pickup

$\phi_0 = 55^\circ$ = angle subtended by one stripline .

The impedance above is quite different from that due to the bellows. As with bellows the reactive part of the impedance below $\omega \approx 1/\sigma_T$ contributes to the frequency shift of mode 0. In addition, however, there is a sizable contribution from the resistive impedance at $\omega \approx 1/\sigma_T$ which contributes to the coupling of modes 0 and -1 and can lead to sizable growth rates. In all the calculations which follow the pickup impedance is included without modification.

5. Transverse Coherent Mode Coupling

In this section we show mode coupling due to the wake fields and impedances calculated in the previous sections. The theory of transverse mode coupling is discussed in Ref. 5 and more briefly in Ref. 6. The SSC parameters used in the calculation are given in Table 2, and the results for the various configurations are shown in Figs. 8 - 11. In each case the BPM impedance was included as well as the wake field from one of the various bellows schemes.

Table 2. SSC Parameters at Injection

Parameters	Notation	Values
Energy	E	1 TeV
Circumference	C	97.2 km
Chamber Radius	b	1.65 cm
Beta Function	β_{ave}	230 m
Energy Spread	σ_E	$1.5 \times 10^{-4} E$
Bunch Length	σ	7 cm
Freq. Slip Factor	η	1.8×10^{-4}
Synchrotron Tune	ν_s	6.0×10^{-3}
Protons per Bunch	N	1.45×10^{10}
Number of Bunches	n_b	9000

In Fig. 8 we show the results which include the BPM'S and simple bellows. Mode 0 moves linearly and collides with mode -1 at about $27\,\mu$A causing an instability. The threshold for this agrees quite well with the estimate given in Eq. (3). Notice also that the modes split apart again and re-stabilize and that modes -2 and -3 collide briefly to cause another 'bubble' of instability. The beam appears stable after $50\,\mu$A; however, this should *not* be taken seriously. In order to calculate the mode coupling accurately past $50\,\mu$A (in this case), it is necessary to include more modes. Roughly speaking, the highest mode which is included should be relatively unaffected if we are to believe the results of the calculation. However, in Fig. 8 we see that both -2 and -3 shift off the graph just past $50\,\mu$A. Thus, at least mode -4 and perhaps mode -5 must be included to calculate further. The growth rate of the instability is quite small ($\sim 0.04\nu_s$) which corresponds to an e-folding time of about 660 turns in the SSC.

The situation is somewhat different in the remaining figures. In Figs. 9 - 11 we show the case of BPM's plus each of the three schemes for shielding the bellows. In these cases the onset of the instability has been delayed and ranges from about $76\,\mu$A in Fig. 9 to about $123\,\mu$A in Fig. 11. Thus, the improvement in the threshold is a factor of 3 to 5. In addition, note that since the higher modes do not move, the calculation *can* be trusted out to the maximum current shown. The transverse mode coupling thresholds are summarized in Table 3 .

5.1 Fast Blow-up Thresholds

It is useful to calculate the threshold for fast blow-up for the case of the simple bellows. We must first assume that we believe the Q and thus the height of the peak in the impedance. If we use the peak value of the impedance at 13.5

Table 3. Transverse Mode Coupling Thresholds

Bellows Type	Threshold Current
simple bellows	$27\,\mu$A
shielded ($d = 5.5$ mm)	$76\,\mu$A
shielded ($d = 4.0$ mm)	$96\,\mu$A
shorted ($d = 4.0$ mm)	$123\,\mu$A

GHz and also include the small contribution of the pickups at that frequency, we find a 'threshold' of $40\,\mu$A. There is no fast blow-up below the threshold, but the actual instability may occur at somewhat larger currents. This indicates that we must be sure to include all the relevant higher modes when calculating transverse mode coupling threshold for currents higher that $40\,\mu$A. In particular, the stability in Fig. 8 above $50\,\mu$A is probably false.

On the other hand we can calculate the threshold for the shielded bellows as well. Here the situation is somewhat different in that the impedance does not have a peak at high frequency. In fact the fast blowup threshold is dominated by the impedance of the pickups at about 2 GHz and occurs at about $50\,\mu$A. This value is lower than the corresponding thresholds for transverse mode coupling; however, this does not indicate *another* instability. Since all the important modes are included for the shielded bellows, the transverse mode coupling threshold is correct. The 'fast blow-up' threshold is consistent with this in that the instability does occur at a larger current and has a rather large growth rate.

6. Feedback as a Cure for Transverse Mode Coupling

It has been shown in Refs. 6 and 16 - 18 that feedback can be used to increase the threshold of the transverse mode coupling instability. In addition there is recent experimental evidence to support this in the case of PEP.[19] For PEP it was found that both reactive feedback and resistive feedback increased the threshold by about a factor of 2. The theoretical prediction was that reactive feedback would increase the threshold significantly while resistive feedback would only increase it slightly.

The feedback used simply acts on the total dipole moment of the bunch. In the case of reactive feedback, a kick is supplied which shifts the coherent tune of the bunch while for resistive feedback the kick damps the dipole motion of the bunch. A simple damping of the dipole motion does not guarantee stability since there are higher modes which may be unstable. For the case of the SSC one would need a feedback system which acts on each bunch independently.

For the SSC we include feedback with sufficient power to shift the coherent tune by ν_s or to yield a damping rate of $i\nu_s$. The results are shown in Figs. 12 and 13 where we treat the case of the BPM's and simple bellows. As in Fig. 6, we cannot trust the results beyond about 0.05 mA since we have only included modes up to -3. However, it seems that both reactive and resistive feedback can increase the threshold by about a factor of 2.

7. Conclusions

In this paper we have presented the calculations of the wake fields and impedances for several different bellows schemes for the SSC and have shown how to scale the results to different designs. After including the additional impedance due to beam position monitors we have examined the transverse mode coupling instability. For the simple bellows we find a threshold for instability of about $26\,\mu$A for the single bunch current. The parameters for the SSC in Table 2 call for a single bunch current of $7.2\,\mu$A. Since there will be other sources of impedance, this is perhaps a bit too close.

We have studied two ways of raising the threshold. First we shielded the bellows with sliding contacts. This increases the threshold by a factor of 3 to 5 depending upon which scheme is used. In addition, we find that both reactive and resistive feedback increase the threshold by at least a factor of 2. Note that these values are for the representative simple and shielded bellows we have chosen for this study. The exact factors, however, will depend on the specific parameters of the bellows chosen.

Unfortunately, for the designs chosen to shield the bellows without a shorting washer, there are significant energy losses which would probably be unacceptable at cryogenic temperatures. However, if the shorted, shielded bellows design is impractical, we feel that it should be possible to design the shielded bellows with losses which are an order of magnitude smaller than those calculated here by simply smoothing the transitions.

8. Acknowledgements

We would like to thank Alex Chao, Albert Hofmann, Perry Wilson, and Bruno Zotter for useful discussions and Tor Raubenheimer for help with computations and figures.

REFERENCES

1. R. D. Ruth, Proc. of the Workshop on Acc. Physics Issues for the SSC, Ann Arbor, MI, p. 151 (1983) and LBL-17253 (1984).
2. H. Henke, LEP Note 454 (1983).
3. R. H. Siemann, private communication.
4. R. D. Ruth and J. M. Wang, IEEE Trans. Nucl. Sci., **NS-28**, No. 3, p. 2405 (1981).
5. R. D. Ruth, Brookhaven Formal Report BNL 51425 (1981).
6. R. D. Ruth, Proc. 12th Int. Conf. on High Energy Acc., Fermilab, Batavia, IL, p. 389 (1983).
7. T. Weiland, DESY **82**-015 (1982) and Nucl. Instr. and Meth. **212**, 13 file (1983).
8. K. Bane and B. Zotter, Proceedings of the 11th Int. Conf. on High Energy Accelerators, CERN (Birkhäuser Verlag, Basel,1980), p. 581.
9. R.K. Cooper, S. Krinsky and P.L. Morton, Particle Accel. **12**, 1 (1982).
10. See for example P. Wilson in *Physics of High Energy Particle Accelerators*, AIP Conf. Proc. No. 87, (Am. Inst. of Physics, New York, 1982), Sec. 11.1.

11. K.Y. Ng, Fermilab Report FN-389.

12. E. Keil, Nucl. Instr. and Meth., **100**, 419 (1972).

13. B. Zotter, private communication.

14. Robert E. Shafer, IEEE Trans. on Nucl. Sci., **NS-32**, No. 5, p. 1933 (1983).

15. R. E. Shafer, contribution to this workshop.

16. R. D. Ruth, CERN-LEP-TH/83-22 (1983).

17. S. Myers, LEP Note 498 (1983).

18. S. Myers, SLAC/AP-30,(1984).

19. M. Donald, A. Hofmann, T. Martin, P. Morton, S. Myers, J. M. Paterson, J.-L. Pellegrin, R. D. Ruth and P. Wilson, *Feedback Experiment at PEP*, to be submitted for publication.

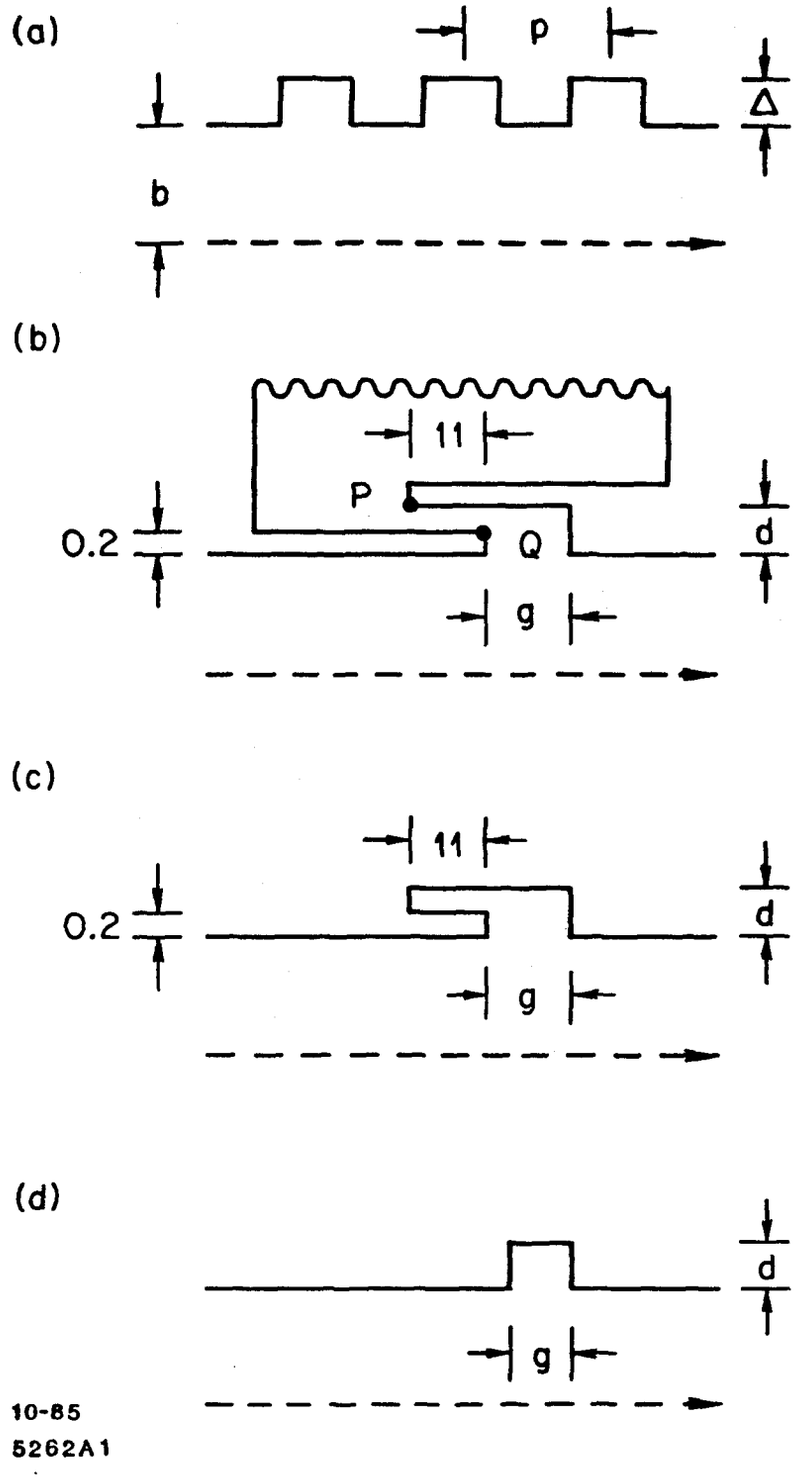

Fig. 1. Schematic Layout of the Bellows Schemes Studied. Dimensions Given are in Centimeters.

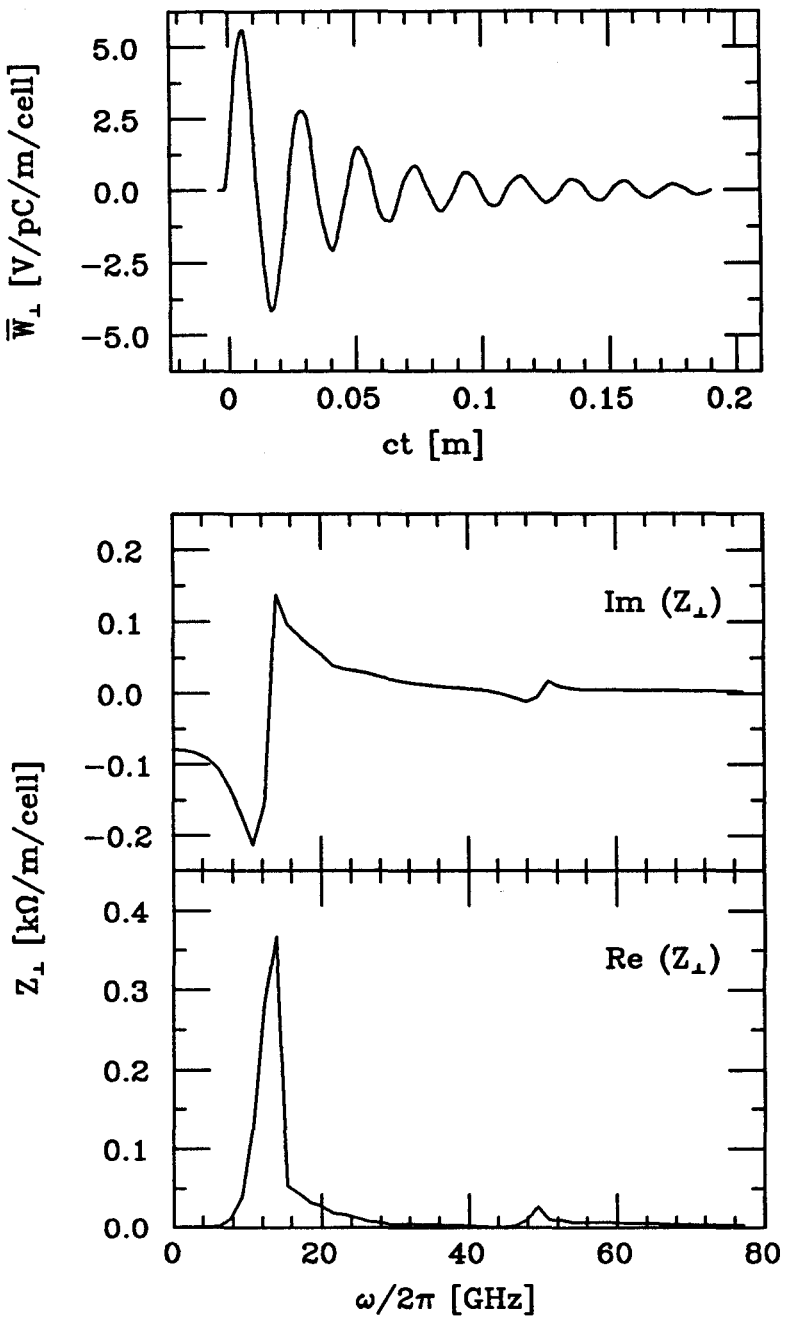

Fig. 2. Simple Bellows Wake Field and Impedance.

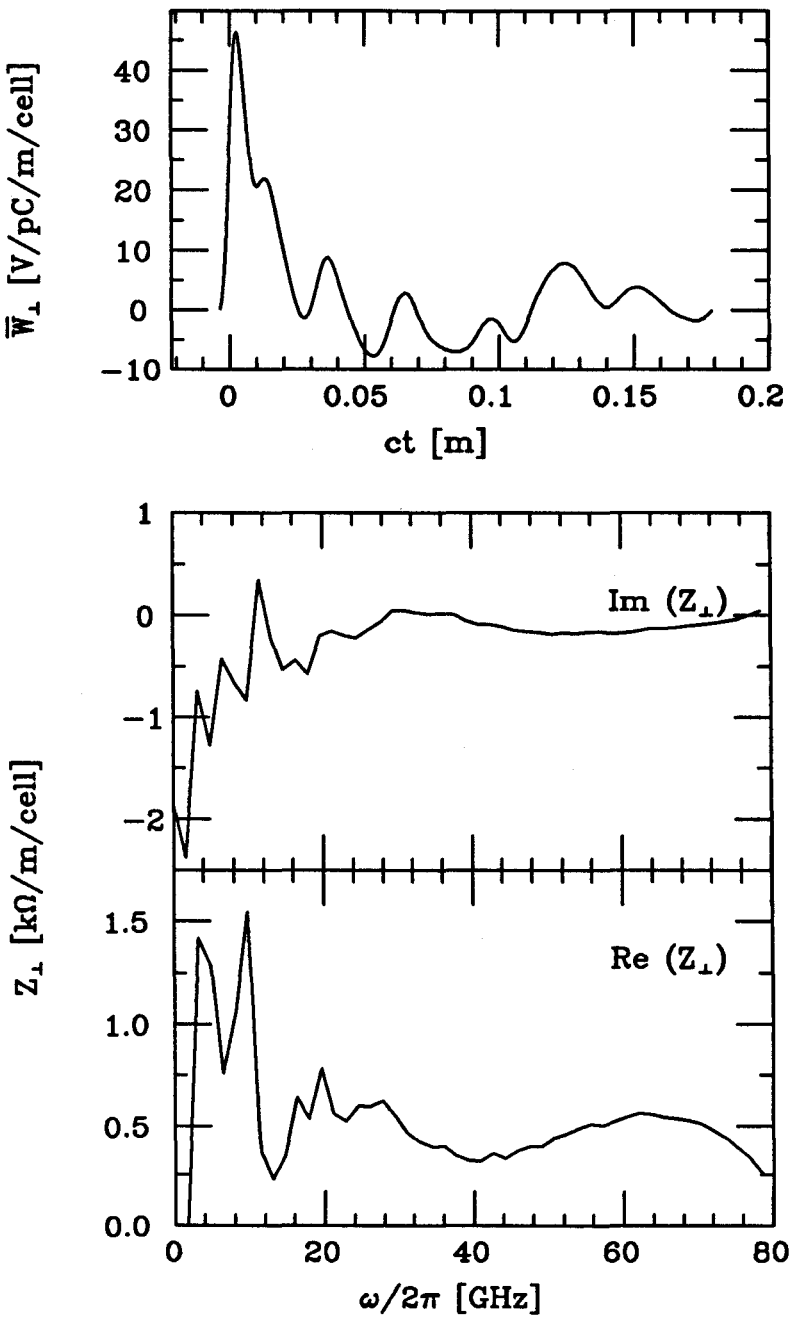

Fig. 3. Sliding Bellows Wake Field and Impedance.

(Depth d = 5.5 mm)

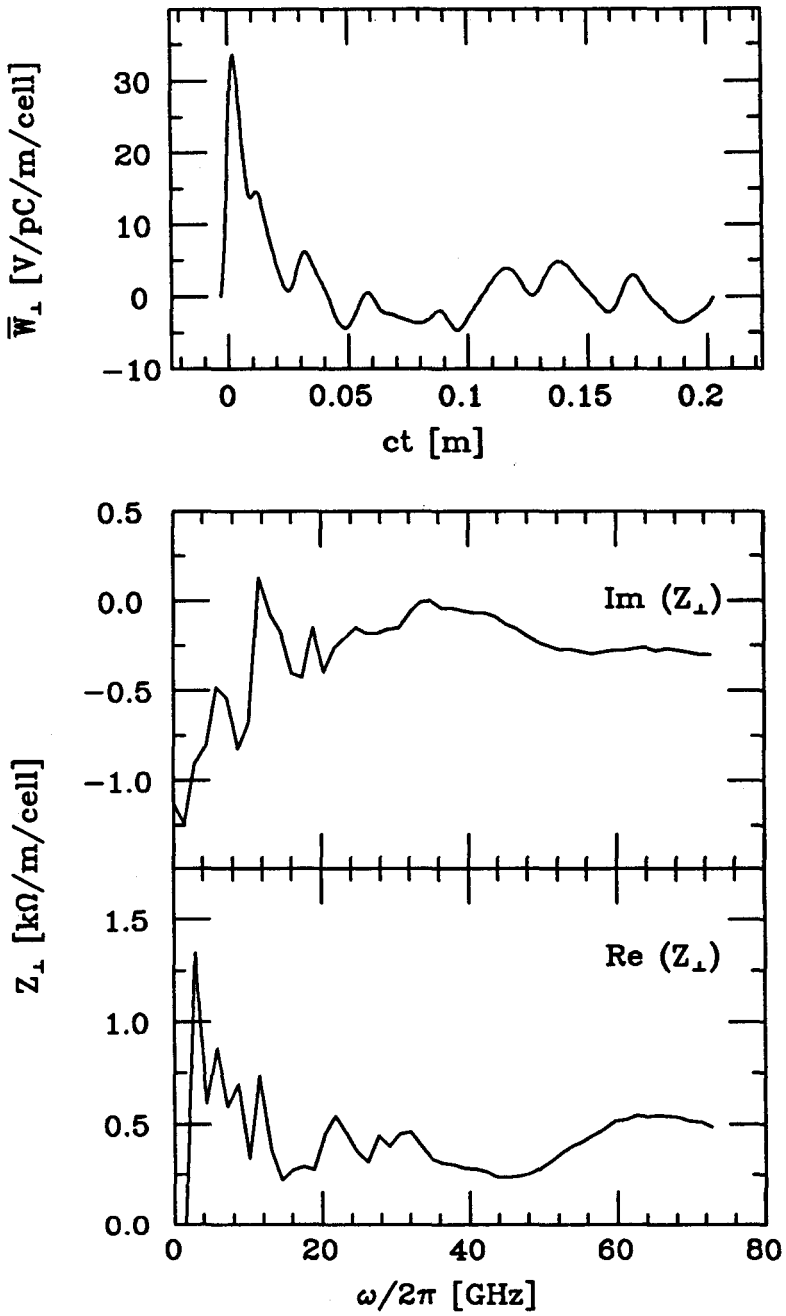

Fig. 4. Sliding Bellows Wake Field and Impedance.

(Depth d = 4.0 mm)

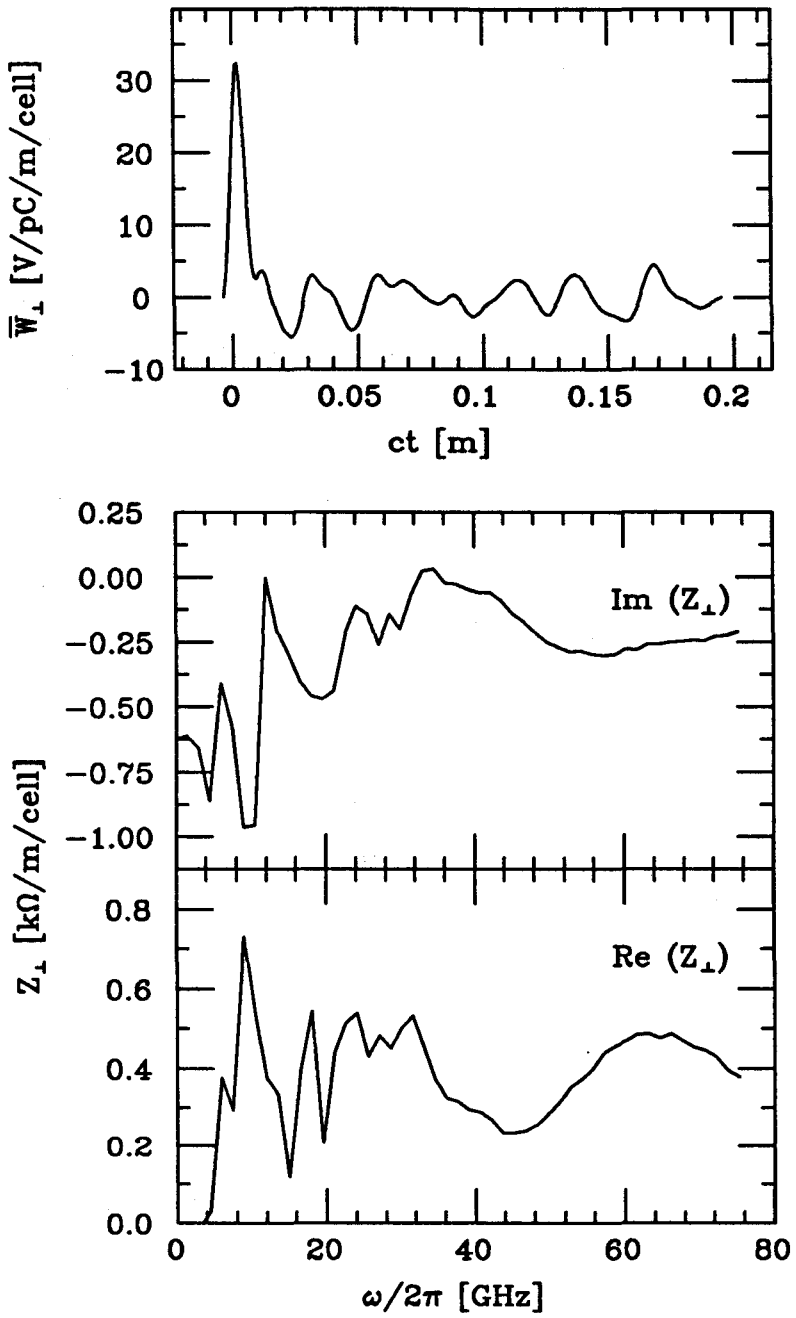

Fig. 5. Shorted Sliding Bellows Wake Field and Impedance.

(Depth d = 4.0 mm)

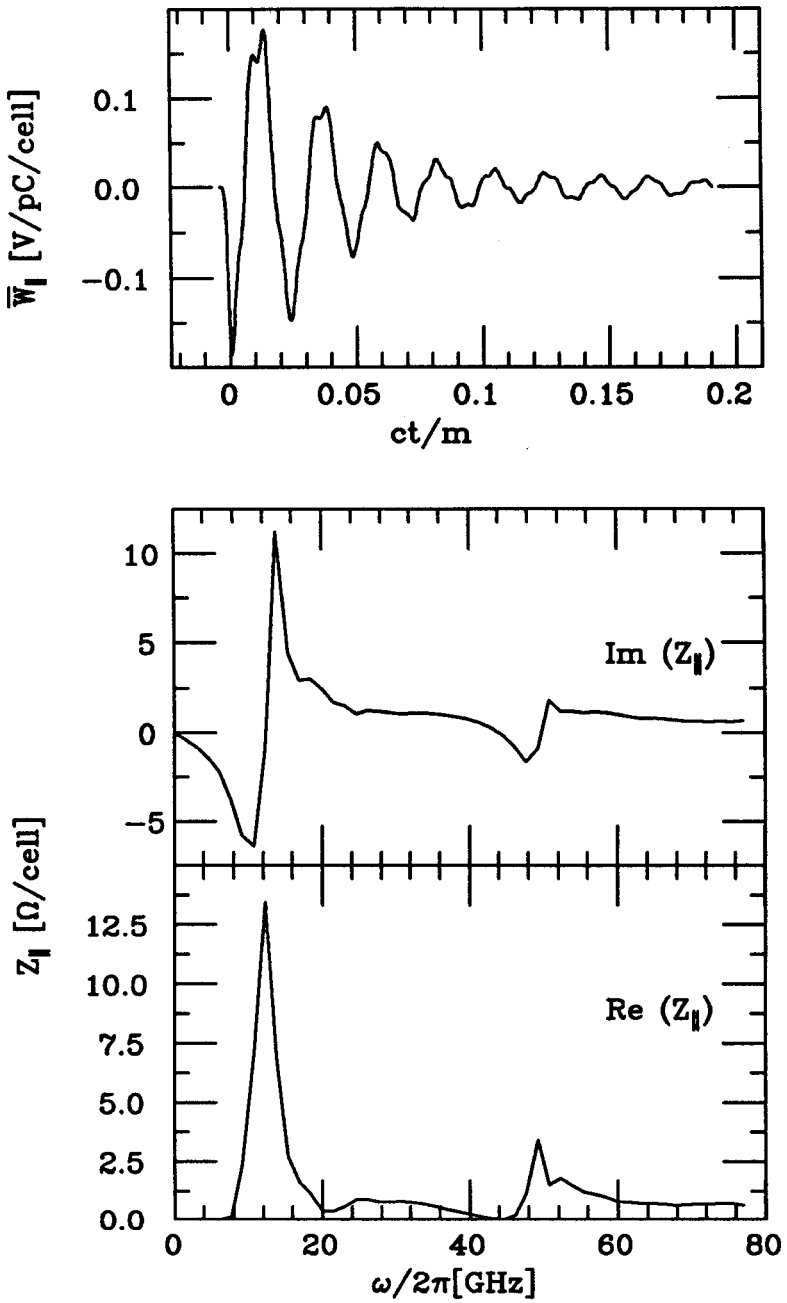

Fig. 6. Simple Bellows Longitudinal Wake Field and Impedance

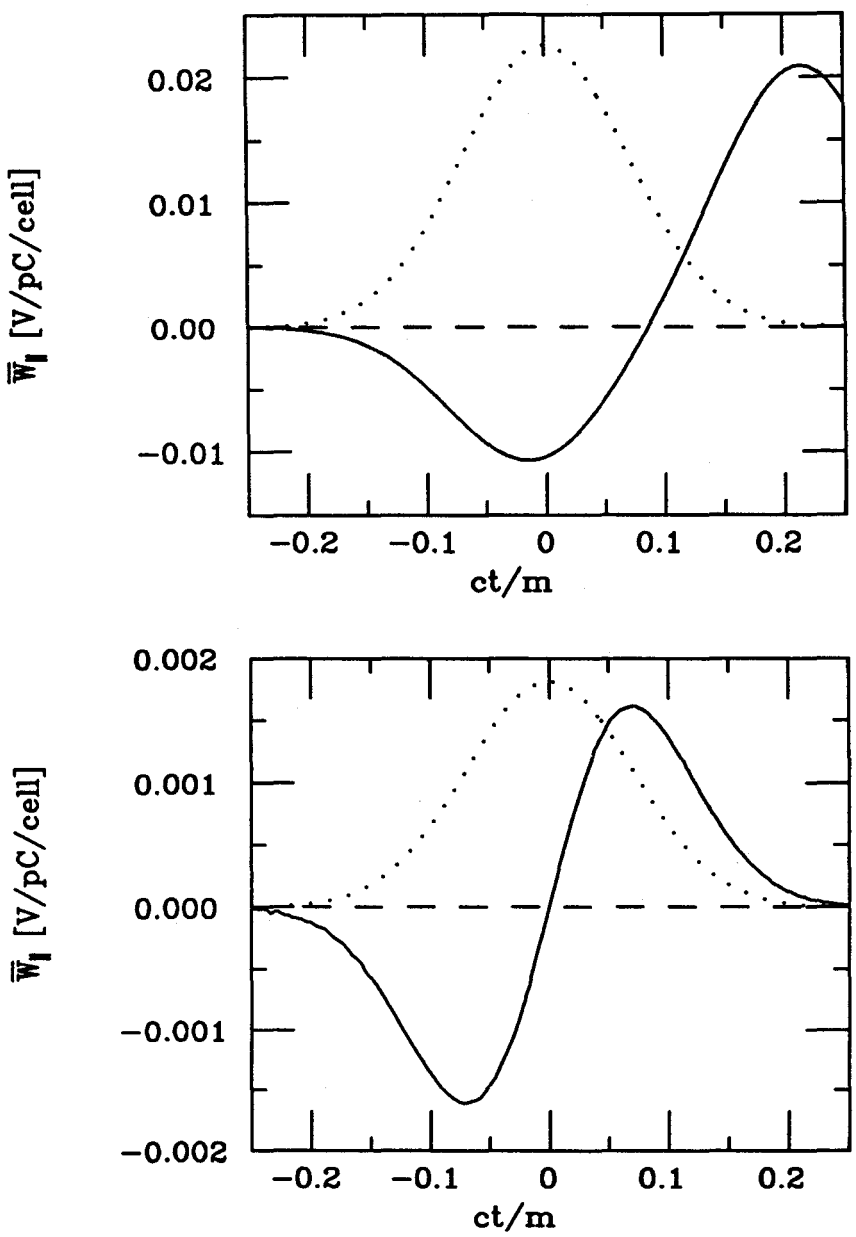

Fig. 7. Wake Field of Shielded (top) and Shielded, Shorted (bot) Bellows when $c\sigma_\tau$= 7cm. d= 4 mm. Dots Show the Bunch Shape with Head to the Left.

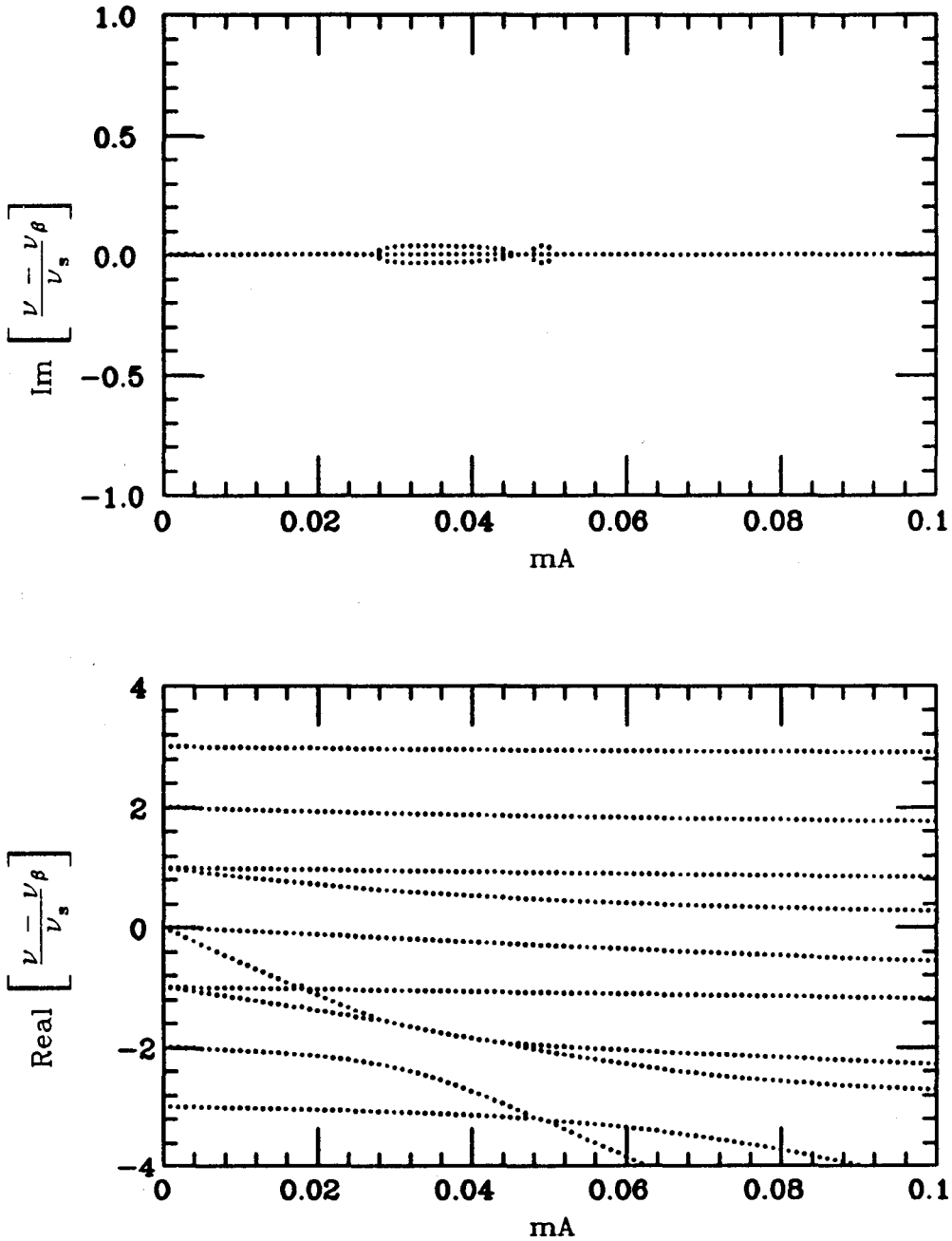

Fig. 8. Transverse Mode Coupling for the case including BPM's and simple bellows.

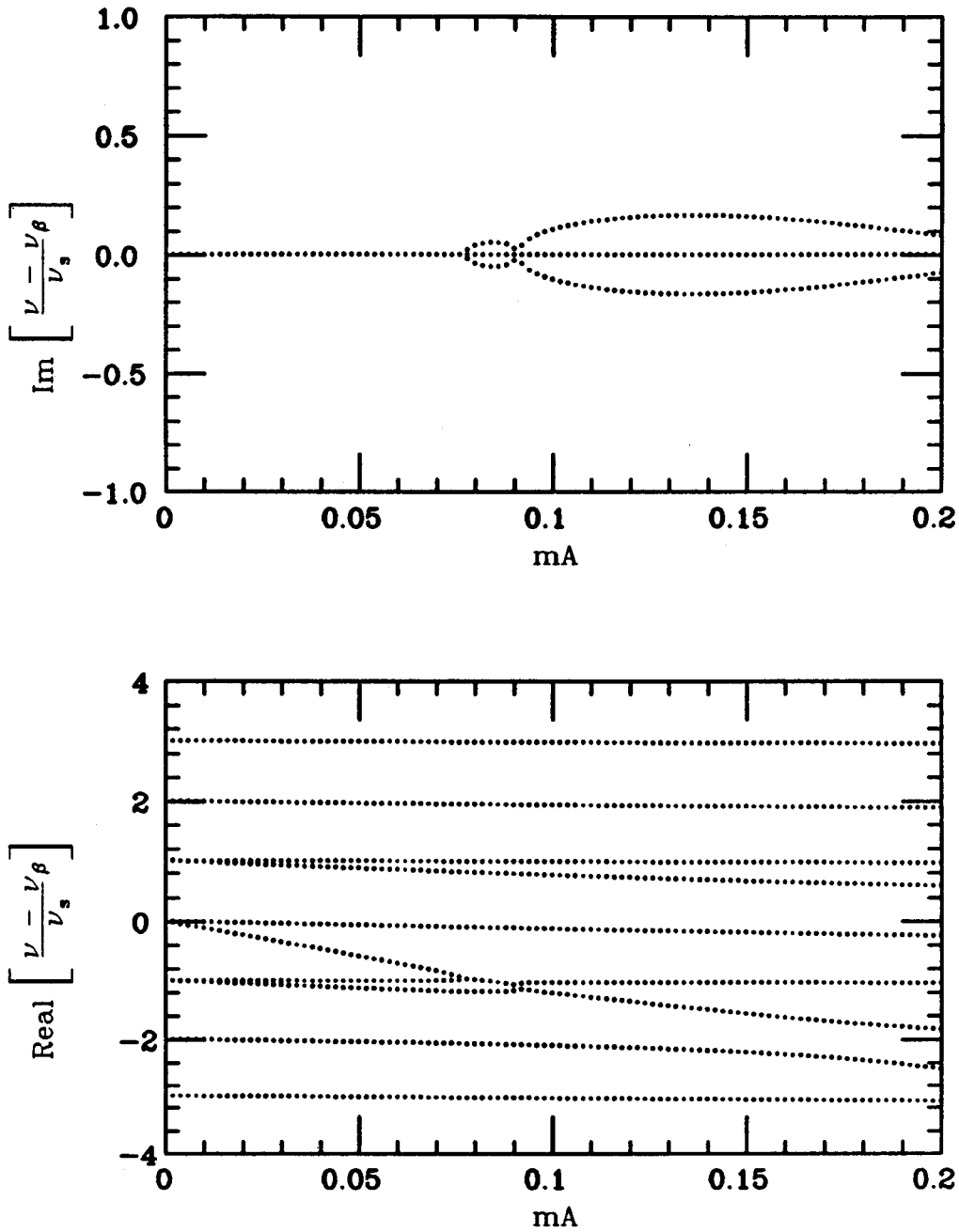

Fig. 9. Transverse Mode Coupling for the case including BPM's and shielded bellows (d = 5.5 mm).

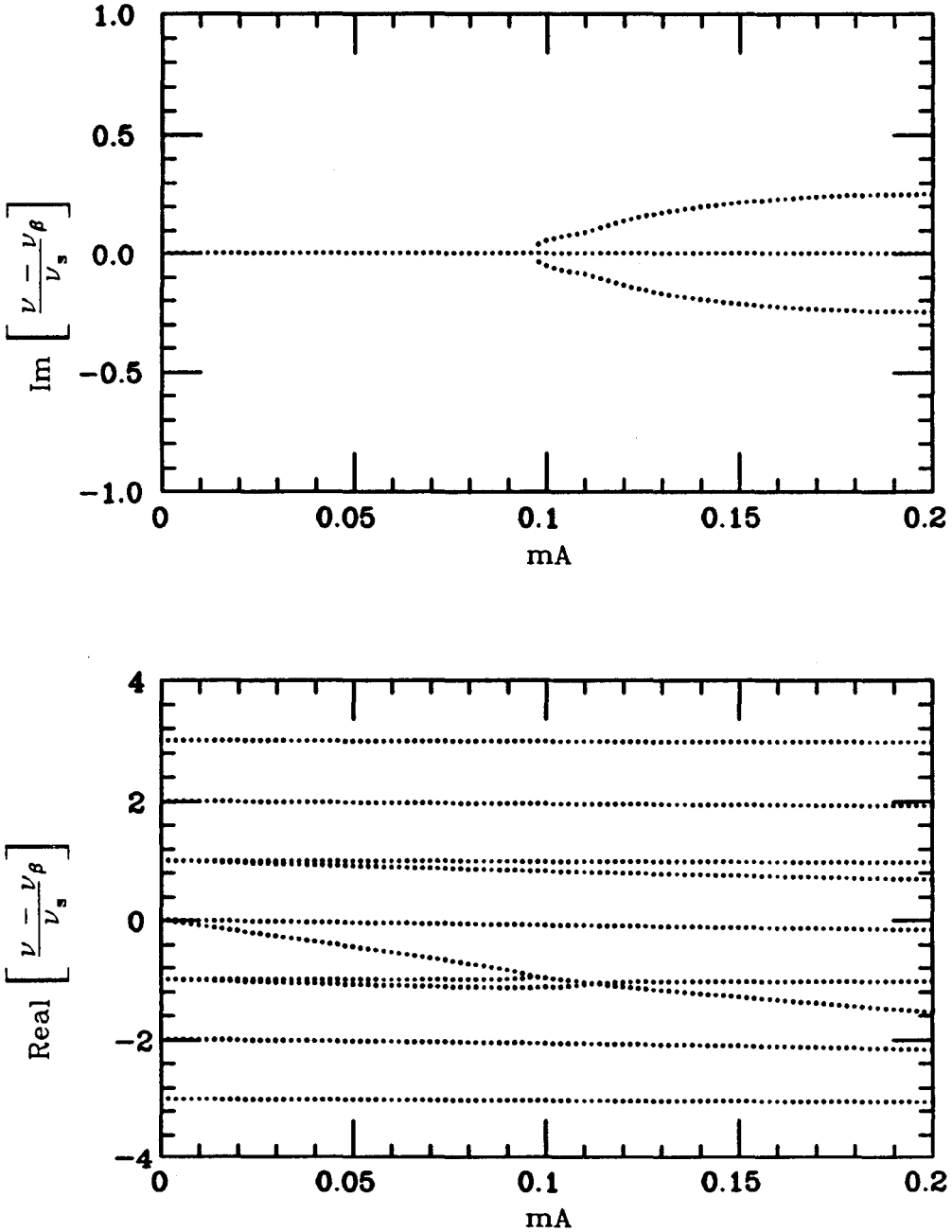

Fig. 10. Transverse Mode Coupling for the case including BPM's and shielded bellows (d = 4.0 mm).

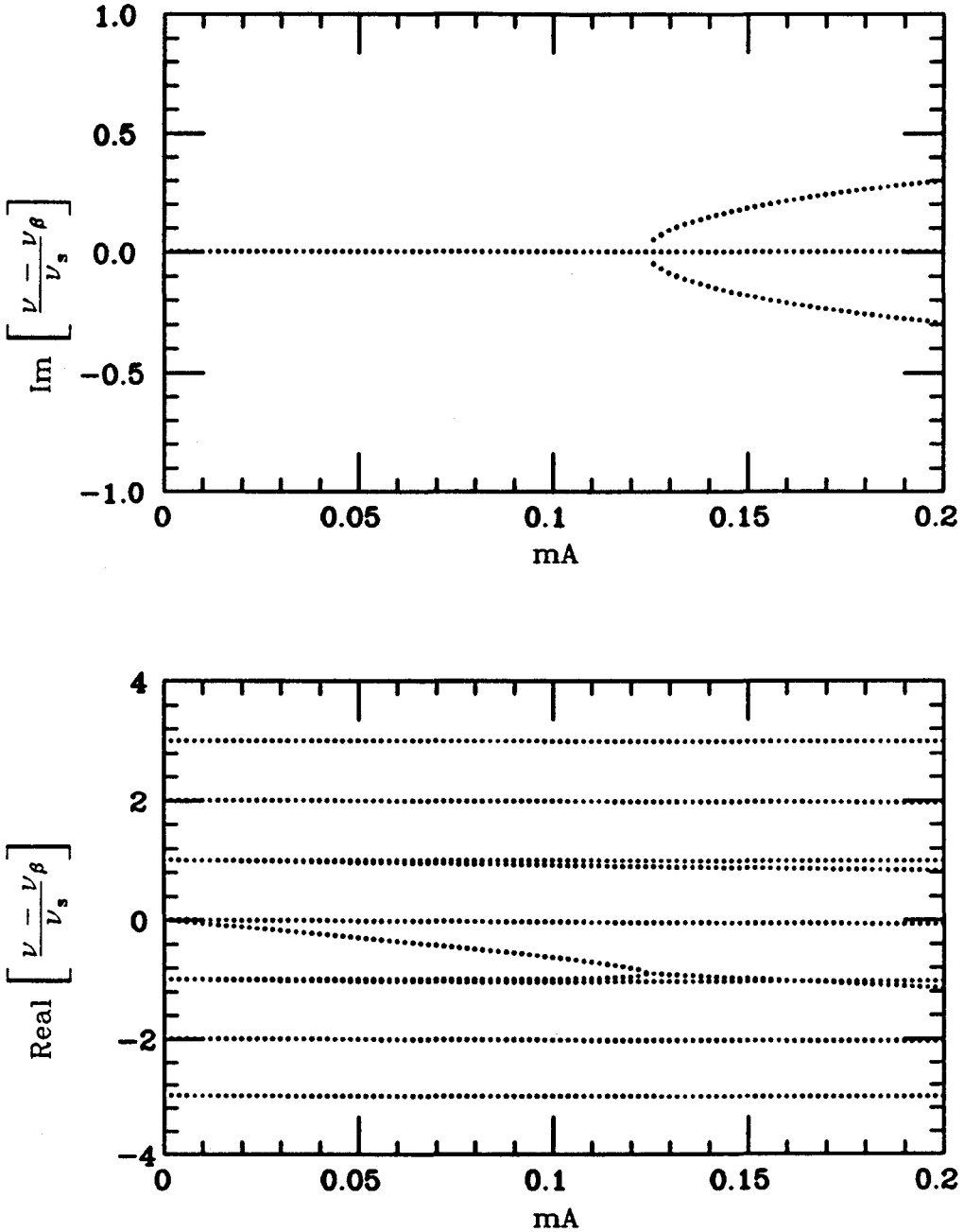

Fig. 11. Transverse Mode Coupling for the case including BPM's and shorted shielded bellows (d = 4.0 mm).

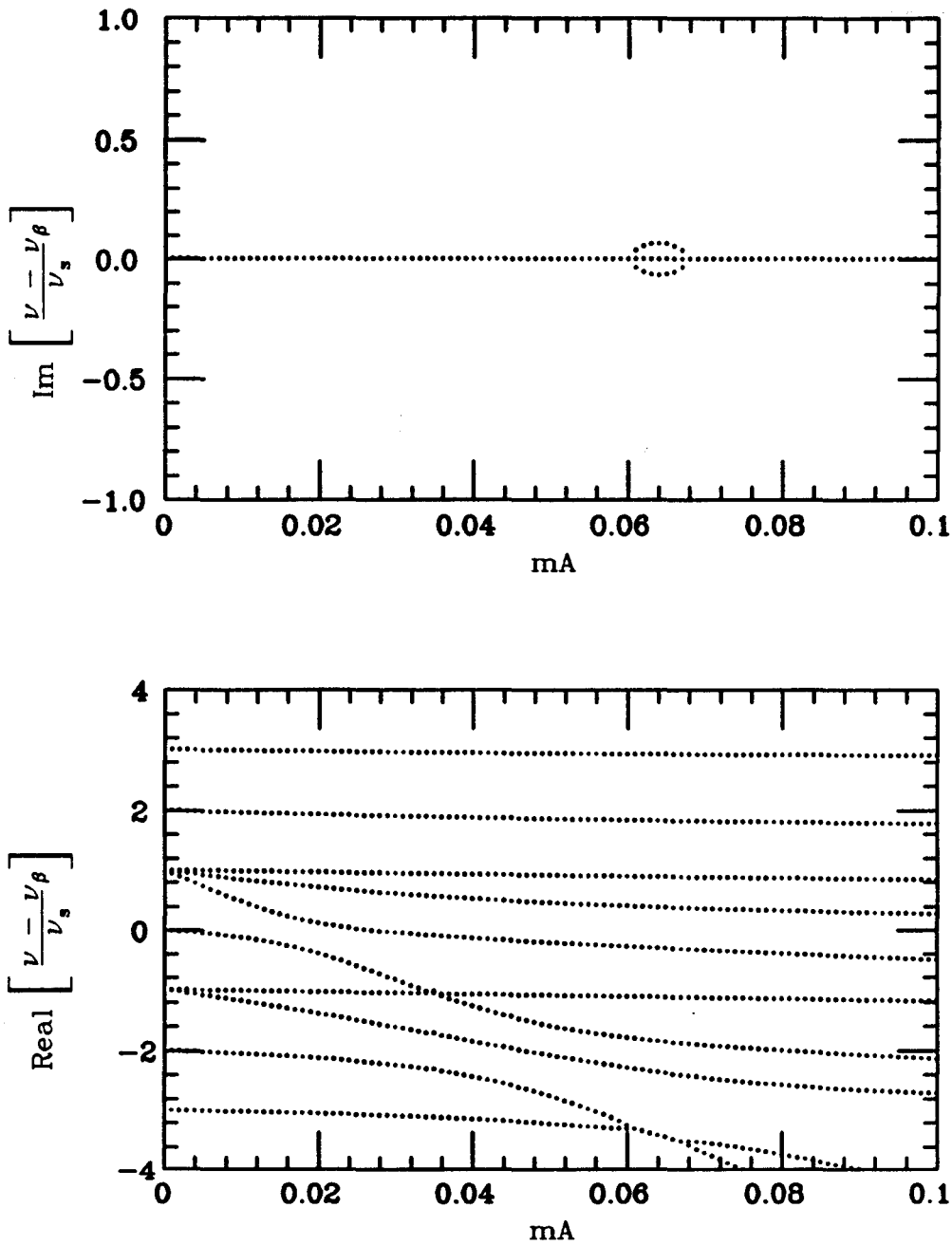

Fig. 12. Transverse Mode Coupling with Reactive Feedback ($\Delta\nu = \nu_s$) including BPM's and simple bellows.

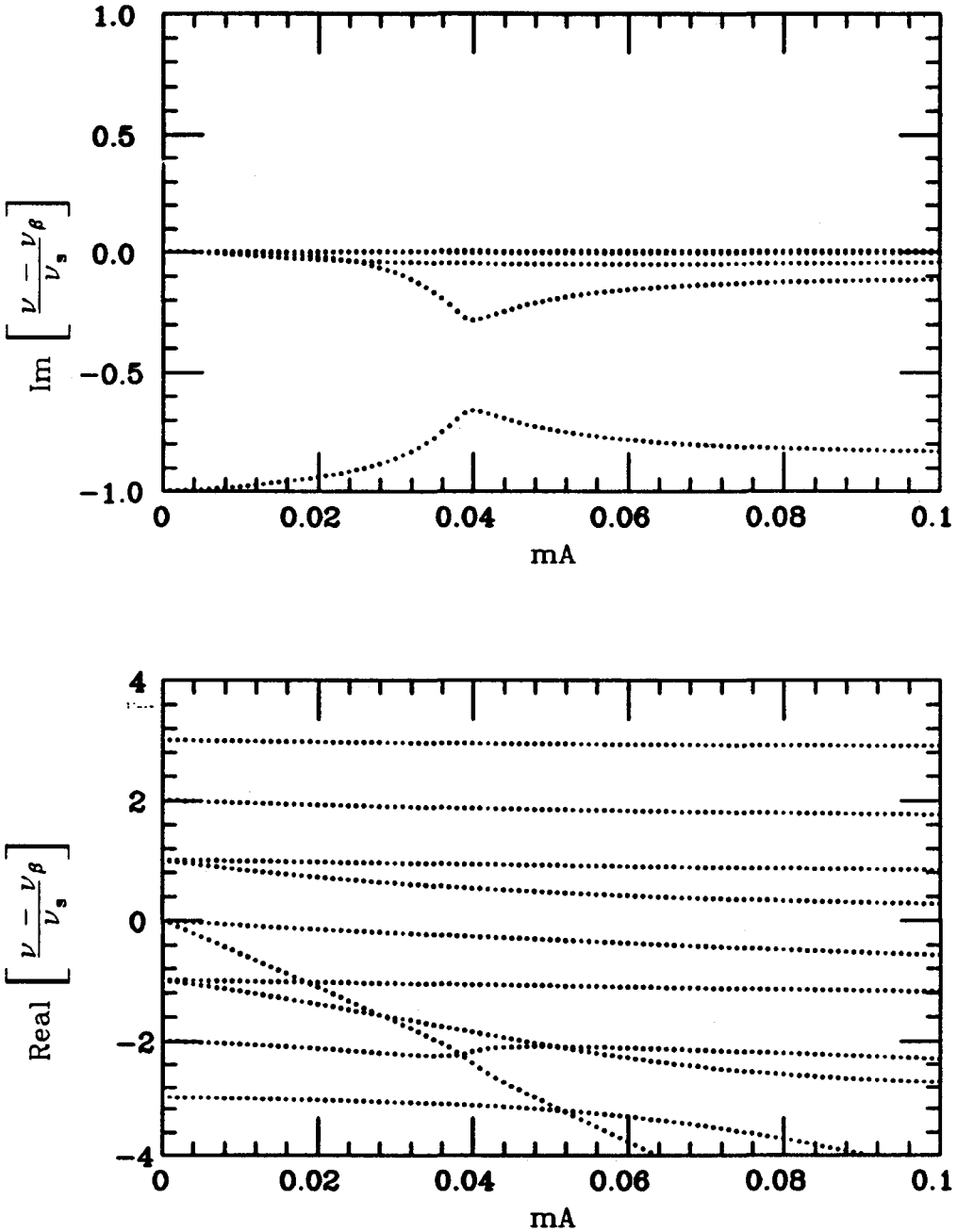

Fig. 13. Transverse Mode Coupling with Resistive Feedback ($\Delta\nu = -i\nu_s$) including BPM's and simple bellows.

AN ESTIMATE OF THE CONTRIBUTIONS OF BELLOWS TO THE IMPEDANCES AND BEAM INSTABILITIES OF THE SSC

Joseph Bisognano
SSC Central Design Group
Lawrence Berkeley Laboratory
Berkeley, CA 94720
and
King Yuen Ng
Fermi National Accelerator Laboratory*
P.O. Box 500
Batavia, IL 60510

July 1985

INTRODUCTION

Between sections of the vacuum chamber, bellows are needed to compensate for thermal expansion and transverse offsets. For beampipe made of stainless steel with a coefficient of linear expansion $19 \times 10^{-6}/^{\circ}C$ and a temperature variation of $\sim 316^{\circ}C$, the allowance for bellows is ~1.2% of the total length of the beampipe, if we assume that the bellows are 50% compressible[1]. This implies 1.08 km of bellows for Design A of the SSC which has a circumference of 90 km, Such a length of bellows will certainly contribute

*Operated by the Universities Research Association, Inc., under contract with the U.S. Department of Energy.

to the longitudinal and transverse impedances of the accelerator and will therefore affect the stability of the beam. In the Reference Designs[2], the actual impedances of the bellows have not been calculated; only an allowance of $Z_{||}/n = 0.05\ \Omega$ and $Z_{\perp} = 7\ M\Omega/m$ is made for miscellaneous discontinuities because all the bellows and pumping ports are assumed totally shielded. It is the purpose of this article to examine the actual contributions by the bellows to the longitudinal and transverse impedances assuming that they are not shielded.

COMPUTATIONS

For the ease of computation, we assume the corrugations of the bellows be rectangular with period $2g = 3$ mm, depth $\tau = 4.875$ mm as shown in Figure 1; the beampipe radius is taken to be $b = 1.5$ cm.

The code TCBI[3] solves directly Maxwell's equations in the time domain and calculate the wake potential $\hat{W}(t)$ of a Gaussian bunch with RMS length σ_ℓ and one unit of charge,

$$\hat{W}(t) = \int d\tau\, q(\tau) W(t-\tau), \tag{1}$$

where W is the wake potential due to a point charge and $q(\tau)$ the charge distribution of the bunch which, in reality, is a truncated Gaussian (in our computation we truncated it at $\pm 5\sigma_\ell$). A Fourier transformation of Eq. (1) gives us $\hat{Z}(\omega)$

the effective impedance seen by the bunch, which is related to the actual impedance seen by a point charge $Z(\omega)$ by

$$\hat{Z}(\omega) = Z(\omega)\, e^{-\frac{1}{2}(\omega\sigma_\ell/c)^2}. \tag{2}$$

In doing the Fourier transform, care must be taken to set the time coordinate correctly so that $\hat{W}(0)$ represents the wake at the center of the bunch. In our computation, we truncated the wake $\hat{W}(t)$ at 60 cm so that the impedance could have a resolution of 0.25 GHz. As will be seen in our resulting plots, ripples of period 0.5 GHz are seen in the curves.

A small bunch length should be used so that the actual impedance at high frequencies will not be smeared away according to Eq. (2). We took σ_ℓ = 1.5 mm so that the impedance would be attenuated to 80% at 21 GHz, 50% at 37.5 GHz and 5% at 78 GHz. The mesh was taken to be 0.375 mm so that there would be four inside each corrugation. Further reduction of σ_ℓ is not possible unless the mesh size is reduced also. We had tried to reduce the mesh size by half; not many changes in the results were observed but the computing time was increased by several times.

We ran TBCI for a bellow of 5 corrugations as shown in Figure 1 for the longitudinal mode m = 0 and the transverse mode m = 1. The results are shown in Figures 2 to 7.

IMPEDANCES AT LOW FREQUENCIES

When the frequency f approaches zero, from Figures 4 and 7, the longitudinal and transverse impedances for one corrugation are respectively

$$Z_{\parallel} = j0.53 \times 10^{-9} f \ \Omega, \tag{3}$$

$$Z_{\perp} = j0.19 \ k\Omega/m . \tag{4}$$

Here, we assume that the impedance of N corrugations is equal to N times the impedance of one corrugation. The above values can be checked by two existing formulas at low harmonics $n \ll 2R/g$ or R/d where R is the radius of the accelerator ring and $d = b+\tau$ is the bigger radius of the bellows. The longitudinal[4] and transverse[5] impedances are

$$Z_{\parallel} = j\left(\frac{Z_0 g}{c} \ln S\right) f \ , \tag{5}$$

$$Z_{\perp} = j Z_0 \left(\frac{g}{\pi b^2}\right)\left(\frac{S^2-1}{S^2+1}\right), \tag{6}$$

with $S = d/b$ and f the frequency in Hz. These give $Z_{\parallel} = j0.53\text{x}10^{-9}$ f Ω and $Z_{\perp} = j219$ Ω/m. Equation (5) is valid when $g/b \ll \pi$ which is certainly satisfied. Equation (6) is valid when $g/b \ll \pi^2/32$ and is not so well satisfied. A more accurate numerical calculation[5] shows that $Z_{\perp} = j198$ Ω/m. As a whole, our computation reproduces the correct results.

RESONANCES

The real part of the longitudinal impedance in Figure 3 and the real part of the transverse impedance in Figure 6 are similar in shape. They have a big resonance near 13 GHz. For the longitudinal mode the lowest resonance is at 7.62 GHz which is below the cutoff frequency of the beampipe $f_{cutoff} = 2.405c/2\pi b = 7.655$ GHz. The loss factor $k = R_s\omega_r/4Q$ can be calculated. Here R_s is the shunt impedance, ω_r is the resonance circular frequency, and Q the quality factor. We find $k_1 = 1.1\text{x}10^9$ volt/coulomb for each corrugation, which is negligible compared with the size of the wake potential. Therefore, this fundamental resonance is not seen in the impedance plot. For a resonance below cutoff, the loss factor is directly proportional to the pillbox width g, which explains why k_1 is so small. The broad resonance near 13 GHz is above cutoff so its loss factor is not governed by the same formula. For the dipole mode, the cutoff frequency is 12.20 GHz and the bellow corrugations have no resonance below this frequency.

There is another smaller resonance near 38 GHz both for the longitudinal mode and the transverse mode. However, because the RMS bunch length of Design A is 7 cm, this resonance will not have any influence on the stability of the beam.

BEAM INSTABILITIES

For a RMS bunch length of σ_ℓ = 7 cm, the bunch bandwidth is ~1 GHz. Thus the impedances of the bellows are of broad band and will therefore drive the single-bunch instabilities. In the Reference Designs[2], the most severe limitation on beam current is set by the transverse mode-coupling instability which arises when the real frequency shift of any mode becomes equal to the synchrotron frequency. Assuming that the largest shift is due to mode $\mu = 0$, the limit on $Z_\perp$ is[2]

$$\bar{Z}_\perp \leqslant \frac{4\sqrt{\pi}\,\eta\,(E/e)(\sigma_E/E)}{I\bar{\beta}}, \tag{7}$$

where

$$\bar{Z}_\perp = \frac{\sigma_\ell}{c\sqrt{\pi}} \int_{-\infty}^{\infty} \mathcal{I}m\, Z_L(\omega)\, e^{-(\omega\sigma_\ell/c)^2} d\omega \tag{8}$$

for a Gaussian bunch. In above, $\eta = 1.3\times10^{-4}$ is the frequency-slip factor, $\sigma_E/E = 1.5\times10^{-4}$ the RMS energy spread at injection energy E = 1 TeV, $\bar{\beta}$ = 150 m the average betatron function and I = 7.7 μA the average single-bunch current. We get for the threshold $Z_\perp$ =120 MΩ/m. For 10.8 km of bellows with a period of 3 mm, there are in total 360,000 corrugations. Using Figure 7, if the integration of Eq. (8) is performed, we get $Z_\perp$ = 68 MΩ/m. If a 100% safety factor is included, the bellow contribution alone will be

higher than the threshold. We note that for the whole machine, the estimate[2] of $Z_{|}$ is only 47 MΩ/m.

The next dangerous instability is the transverse microwave which has a risetime fast compared with a synchrotron period and is driven by disturbances of wavelengths much shorter than the bunch length. The impedance limit[6] for a broad band at f ~13 GHz is

$$|Z_{\perp}| \leq \frac{4\eta(E/e)(\sigma_E/E)(\sigma_\ell/R)(2\pi Rf/c)}{I\bar{\beta}} = 1287\ M\Omega/m. \qquad (9)$$

This limit will be very much lower if the traditional cutoff frequency is used for f instead. Figures 6 and 7, $|Z_{\perp}|$ has a maximum of 3.8 kΩ/m for 5 corrugations or 274 MΩ for 360,000 corrugations which is dangerously to high.

As for longitudinal microwave instability[7], the limit on $Z_{||}/n$ is

$$|Z_{\parallel}/n| \leq \frac{\sqrt{2\pi}\,\eta(E/e)(\sigma_\ell/R)(\sigma_E/E)^2}{I} = 4.7\Omega. \qquad (10)$$

From Figures 3 and 4, we get, at ~13 GHz, $|Z_{||}/n| = 2.3\ \Omega$ for all the corrugations which is rather too high.

The longitudinal mode-coupling instability occurs when two modes collide as the real frequencies shift. For a short bunch the lowest mode $\mu = 1$ is shifted most, the stability limit for $Z_{||}/n$ is given by[7]

$$\mathrm{Im}\, Z_{\parallel}/n \leq \frac{8\sqrt{\pi}\,\eta(E/e)(\sigma_E/E)^2(\sigma_\ell/R)}{I} = 27\Omega. \qquad (11)$$

The bellow contribution from Figure 4 is 0.64 Ω which is very much lower than the above limit.

DISCUSSIONS

1. We learn from above that the bellow contributions to the impedances will upset the single-bunch stabilities, among which the dangerous ones are the transverse mode-coupling, transverse microwave, and longitudinal microwave instabilities. Therefore, the corrugations must be shielded in some way to preserve beam stability.

2. In our analysis, we make the assumption that the impedance of N corrugations is N times the impedance of one corrugation. Strictly speaking, this is true only when the wavelength is much shorter than the period of the corrugations. We had run TBCI for 1 corrugation, 3 corrugations, 5 corrugations and 9 corrugations and found that the impedance per corrugation decreased slightly with the number of corrugations. For example, near zero frequency, the imaginary parts of the transverse impedance per corrugation are respectively 0.198, 0.190, 0.186 and 0.185 kΩ/m when 1, 3, 5 and 9 corrugations are considered. For this reason, we believe that our estimates for 360,000 corrugations might have been slightly too high but nevertheless of the correct order of magnitude.

REFERENCES

1. L. Vos, CERN-SPS/84-10 (DI-MST)
2. Report of the Reference Designs Study Group on the Superconducting Super Collider, May 8, 1984
3. T. Weiland, DESY 82-015, 1982
4. E. Keil and B. Zotter, Particle Accelerators 3, 11 (1972)
5. K.Y. Ng, Fermilab Report FN-389
6. R.D. Ruth, Proceedings of the Workshop on Accelerator Physics Issues for a Superconducting Super Collider, Ann Arbor, MI, 1983, p. 151
7. S. Krinsky and J.M. Wang, BNL-33867

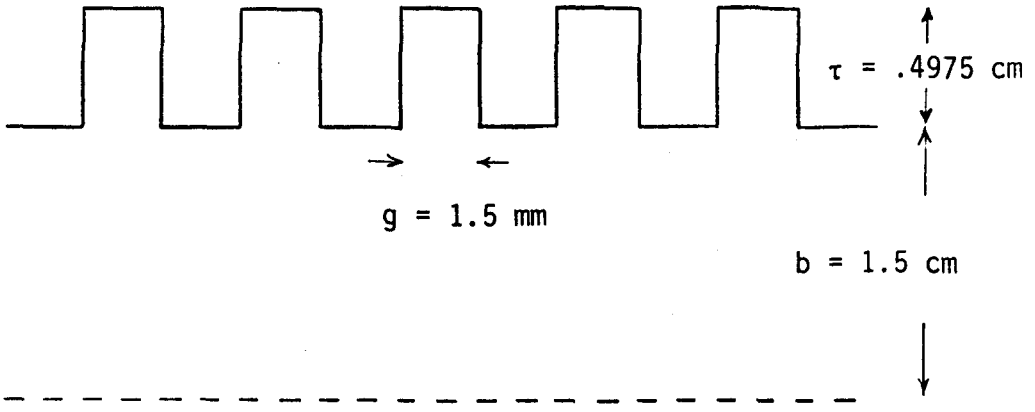

Figure 1. Five corrugations of a bellow

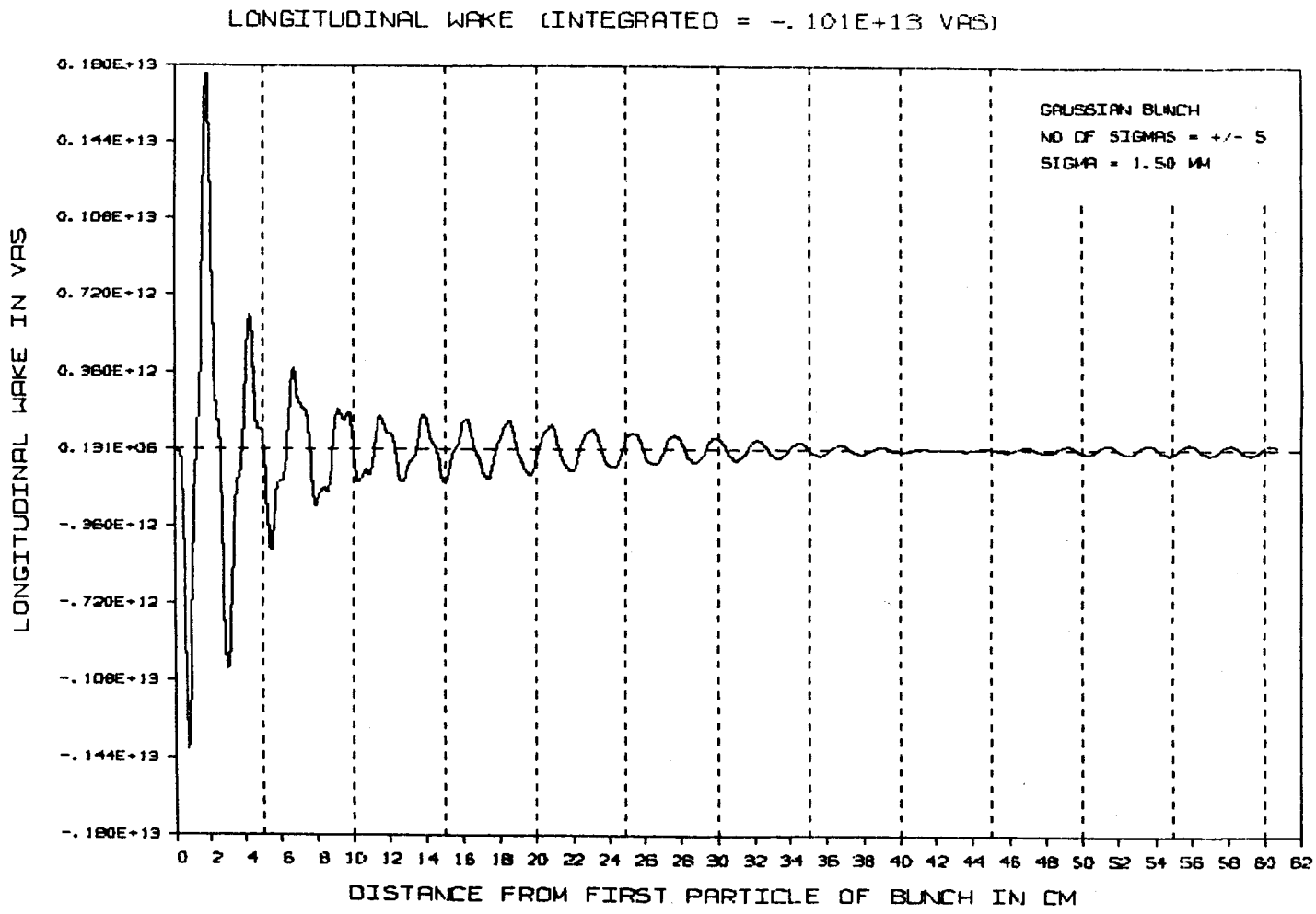
LONGITUDINAL WAKE (INTEGRATED = -.101E+13 VAS)
GAUSSIAN BUNCH
NO OF SIGMAS = +/- 5
SIGMA = 1.50 MM
LONGITUDINAL WAKE IN VAS
0.180E+13
0.144E+13
0.108E+13
0.720E+12
0.360E+12
0.131E+06
-.360E+12
-.720E+12
-.108E+13
-.144E+13
-.180E+13
0 2 4 6 8 10 12 14 16 18 20 22 24 26 28 30 32 34 36 38 40 42 44 46 48 50 52 54 56 58 60 62
DISTANCE FROM FIRST PARTICLE OF BUNCH IN CM

Fig. 2

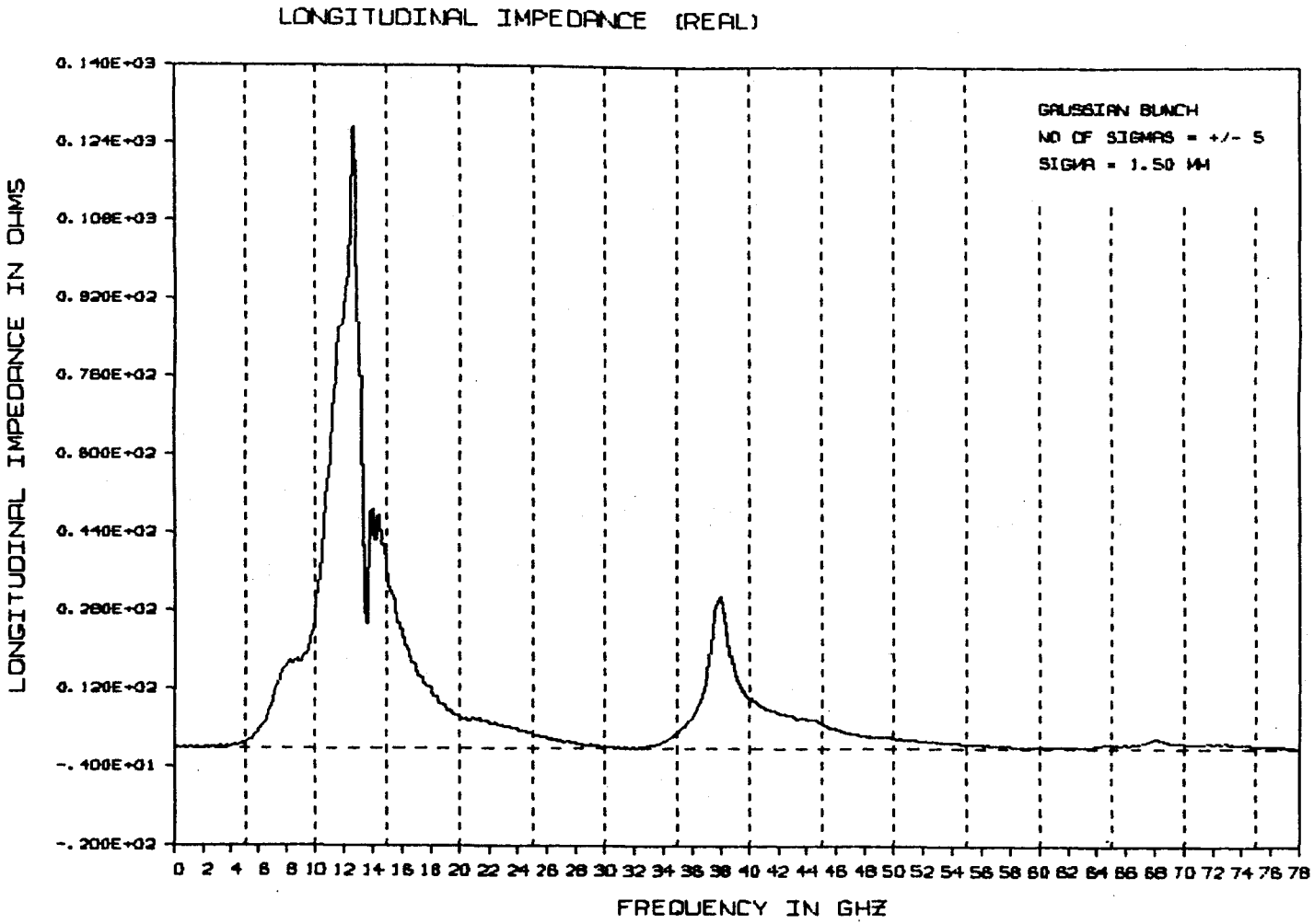
LONGITUDINAL IMPEDANCE (REAL)
GAUSSIAN BUNCH
NO OF SIGMAS = +/- 5
SIGMA = 1.50 MM
LONGITUDINAL IMPEDANCE IN OHMS
0.140E+03
0.124E+03
0.108E+03
0.920E+02
0.760E+02
0.600E+02
0.440E+02
0.280E+02
0.120E+02
-.400E+01
-.200E+02
0 2 4 6 8 10 12 14 16 18 20 22 24 26 28 30 32 34 36 38 40 42 44 46 48 50 52 54 56 58 60 62 64 66 68 70 72 74 76 78
FREQUENCY IN GHZ

Fig. 3

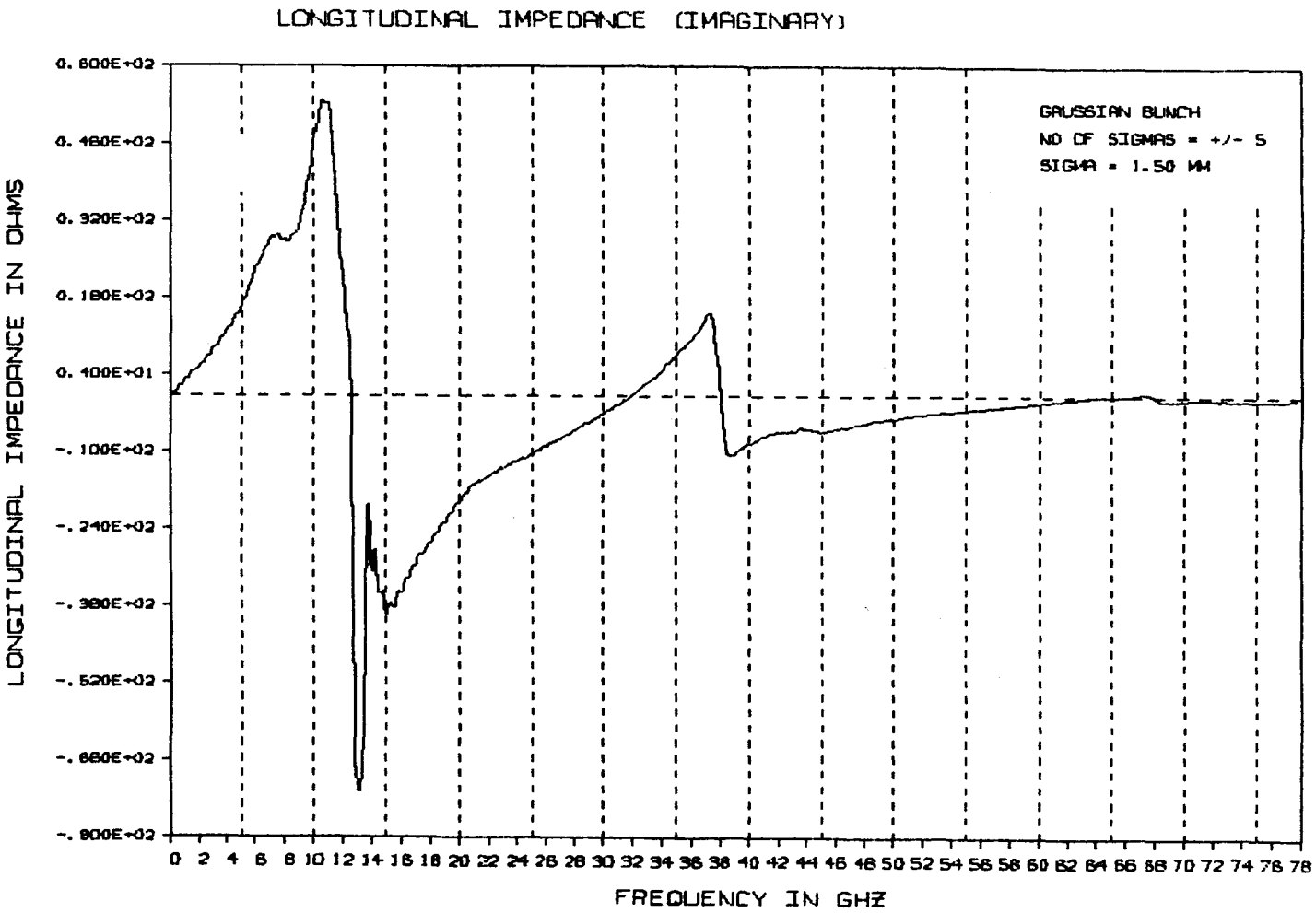
LONGITUDINAL IMPEDANCE (IMAGINARY)
GAUSSIAN BUNCH
NO OF SIGMAS = +/- 5
SIGMA = 1.50 MM
LONGITUDINAL IMPEDANCE IN OHMS
0.800E+02
0.480E+02
0.320E+02
0.160E+02
0.400E+01
-.100E+02
-.240E+02
-.380E+02
-.520E+02
-.660E+02
-.800E+02
0 2 4 6 8 10 12 14 16 18 20 22 24 26 28 30 32 34 36 38 40 42 44 46 48 50 52 54 56 58 60 62 64 66 68 70 72 74 76 78
FREQUENCY IN GHZ

Fig. 4

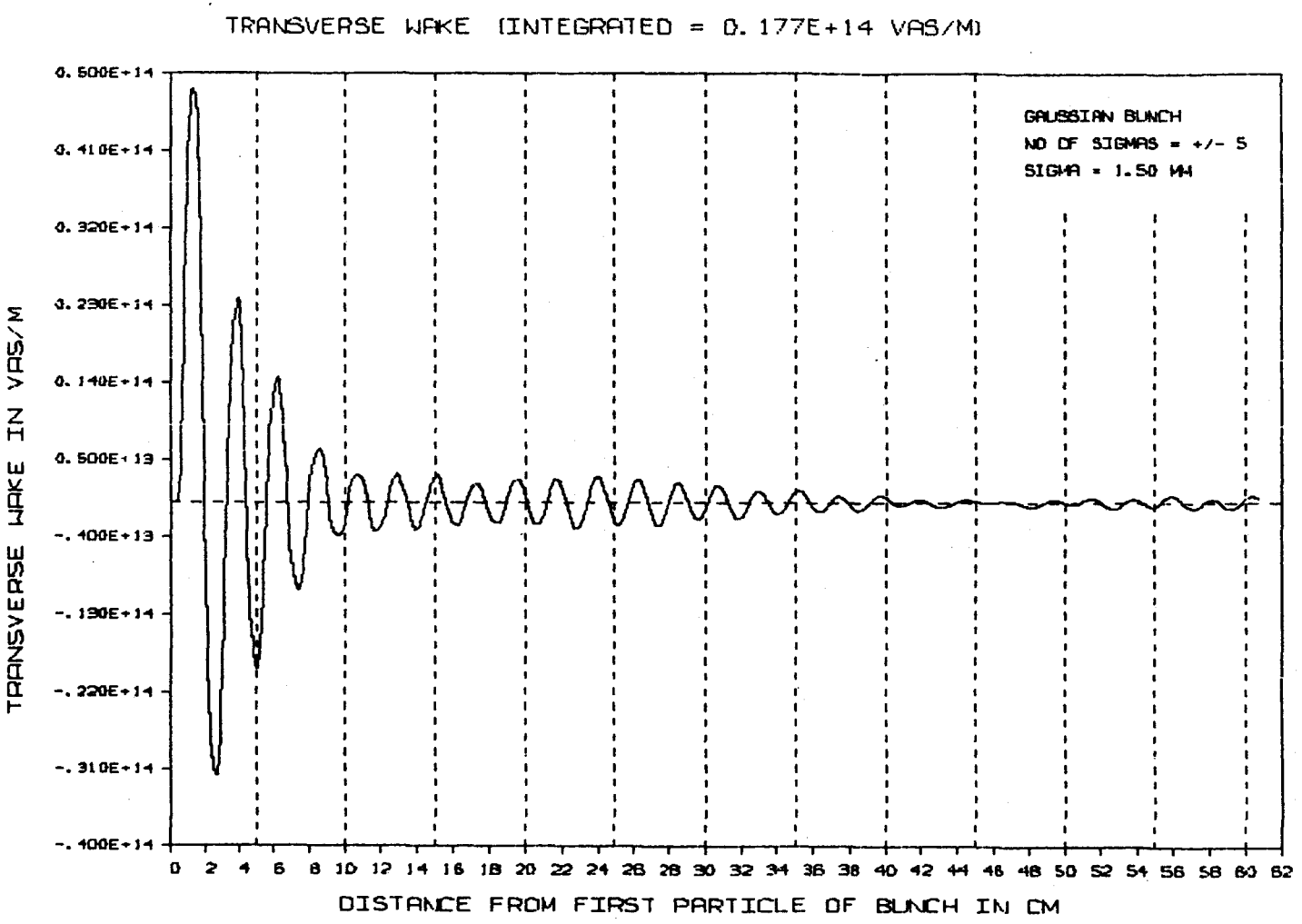
TRANSVERSE WAKE (INTEGRATED = 0.177E+14 VAS/M)
GAUSSIAN BUNCH
NO OF SIGMAS = +/- 5
SIGMA = 1.50 MM
TRANSVERSE WAKE IN VAS/M
0.500E+14
0.410E+14
0.320E+14
0.230E+14
0.140E+14
0.500E+13
-.400E+13
-.130E+14
-.220E+14
-.310E+14
-.400E+14
0 2 4 6 8 10 12 14 16 18 20 22 24 26 28 30 32 34 36 38 40 42 44 46 48 50 52 54 56 58 60 62
DISTANCE FROM FIRST PARTICLE OF BUNCH IN CM

Fig. 5

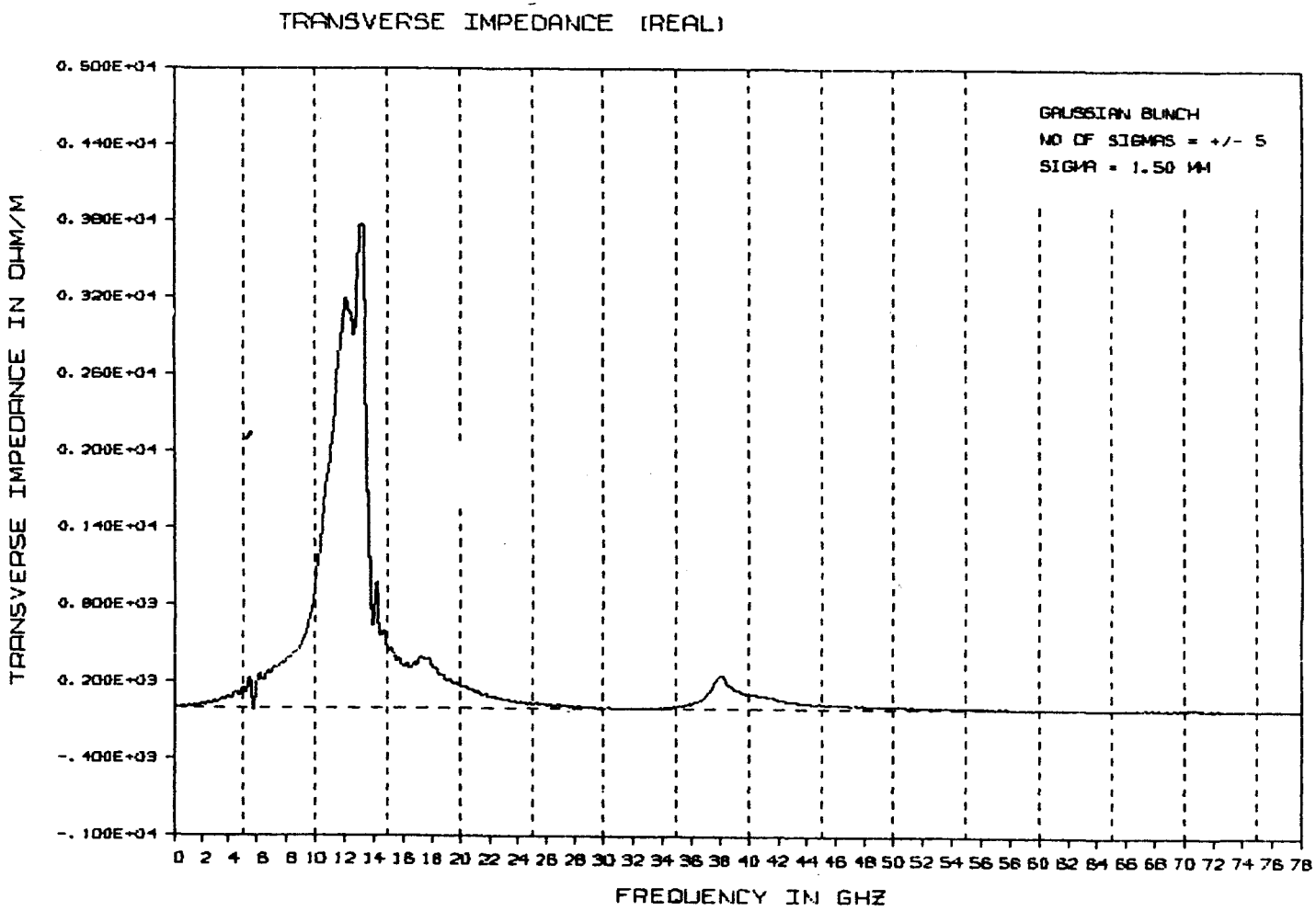
TRANSVERSE IMPEDANCE (REAL)
GAUSSIAN BUNCH
NO OF SIGMAS = +/- 5
SIGMA = 1.50 MM
TRANSVERSE IMPEDANCE IN OHM/M
0.500E+04
0.440E+04
0.380E+04
0.320E+04
0.260E+04
0.200E+04
0.140E+04
0.800E+03
0.200E+03
-.400E+03
-.100E+04
0 2 4 6 8 10 12 14 16 18 20 22 24 26 28 30 32 34 36 38 40 42 44 46 48 50 52 54 56 58 60 62 64 66 68 70 72 74 76 78
FREQUENCY IN GHZ

Fig. 6

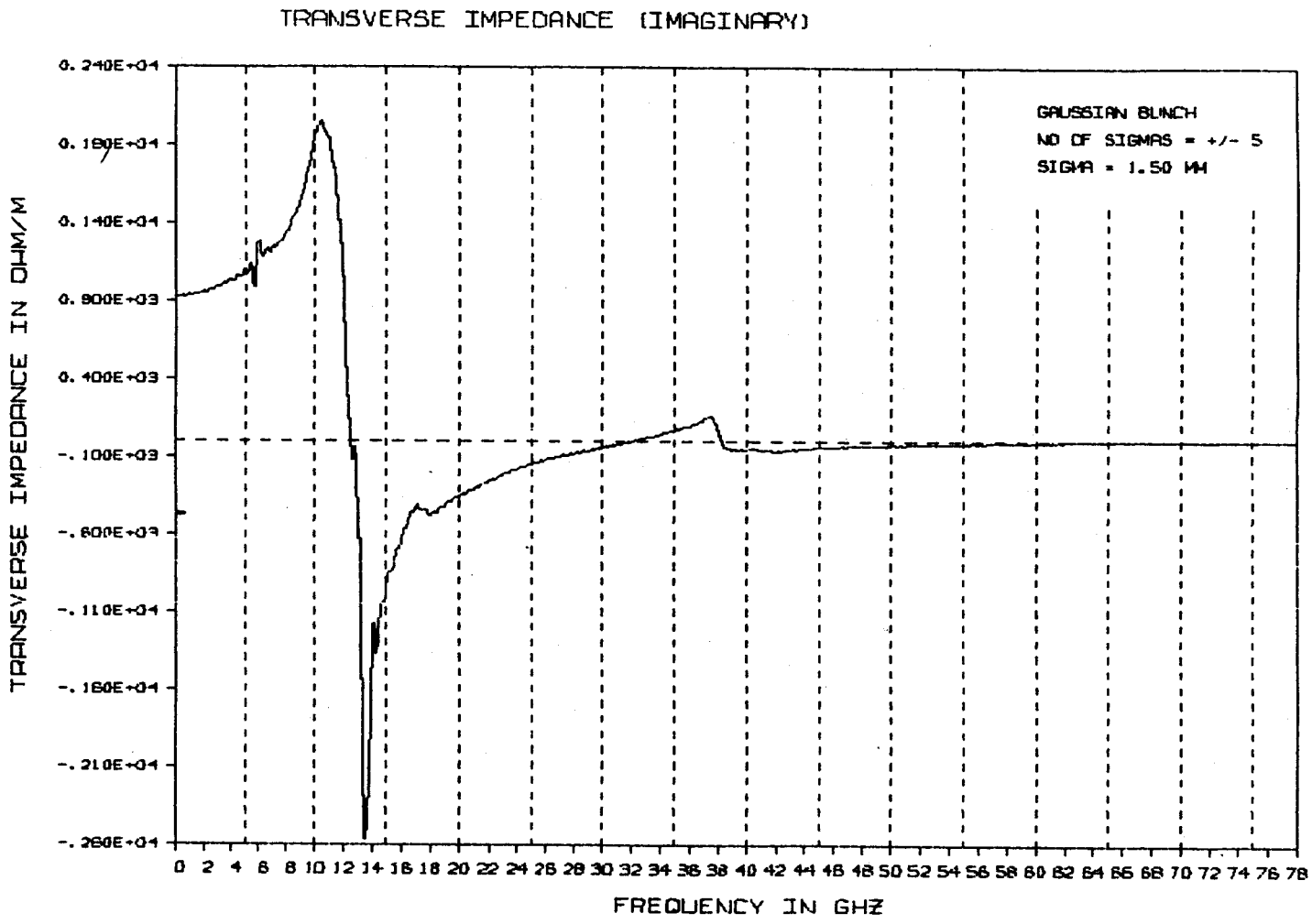
TRANSVERSE IMPEDANCE (IMAGINARY)
GAUSSIAN BUNCH
NO OF SIGMAS = +/- 5
SIGMA = 1.50 MM
TRANSVERSE IMPEDANCE IN OHM/M
0.240E+04
0.180E+04
0.140E+04
0.900E+03
0.400E+03
-.100E+03
-.600E+03
-.110E+04
-.160E+04
-.210E+04
-.260E+04
0 2 4 6 8 10 12 14 16 18 20 22 24 26 28 30 32 34 36 38 40 42 44 46 48 50 52 54 56 58 60 62 64 66 68 70 72 74 76 78
FREQUENCY IN GHZ

Fig. 7

IMPEDANCES OF THE SHIELDED BELLOWS IN THE SSC AND THE EFFECTS ON BEAM STABILITY

King Yuen Ng

Fermi National Accelerator Laboratory*

P.O. Box 500

Batavia, IL 60510

July 1985

INTRODUCTION

The 1.08 km of bellows in Design A of the SSC[1] will contribute to single-bunch instabilities:[2]

1. transverse mode-coupling

   bellow contribution $\bar{Z}_\perp$ = 68 MΩ/m,

   allowance for stability $\bar{Z}_\perp$ < 120 MΩ/m,

2. transverse microwave (for broad band at 13 GHz)

   bellow contribution $|Z_\perp|$ = 274 MΩ/m,

   allowance for stability $|Z_\perp|$ < 1287 MΩ/m,

3. longitudinal microwave

   bellow contribution $|Z_{||}/n|$ = 2.3 Ω,

   allowance for stability $|Z_{||}/n|$ < 4.7 Ω.

In above, we have assumed an average single-bunch current I = 7.7 μA, RMS energy spread $\sigma_E/E = 1.5\times10^{-4}$ at injection energy of 1 TeV, RMS bunch length σ_ℓ = 7 cm, average

* Operated by the Universities Research Association, Inc., under contract with the U.S. Department of Energy.

betatron function $\bar{\beta}$ = 150 m, and frequency-slip factor η = 1.3×10^{-4}. In order to support a stable bunch beam of the designed intensity, the bellow corrugations must be shielded. This shielding also needs itself to have low enough impedances. A suggestion is to use two circular tubes each of thickness 2 mm as shown in Figure 1. The separation between the tubes is 2 mm; inside the separation, balls or fingers can be placed for contacts. There will be roughly 5000 bellows each of which contains 72 corrugations (period = 3 mm). The design is to have a bellow of length 50 cm. At room temperature, the two shielding tubes overlap completely while at superconducting temperature, they overlap for only 30 cm leaving a gap of g = 10 cm at each end. We want to study the impedances of such a configuration and the dependence on the gap length g.

COMPUTATIONS

Since the corrugations are shielded, we can approximate the configuration by forgetting all the corrugations. The code TBCI[3] is used to calculate the wake potentials of a Gaussian bunch with RMS length σ_ℓ and truncated at $\pm5\sigma$. A Fourier transformation of the wake potential will give us $\hat{Z}(\omega)$, the effective impedance seen by the bunch, which is related to the actual impedance seen by a point charge $Z(\omega)$ by

$$\hat{Z}(\omega) = Z(\omega)\, e^{-\frac{1}{2}(\omega\sigma_\ell/c)^2}. \tag{1}$$

We truncated the wake potential at 30 cm so that the impedance would have a resolution of 0.5 GHz. A bunch length of σ_ℓ = 2.5 mm was used so that the impedance Z was attenuated to 5% at ~48 GHz. The mesh was taken to be 0.5 mm so that there would be four between the two shielding tubes. We had tried to reduce the mesh size by half; not many changes in the results were observed but the computation time was increased by several times.

IMPEDANCES

In general the impedances of a shielded bellow look very different from those of an unshielded one. The longitudinal impedance in Figures 3 and 4 looks very similar in shape to the impedance of a cavity formed by closing the gap between the two shielding tubes. But the effect of the gap does show up in Figure 3 by contributing 6.67 Ω (instead of zero) at low frequencies and a broad resonance near 48 GHz. This 6.67 Ω can be understood by the fact that electromagnetic energy is leaking through this gap. In fact this gap can be viewed as a coaxial transmission line of infinite length and inner and outer radii 1.7 and 1.9 cm, connected in parallel to the beampipe. Thus the impedance is just $Z_c = (Z_o/2\pi)\ln(1.9/1.7) = 6.67\ \Omega$, the characteristic impedance of the transmission line.

At low frequencies, the cavity of length g = 10 cm and radius d formed by closing the gap between the shielding tubes can also be considered as a transmission line connected in series with the beampipe which is of radius b. The impedance[4] at frequency f is

$$Z_{\parallel}/f = j\,\frac{Z_0 g_e}{c}\,\ln\frac{d}{b}\,, \tag{2}$$

where the effective attenuated cavity length g_e is related to the true length g by

$$g_e/g = (1 - e^{-\gamma g})(\gamma g)^{-1}\,, \tag{3}$$

with the attenuation constant $\gamma = 2.405/d$. With b = 1.5 cm and d = 1.9 cm, we get $Z_{||} = 2.35\times10^{-9} f\Omega$ in agreement with the initial slope in Figure 3. This cavity gives a resonance at 6.2 GHz, which is also seen in the plot. We want to point out that what we have described so far are independent of the length g since g>>b and the overlap length of the shielding tubes is also >>b. At higher frequencies, the plots exhibit a broad band from 12 to 25 GHz which is the characteristic of the closed cavity described above.

For the transverse impedance, the first resonance comes at 2.8 GHz. This is the so called "ring mode" (a TM mode) if we consider the gap between the two shielding tubes as a

coaxial transmission line, which starts transmitting in the dipole mode when the azimuthal wave length is equal to the circumference of the line. The imaginary part of the transverse impedance starts from ~1.35 kΩ/m which is due to the inductive property of the cavity formed by closing the gap between the two shielding tubes. Again, these low-frequency impedances are not dependent on the length of the "closed" cavity g or the length of the overlap of the shieldings. We have performed computations with g = 5 cm, 10 cm, 15 cm, 20 cm and found no appreciable changes in the impedances at low frequencies. At higher frequencies, some more resonances are seen.

STABILITIES

The effective transverse impedance $\bar{Z}_\perp$ that contributes to the transverse mode-coupling instability is given by

$$\bar{Z}_\perp = \frac{\sigma_\ell}{c\sqrt{\pi}} \int_{-\infty}^{\infty} \mathrm{Im}\, Z_\perp(\omega)\, e^{-(\omega\sigma_\ell/c)^2} d\omega . \qquad (4)$$

For a RMS bunch length σ_ℓ = 7 cm, our computation yields for 5000 bellows $\bar{Z}_\perp$ ~ 5000x1.35 = 6.75 MΩ/m which is 10 times smaller than the unshielded bellows and will not lead not mode-coupling instability.

For the transverse microwave, we have from our results $|Z_\perp|$ = 5000x2.4 = 12 MΩ/m at ~3 GHz, which is 22 times smaller than the unshielded bellows.

For the longitudinal microwave, we have a broad band of $Z_{||} \approx 35\ \Omega$ at $f \approx 15$ GHz. For 5000 bellows this yields $Z_{||}/n \approx 0.039\ \Omega$ which is about 60 times smaller than the unshielded bellows.

For the longitudinal mode-coupling, the total bellow contribution to $\mathrm{Im}Z_{||}/n$ is $\sim 0.039\ \Omega$ which is about 16 times smaller than the unshielded bellows[2].

Since the contribution to the impedances is lowered by so much, all types of single-bunch instabilities can be avoided and the shielding scheme in Figure 1 is workable.

REMARKS

We are interested in the stability of a single bunch which has a RMS bunch length $\sigma_\ell = 7$ cm according to the Reference Designs. Thus, wake potentials calculated up to 30 cm ($>4\sigma$ including 95.5% of the bunch particles) will be long enough for our purpose. However, one may think that, since the overlap length of the shieldings is 30 cm, the reflected waves will show appreciate effects to the wakes at 60 cm. When these effects are Fourier transformed, the impedances will be very much modified from those obtained from the wakes truncated at 30 cm. With this in mind, we compute the longitudinal wake up to 110 cm. The result is shown in Figure 8, which exhibits, as expected due to the reflected waves, a big eruption around (60+5x0.5) cm, where

0.5 cm is the RMS length of the test bunch. The longitudinal impedance shown in Figures 9 and 10 is indeed different from our former one in Figures 3 and 4. Here, we see resonances at 0.0, 0.5, 1.0, 1.5,... GHz which are resonances of an open-end transmission line of length 30 cm. The transverse counterparts, on the other hand, are not much different from those shown in Figure 5 - 7.

However, although the impedance plots are different in the actual computations of the thresholds of single-bunch instabilities, for example, in formulas similar to Eq. (4), the different impedances will lead to exactly the same results. Thus, we can conclude that, by computing the wakes up to only 30 cm, although the impedances obtained through Fourier transformation may differ from the actual ones, nevertheless, they are completely adequate for the study of single-bunch instabilities. As a result, we can perform a simplified TCBI computation by closing the shielding gap at the point A (Figure 1) without losing anything but gaining quite a lot in the reduction of computer time.

REFERENCES

1. Report of the Reference Designs Study Group on the Superconducting Super Collider, May 8, 1984
2. J. Bisognano and K.Y. Ng, this workshop
3. T. Weiland, DESY 82-015, 1982
4. L. Vos, CERN SPS/DI-MST/Note/84-2

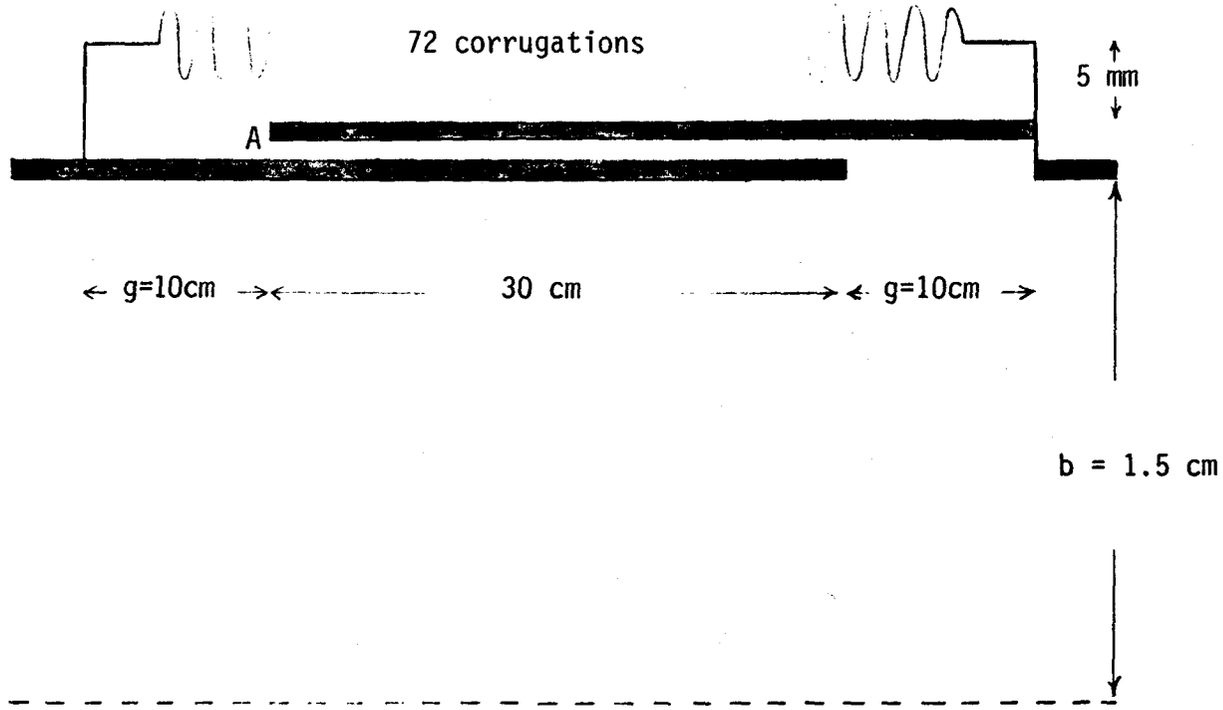

Figure 1. A shielded bellow
Thickness of each shielding tube = 2 mm.
Gap between two shielding tubes = 2 mm.

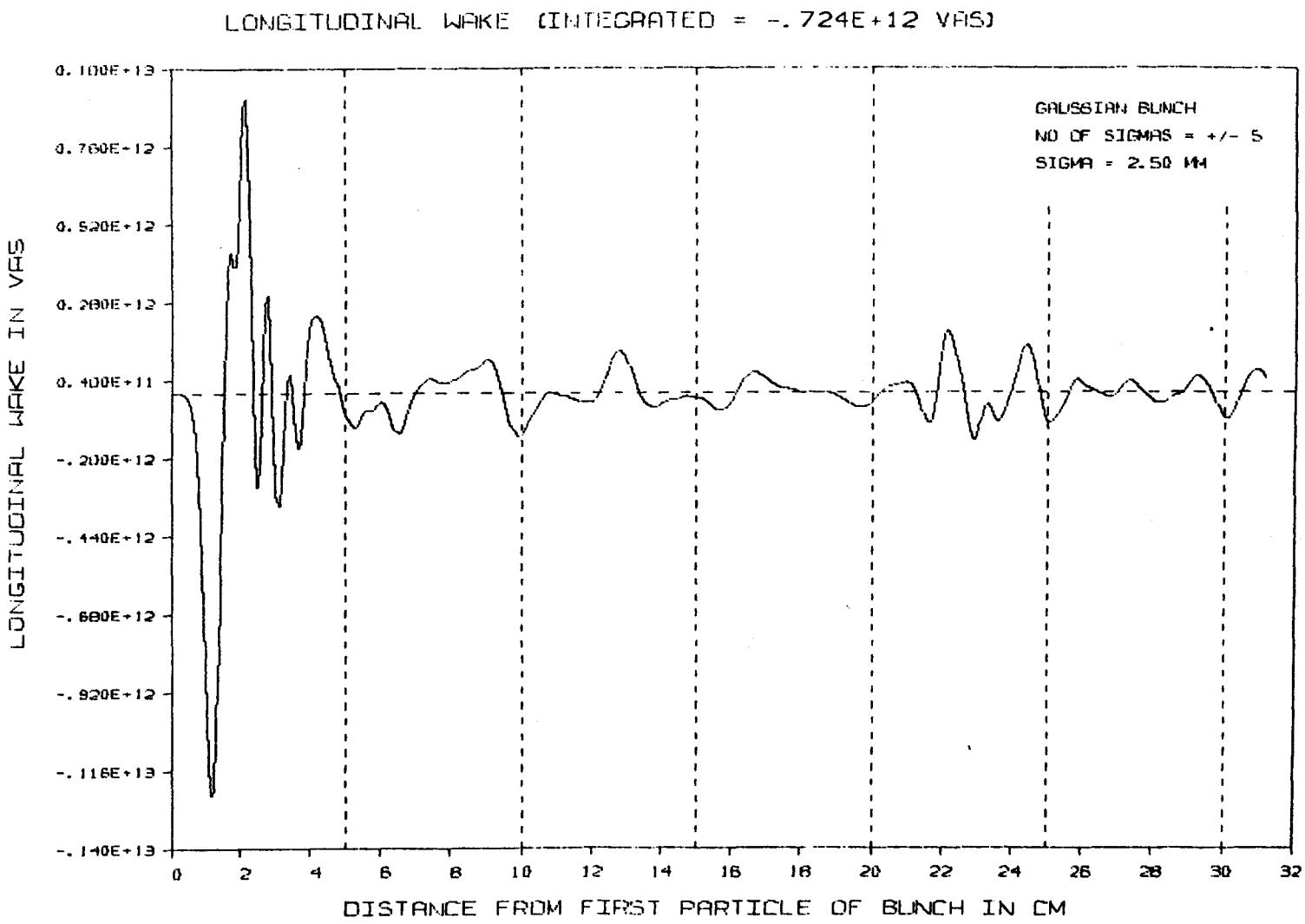
LONGITUDINAL WAKE (INTEGRATED = -.724E+12 VAS)
GAUSSIAN BUNCH
NO OF SIGMAS = +/- 5
SIGMA = 2.50 MM
LONGITUDINAL WAKE IN VAS
0.100E+13
0.760E+12
0.520E+12
0.280E+12
0.400E+11
-.200E+12
-.440E+12
-.680E+12
-.920E+12
-.116E+13
-.140E+13
0
2
4
6
8
10
12
14
16
18
20
22
24
26
28
30
32
DISTANCE FROM FIRST PARTICLE OF BUNCH IN CM

Fig. 2

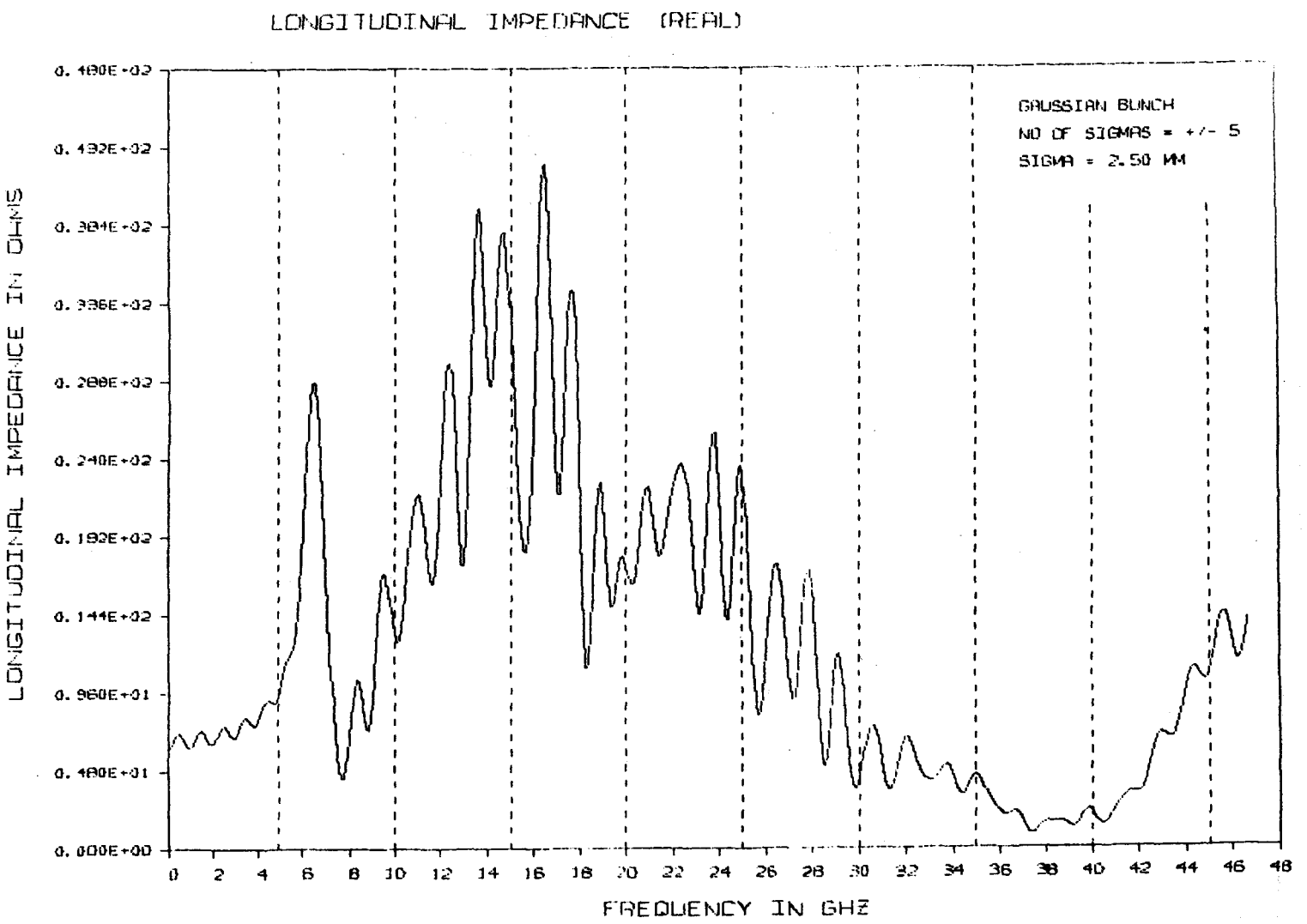
LONGITUDINAL IMPEDANCE (REAL)
GAUSSIAN BUNCH
NO OF SIGMAS = +/- 5
SIGMA = 2.50 MM
LONGITUDINAL IMPEDANCE IN OHMS
0.480E+02
0.432E+02
0.384E+02
0.336E+02
0.288E+02
0.240E+02
0.192E+02
0.144E+02
0.960E+01
0.480E+01
0.000E+00
0 2 4 6 8 10 12 14 16 18 20 22 24 26 28 30 32 34 36 38 40 42 44 46 48
FREQUENCY IN GHZ

Fig. 3

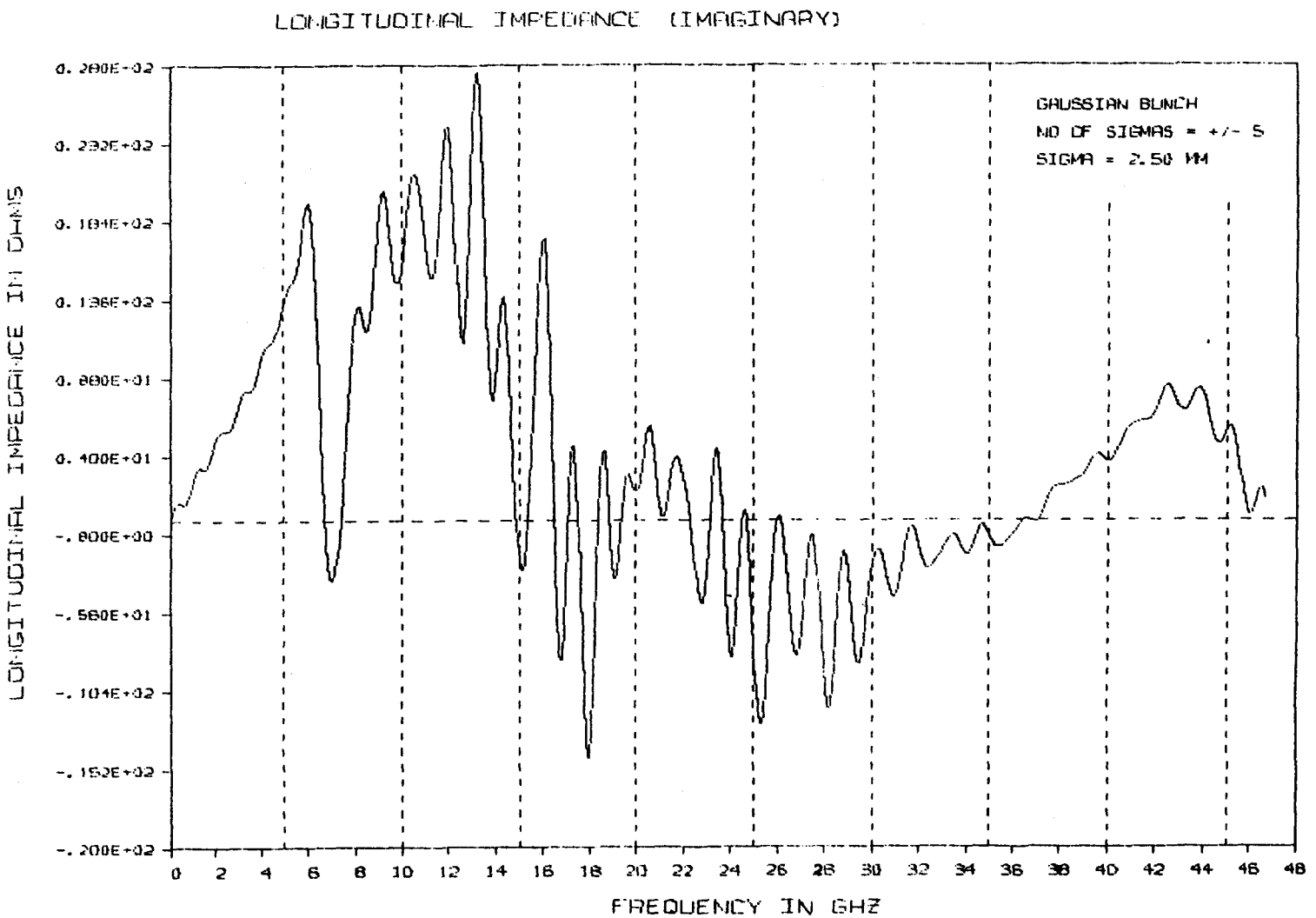
LONGITUDINAL IMPEDANCE (IMAGINARY)
GAUSSIAN BUNCH
NO OF SIGMAS = +/- 5
SIGMA = 2.50 MM
LONGITUDINAL IMPEDANCE IN OHMS
0.200E+02
0.232E+02
0.104E+02
0.136E+02
0.800E+01
0.400E+01
-.800E+00
-.560E+01
-.104E+02
-.152E+02
-.200E+02
0 2 4 6 8 10 12 14 16 18 20 22 24 26 28 30 32 34 36 38 40 42 44 46 48
FREQUENCY IN GHZ

Fig. 4

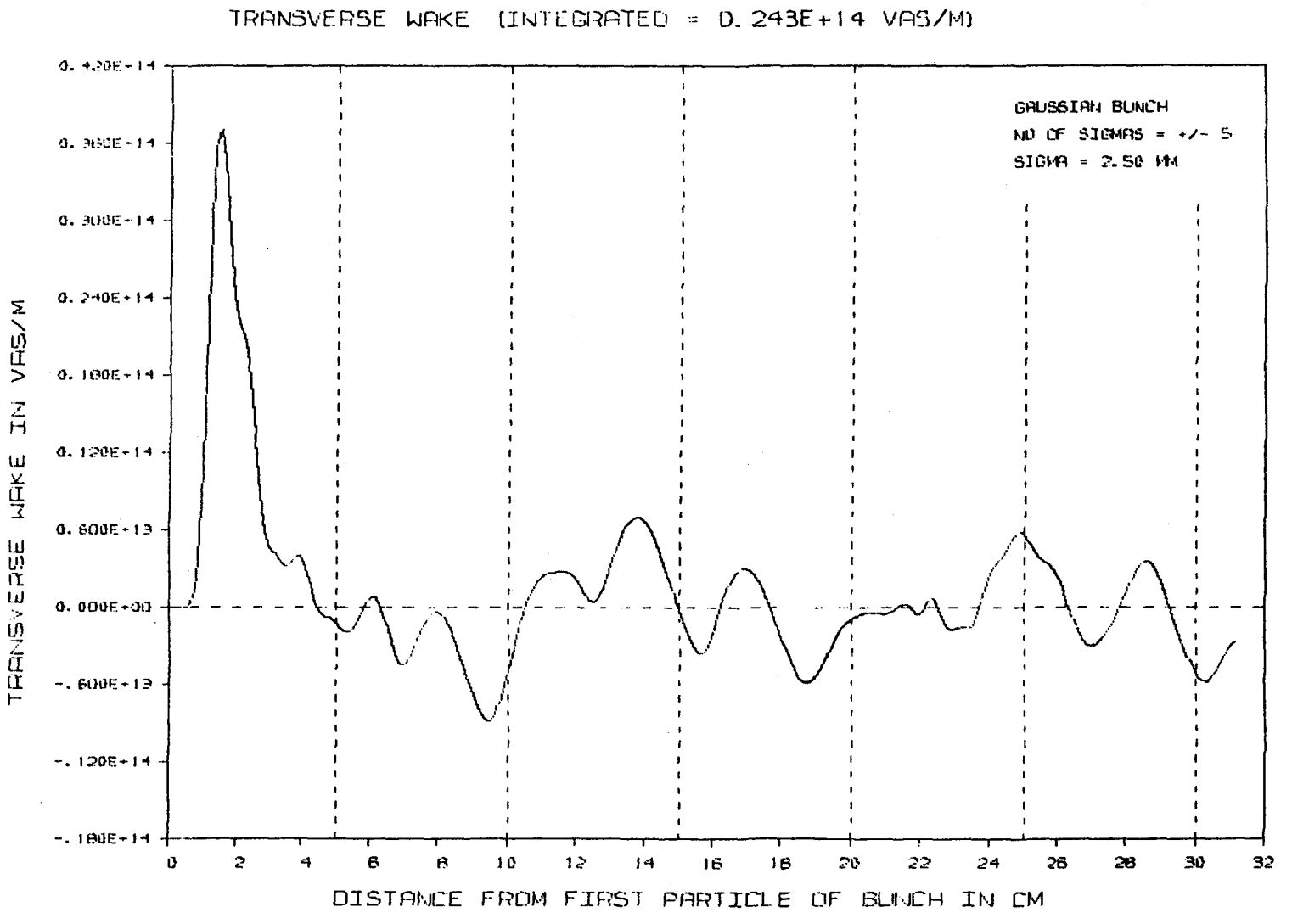
TRANSVERSE WAKE (INTEGRATED = 0.243E+14 VAS/M)
GAUSSIAN BUNCH
NO OF SIGMAS = +/- 5
SIGMA = 2.50 MM
TRANSVERSE WAKE IN VAS/M
0.420E+14
0.360E+14
0.300E+14
0.240E+14
0.180E+14
0.120E+14
0.600E+13
0.000E+00
-.600E+13
-.120E+14
-.180E+14
0
2
4
6
8
10
12
14
16
18
20
22
24
26
28
30
32
DISTANCE FROM FIRST PARTICLE OF BUNCH IN CM

Fig. 5

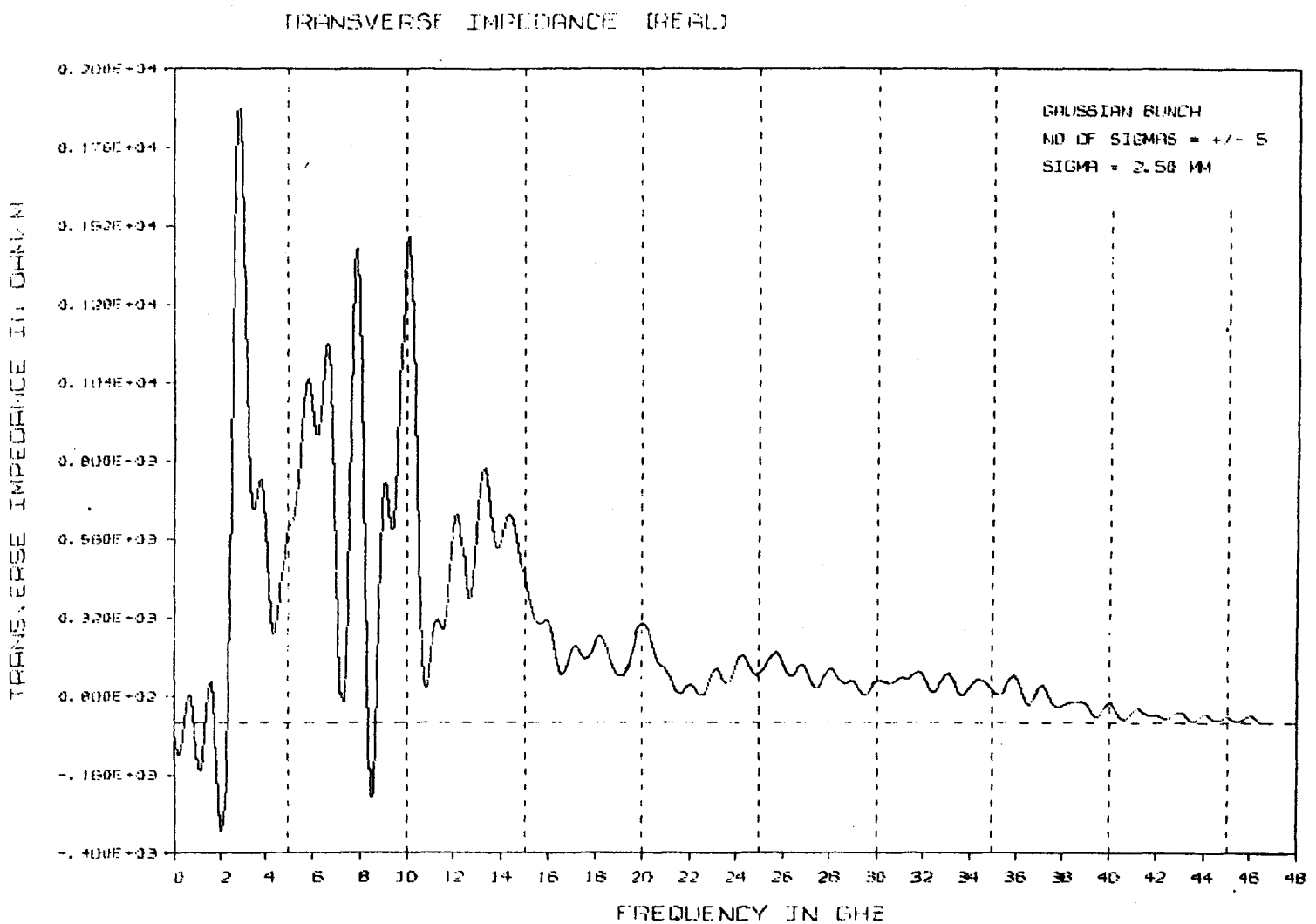
TRANSVERSE IMPEDANCE (REAL)
GAUSSIAN BUNCH
NO OF SIGMAS = +/- 5
SIGMA = 2.50 MM
TRANSVERSE IMPEDANCE IN OHM/M
0.200E+04
0.176E+04
0.152E+04
0.128E+04
0.104E+04
0.800E+03
0.560E+03
0.320E+03
0.800E+02
-.160E+03
-.400E+03
0 2 4 6 8 10 12 14 16 18 20 22 24 26 28 30 32 34 36 38 40 42 44 46 48
FREQUENCY IN GHZ

Fig. 6

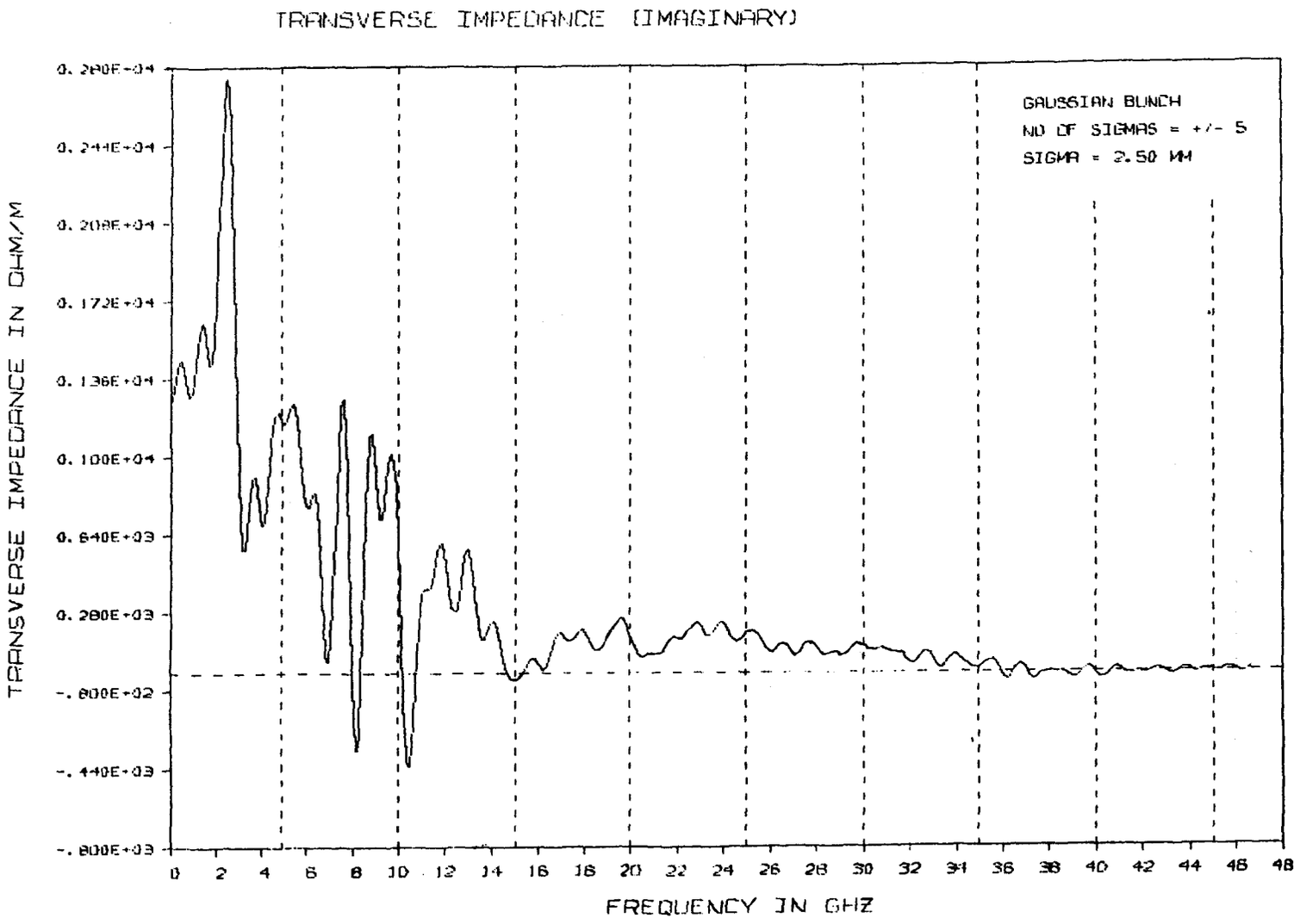
TRANSVERSE IMPEDANCE (IMAGINARY)
GAUSSIAN BUNCH
NO OF SIGMAS = +/- 5
SIGMA = 2.50 MM
TRANSVERSE IMPEDANCE IN OHM/M
0.280E+04
0.244E+04
0.208E+04
0.172E+04
0.136E+04
0.100E+04
0.640E+03
0.280E+03
-.800E+02
-.440E+03
-.800E+03
0 2 4 6 8 10 12 14 16 18 20 22 24 26 28 30 32 34 36 38 40 42 44 46 48
FREQUENCY IN GHZ

Fig. 7

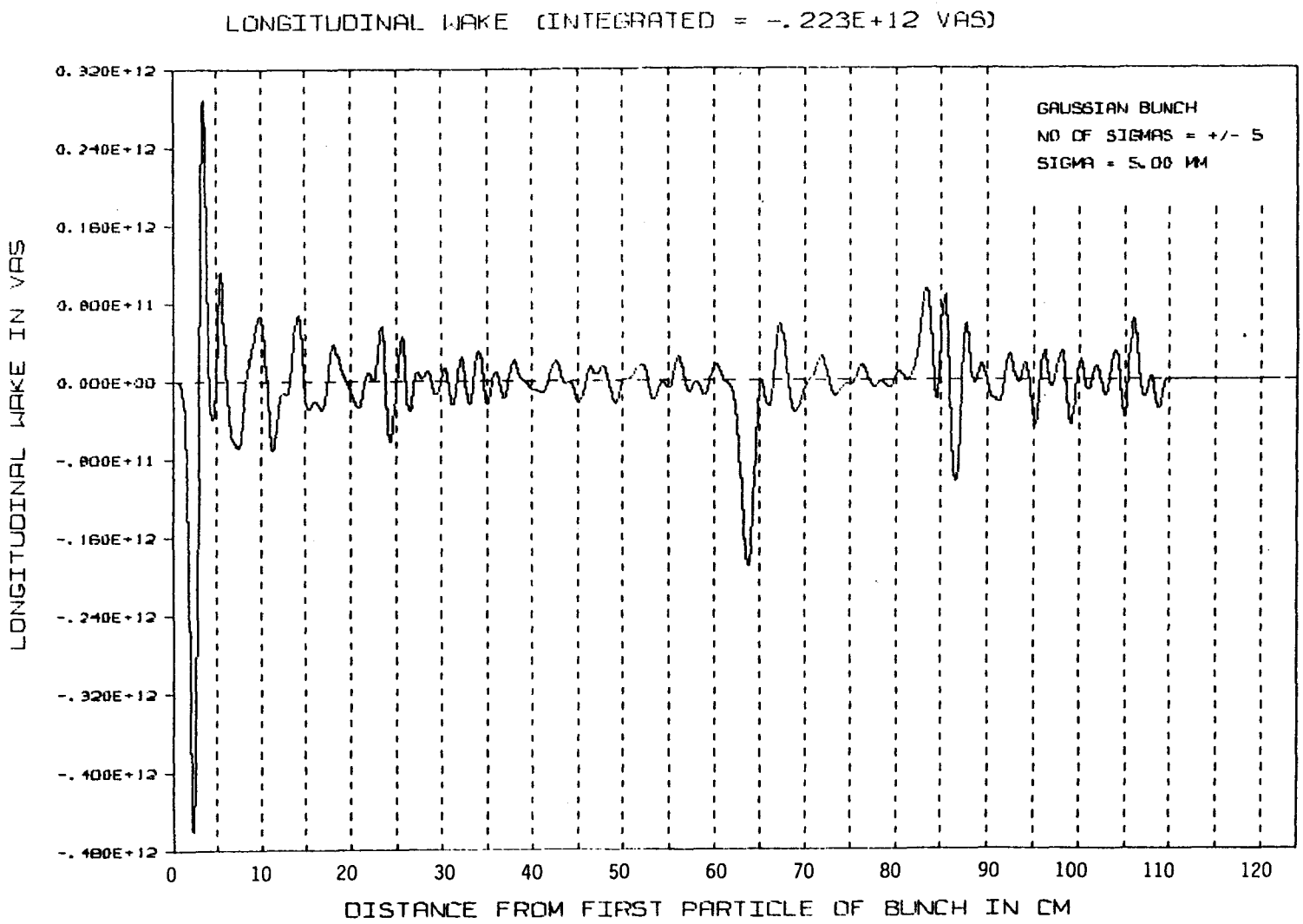
LONGITUDINAL WAKE (INTEGRATED = -.223E+12 VAS)
GAUSSIAN BUNCH
NO OF SIGMAS = +/- 5
SIGMA = 5.00 MM
LONGITUDINAL WAKE IN VAS
0.320E+12
0.240E+12
0.160E+12
0.800E+11
0.000E+00
-.800E+11
-.160E+12
-.240E+12
-.320E+12
-.400E+12
-.480E+12
0
10
20
30
40
50
60
70
80
90
100
110
120
DISTANCE FROM FIRST PARTICLE OF BUNCH IN CM

Fig. 8

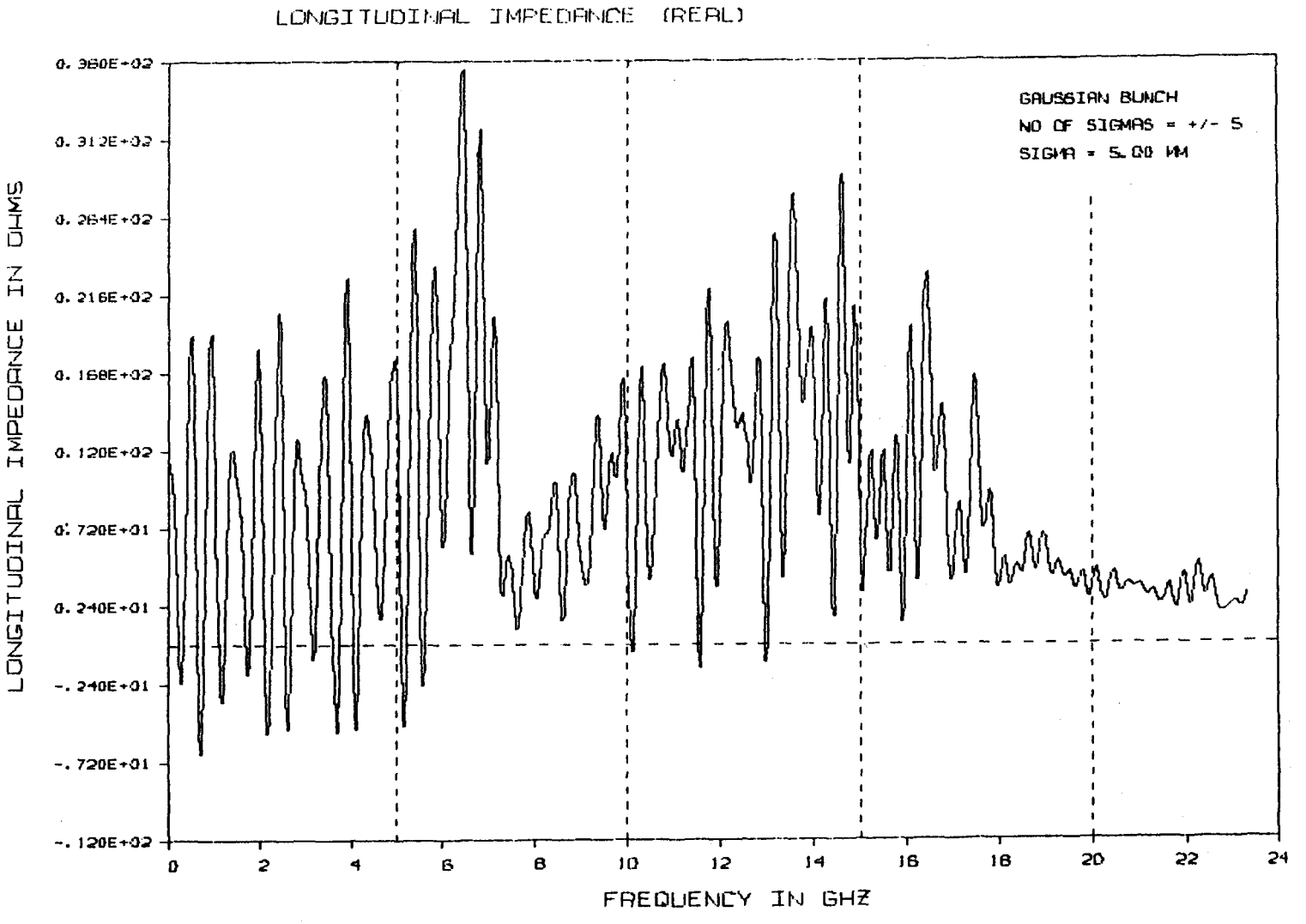
LONGITUDINAL IMPEDANCE (REAL)
GAUSSIAN BUNCH
NO OF SIGMAS = +/- 5
SIGMA = 5.00 MM
LONGITUDINAL IMPEDANCE IN OHMS
0.360E+02
0.312E+02
0.264E+02
0.216E+02
0.168E+02
0.120E+02
0.720E+01
0.240E+01
-.240E+01
-.720E+01
-.120E+02
0
2
4
6
8
10
12
14
16
18
20
22
24
FREQUENCY IN GHZ

Fig. 9

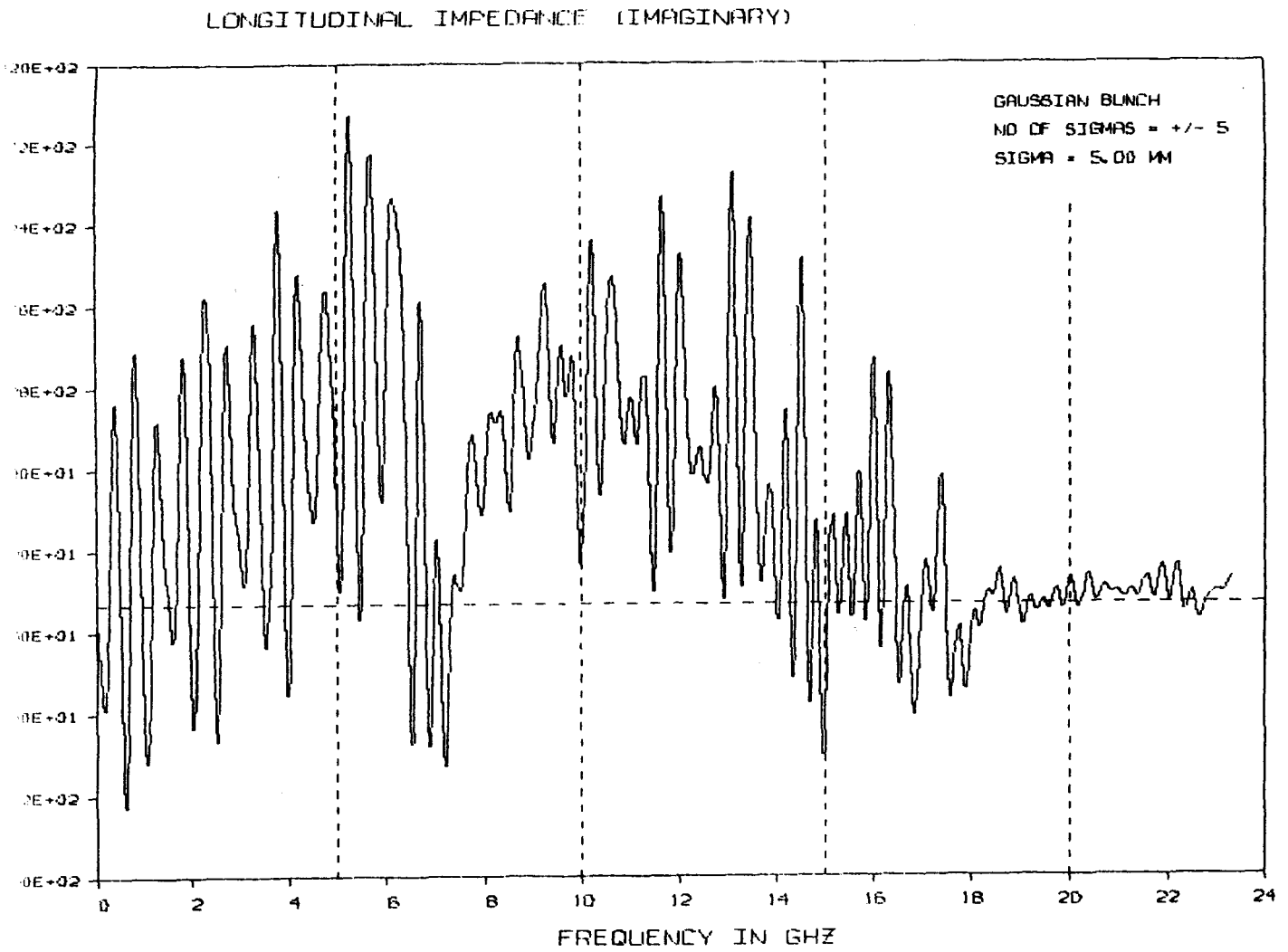
LONGITUDINAL IMPEDANCE (IMAGINARY)
GAUSSIAN BUNCH
NO OF SIGMAS = +/- 5
SIGMA = 5.00 MM
0
2
4
6
8
10
12
14
16
18
20
22
24
FREQUENCY IN GHZ

Fig. 10

AN INVESTIGATION OF THE SKIN DEPTH EFFECT OF A METALLIC COATING ON A CERAMIC BEAMPIPE INSIDE A KICKER

King-Yuen Ng

Fermi National Accelerator Laboratory*

P.O. Box 500

Batavia, IL 60510

July 1985

INTRODUCTION

Inside a kicker magnet, metallic beampipe cannot be used because it will screen off the rapid rising of the kickers's magnetic field. When a ceramic beampipe is used, one usually coats the inside with a thin layer of metal so as to carry at least part of the beam's image current and to prevent static charge buildup. The purpose of this article is to investigate whether such a coating will alter the risetime constant of the magnetic field significantly, whether such a coating can withstand the strong transient current induced by the fast rising magnetic field, and whether the back magnetic field generated by this transient current is strong enough to upset the designed risetime of the kicker.

---

*Operated by the Universities Research Association, Inc., under contract with the U.S. Department of Energy.

The magnetic field inside the ceramic beampipe is affected by the metallic coating in two ways. Firstly, there is the "shielding effect". Even when the kicker's magnetic field rises abruptly as step function, the field inside the beampipe has a nonzero risetime

$$\tau_c = \frac{\mu b \Delta}{2\rho}, \tag{1.1}$$

where b is the radius of the beampipe, Δ the thickness of the metallic coating, ρ the resistivity of the coating and $\mu = 4\pi x10^{-7}$ henry/m is the magnetic permeability. Here, the azimuthal electric field and the radial magnetic field are assumed to be continuous across the coating. If we take Δ = 1 mil, b = 1.5 cm, $\rho = 1.7x10^{-8}$ ohm-m for copper, we get τ_c = 14 μsec or $\omega_c/2\pi = 1/2\pi\tau_c$ = 11 kHz. Thus, this is a low-frequency effect. The "shielding effect" has been considered in detail by Shafer[1] and will not be included in this article.

The second is the "skin-depth" effect. Here the fields "diffuse" from one side of the coating to the other. (The term "diffusion" is explained in the Appendix.) Thus, the azimuthal electric field and the radial magnetic field become discontinuous across the coating. This effect can be represented by the time scale

$$\tau_s = \frac{\mu \Delta^2}{2\rho}. \tag{1.2}$$

At the characteristic angular frequency $\omega_s = 1/\tau_s$, the fields will be attenuated by a factor of e^{-1} across the coating. Comparing Eqs. (1.1) and (1.2), we find $\tau_s/\tau_c = \Delta/b$. Thus the "skin-depth" effect occurs at a frequency much higher than that of the "shielding" effect. For a 1 mil coating with the same ρ, $\omega_s/2\pi = 6.7$ MHz. The injection and injection-abort kickers of the SSC have risetimes 10 ns to 100 ns, or have characteristic frequencies 1.6 MHz to 16 MHz. Thus, these kickers will be affected by the skin-depth effect, which we will study in detail below.

MAGNETIC FIELD ACROSS THE COATING

For simplicity, we assume the beampipe to be of square cross section with horizontal coatings of thickness Δ at the top and bottom walls as shown in Figure 1. The magnetic field generated by the kicker perpendicular to the coating is

$$B_{in}(t) = B_0 \left(1 - e^{t/\tau}\right) \theta(t), \tag{2.1}$$

where τ is the risetime of the kicker. This can be Fourier transformed into

$$B_{in}(t) = \int_{-\infty}^{\infty} d\omega \, B_{in}(\omega) e^{j\omega t}, \tag{2.2}$$

with

$$B_{in}(\omega) = -\frac{B_0}{\pi} \frac{\omega_\tau}{(\omega - j\xi)(\omega - j\omega_\tau)}, \tag{2.3}$$

where $\omega_\tau = 1/\tau$ is the characteristic angular frequency of the kicker and ξ is a positive infinitesimal number. The position of the pole near $\omega = 0$ has been carefully chosen so that the step function in Eq. (2.1) can be reproduced through the integration of Eq. (2.2).

Due to the time variation of the magnetic field $\vec{B}$, electric field $\vec{E}$ is also present. Inside the metallic coating, the corresponding Fourier components satisfy the Maxwell equations

$$\vec{\nabla} \times \vec{B} = \mu\sigma\vec{E} + j\omega\epsilon\mu\vec{E},$$

$$\vec{\nabla} \times \vec{E} = -j\omega\vec{B}, \tag{2.4}$$

where ϵ is the electric permitivity of the coating which we assume to be approximately the value at vacuum. The frequency of $\vec{B}$ and $\vec{E}$ for the kicker will be at most $\sim\omega_\tau/2\pi$; as a result, the displacement current can be neglected for most metal. Eliminating E, one gets the familiar equation,

$$\nabla^2\vec{B} = j\omega\mu\sigma\vec{B}. \tag{2.5}$$

The component of $\vec{B}$ perpendicular to the coating is continuous at both surfaces. Thus, after penetrating a thickness Δ, the emerging perpendicular magnetic field is

$$B_{out}(\omega) = B_{in}(\omega)\, e^{-(1\pm j)\sqrt{|\omega|\tau_s}}, \tag{2.6}$$

where τ_s is the characteristic time of the skin-depth effect and is given by Eq. (12). The ± sign in the exponent applies when ω is positive (negative). The time variation of the emerging magnetic field is therefore

$$B_{out}(t) = -\frac{B_o}{2\pi}\int_{-\infty}^{\infty} d\omega \, \frac{\omega_\tau}{(\omega - j\xi)(\omega - j\omega_\tau)} \, e^{-(1\pm j)\sqrt{|\omega|\tau_s}} \, e^{j\omega t} . \tag{2.7}$$

When $B_{out}(t)/B_o$ is viewed as a function of t/τ, the only parameter is

$$a = (\tau_s/\tau)^{\frac{1}{2}} . \tag{2.8}$$

When $t<0$, simple contour integration gives $B_{out}(t) = 0$ as expected. (See Appendix for detail.) When $t>0$, because of the existence of a branch point at $\omega = 0$, contour integration cannot be performed simply. Instead a numerical integration is attempted. The result is plotted in Figure 2. The rise of magnetic field inside the ceramic pipe at fixed kicker's risetime τ but at difference coating thicknesses can be read off directly. For example, with Δ = 1 mil and τ = 50 ns, i.e., a = 0.69, the effective risetime [the time for the field to increase to (1-1/e) of its maximum value] is roughly 3.5 times the kicker's risetime. If the thickness of the coating is reduced to 0.5 mil (a = 0.49), the effective risetime is still ~2.5 τ. Thus, the effect of the coating is not small at all.

We can also fix the coating thickness, and observe the rise of magnetic field at different kicker's risetime. Then we take t/τ_s as the time variable in Eq.(2.7) and take $a^{-1} = (\tau/\tau_s)^{1/2}$ as the parameter. This is plotted in Figure 3. We see that even when the kicker has zero risetime $a^{-1} = 0$, the field inside the coated beampipe has an effective risetime of ~4.5 τ_s.

EDDY CURRENT IN THE COATING AND BACK MAGNETIC FIELD

With the coordinate system in Figure 1, electric field E_y induced by magnetic field $B_z(t)$ at a distance x from the center of the coating is

$$E_y(x,t) = -x \frac{\partial}{\partial t} B_z(t). \tag{3.1}$$

As an overestimate, the magnetic field at the top of the coating surface is used, therefore

$$E_y(x,t) = -\frac{x}{\tau} B_o e^{-t/\tau} \theta(t). \tag{3.2}$$

Thus the current induced in one half of the coating is

$$\begin{aligned} I(t) &\sim \int_o^W \frac{\Delta}{\rho} E_y(x,t)\, dx \\ &= \frac{W^2 \Delta}{2\tau\rho} B_o e^{-t/\tau} \theta(t), \end{aligned} \tag{3.3}$$

where 2W is the width of the coating. Taking W = 1.5 cm, B_o = 0.5 Tesla, $\rho = 1.7\text{x}10^{-8}$ ohm-m for copper, τ = 50 ns and

Δ = 1 mil, this current is ~1.7×10^6 amp when $t \ll \tau$. The total energy dissipated in a unit length of coating (two halves) is

$$\mathcal{E} = \frac{\Delta W^3 B_0^2}{6\tau\rho} = 4200 \text{ joules/m} . \tag{3.4}$$

This leads to a rise in temperature of

$$\Delta T = \frac{W^2 B_0^2}{12\tau\rho d s H} = 1600°C , \tag{3.5}$$

where d~9 gm/cm^3 and s = 0.092 are the density and specific heat of copper respectively and H = 4.18 joules/calorie is the mechanical equivalence of heat. In order to reduce this temperature rise, we have to choose a coating metal with high density, resistivity and specific heat. Nickel can lower the temperature rise by 5.4 times, wrought iron 6.4 times and steel ~50 times. Otherwise, some heat sink must be installed.

At the same time, the eddy current in the coating will generate a back magnetic field in the opposite direction of the kicker's field. At the center of the coating, this back field is

$$B_{back} \sim \frac{\mu}{4\pi} \int_{-W}^{W} \frac{2E_y \Delta}{x\rho} dx$$

$$= \frac{\Delta \mu W B_0}{\pi\rho\tau} e^{-t/\tau} , \tag{3.6}$$

which comes out to be ~180 B_o at $t \ll \tau$. Thus, special care must be taken for the kicker's current source so that the kicker's current will not be disturbed. Again, choosing a coating with a high resistivity can reduce this back magnetic field.

If the coatings are on the vertical walls of the beampipe instead, the rise in temperature and the strength of the induced transient magnetic field will be of the same order of magnitude, although there is no screening of the kicker's field at all in this case.

DISCUSSIONS

We see from above that a metallic coating will affect the transience of the kicker very much when the kicker's risetime is as small as τ = 50 ns. A coating of 1 mil copper can increase the risetime 3.5 times. The eddy current in the coating can lead to a temperature rise of ~ a thousand degrees. The back magnetic field can be ~180 times the maximum kicker's field when $t \ll \tau$. To overcome these effects we can choose a metallic coating with the highest resistivity. If we use steel whose resistivity is ~40 times that of copper, the risetime increases by only ~20%, the rise in temperature becomes ~32°C and the back magnetic field becomes ~5 B_o. Such a high resistive coating may still serve the purpose of preventing static charge buildup.

To carry the image current some other methods must be derived. One suggestion is to use metallic strips at the vertical walls of the ceramic beampipe with capacitance in series. The capacitance is so chosen that it will allow the flow of the image current which is of high frequencies ($>\omega_{rf}/2\pi$ = 360 MHz) but block the flow of the eddy current which is of frequencies $<\omega_{\tau}/2\pi$ (= 3.2 MHz when the kicker's risetime is 50 ns).

The author would like to thank Dr. R. Shafer for useful discussion.

APPENDIX

Solution of Eq. (2.5) gives

$$B_{out}(t) = -\frac{B_0}{2\pi}\int_{-\infty}^{\infty} d\omega \frac{\omega_\tau}{(\omega - j\xi)(\omega - j\omega_\tau)} e^{\sqrt{2j\tau_s\omega}} e^{j\omega t} . \tag{A.1}$$

There is a branch point at $\omega = 0$ and we choose the branch cut along the negative ω-axis. For ω real and positive, the physical sheet is characterized by the physical condition that the integrand decreases as the coating thickness $\Delta(\sim\sqrt{\tau_s})$ increases; i.e.,

$$\sqrt{2j\tau_s\omega} \longrightarrow -(1+j)\sqrt{\tau_s\omega}$$

The same physical condition also applies when ω is real and negative; i.e.,

$$\sqrt{2j\tau_s\omega} \longrightarrow -(1-j)\sqrt{\tau_s|\omega|}$$

and is below the cut. The path of integration of Eq. (A.1) is shown in Figure 4. The pole-part of the integrand gives poles at $j\xi$ and $j\omega_c$ in the upper halves of both sheets. Therefore, when $t<0$, we complete the path of integration in the lower half of the physical sheet and get $B_{out}(t<0) = 0$. When $t>0$, if we complete the path of integration in the upper half of the physical sheet, we need to integrate around the cut too which is not easy at all. Instead, we do the integration directly by breaking it up into two parts: (i) along a semicircle of radius η in the lower half-plane to bypass the pole at the origin and (ii) from $-\infty$ to $-\eta$ below the cut and then from η to ∞. Finally we let $\eta \to 0$. The first part gives 1/2 B_o while the second part reduces to

$$B_2(t) = \frac{2B_o}{\pi}\int_0^\infty du\, \frac{e^{-au}}{1+u^4}\left\{\sin\frac{u^2t}{\tau}\left(\frac{\cos au}{u} - u\sin au\right)\right.$$
$$\left. - \cos\frac{u^2t}{\tau}\left(\frac{\sin au}{u} + u\cos au\right)\right\}, \qquad \text{(A.2)}$$

where $a = (\tau_s/\tau)^{1/2}$. Numerical integration then leads to the curves in Figure 2.

Equation (A.2) can also be written as

$$B_2(t) = \frac{2B_o}{\pi}\int_0^\infty du\, \frac{e^{-u}}{1+a^{-4}u^{-4}}\left\{\sin\frac{u^2t}{\tau_s}\left(\frac{\cos u}{u} - a^{-2}u\sin u\right)\right.$$
$$\left. + \cos\frac{u^2t}{\tau_s}\left(\frac{\sin u}{u} + a^{-2}u\cos u\right)\right\}, \qquad \text{(A.3)}$$

which gives the curves in Figure 3.

The transient electric field is given by Eq. (3.1). Using Eq. (A.2), we get

$$E_y(t) = -\frac{2\varkappa B_0}{\pi}\int_0^\infty du\,\frac{e^{-au}}{1+u^4}\,\frac{u^2}{\tau}\left\{\cos\frac{u^2t}{\tau}\left(\frac{\cos au}{u} - u\sin au\right)\right.$$

$$\left. + \sin\frac{u^2t}{\tau}\left(\frac{\sin au}{u} + u\cos au\right)\right\},$$

where a = 0 denotes the field on the top of the coating and a>0 the field inside or on the bottom of the coating. For t = 0, E_y = 0 independent of whether a = 0 or a>0. But for t = 0_+ we get

$$E_y = \begin{cases} -\varkappa B_0/\tau & a = 0 \\ 0 & a > 0 . \end{cases}$$

Care must be exercised in the evaluation of Eq. (A.4) because the sin u^2t/τ term gives nonzero contribution with opposite signs when t = $0_\pm$. Equation (A.5) says that although there is a surge of eddy current on the top of the coating at t = 0_+, the eddy current on the other side of the coating always starts from zero no matter how thin the coating is. The same applies to B_z. If the kicker's risetime τ = 0, we get with the aid of Eq. (A.3),

$$B_z = \begin{cases} B_0 & \tau_s = 0 \\ 0 & \tau_s > 0 \end{cases}$$

at t = 0_+. This behavior can also be understood from the Maxwell equations. Both B_z and E_y satisfy Eq. (2.5), which in the time domain reads

$$\frac{\partial^2 E_y}{\partial z^2} = \mu\sigma\dot{E}_y , \qquad \frac{\partial^2 B_z}{\partial z^2} = \mu\sigma\dot{B}_z .$$

These are just diffusion equations. If there is a surge of fields at $z = 0$, it takes finite time for them to diffuse to the location $z \neq 0$. Thus no matter how small z is, the fields there always start from zero.

REFERENCE

1. R. Shafer, "On Shielding the Beam from Kicker Magnets at High Frequencies", this workshop. R. Shafer, Fermilab report TM-991.

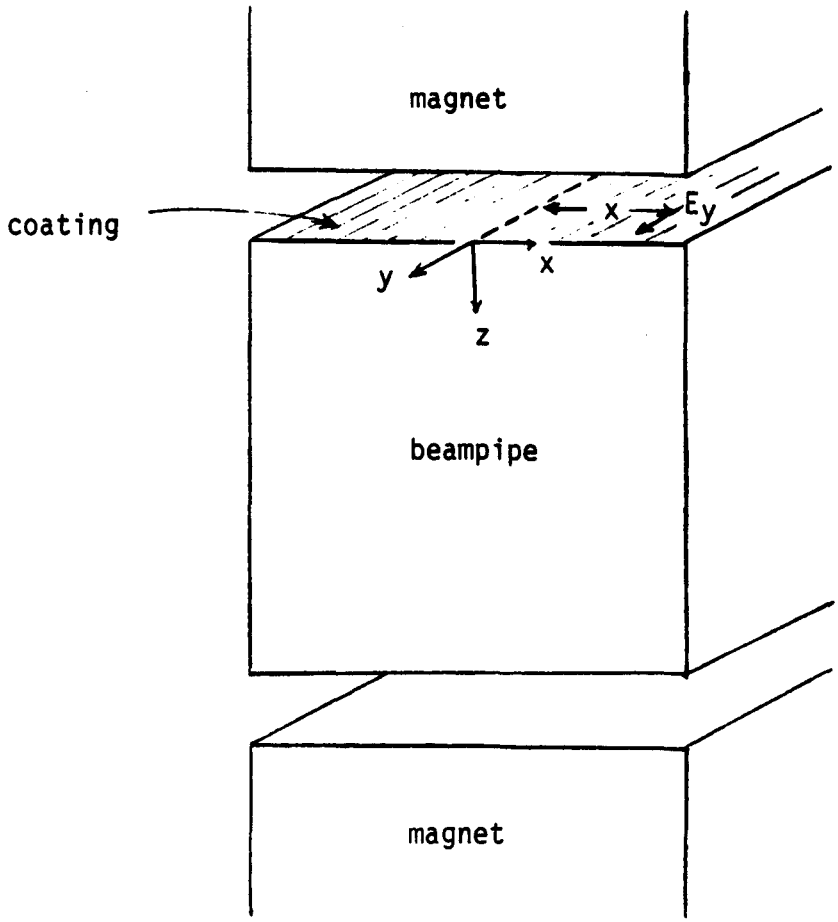

Fig. 1 Magnet and beampipe configuration

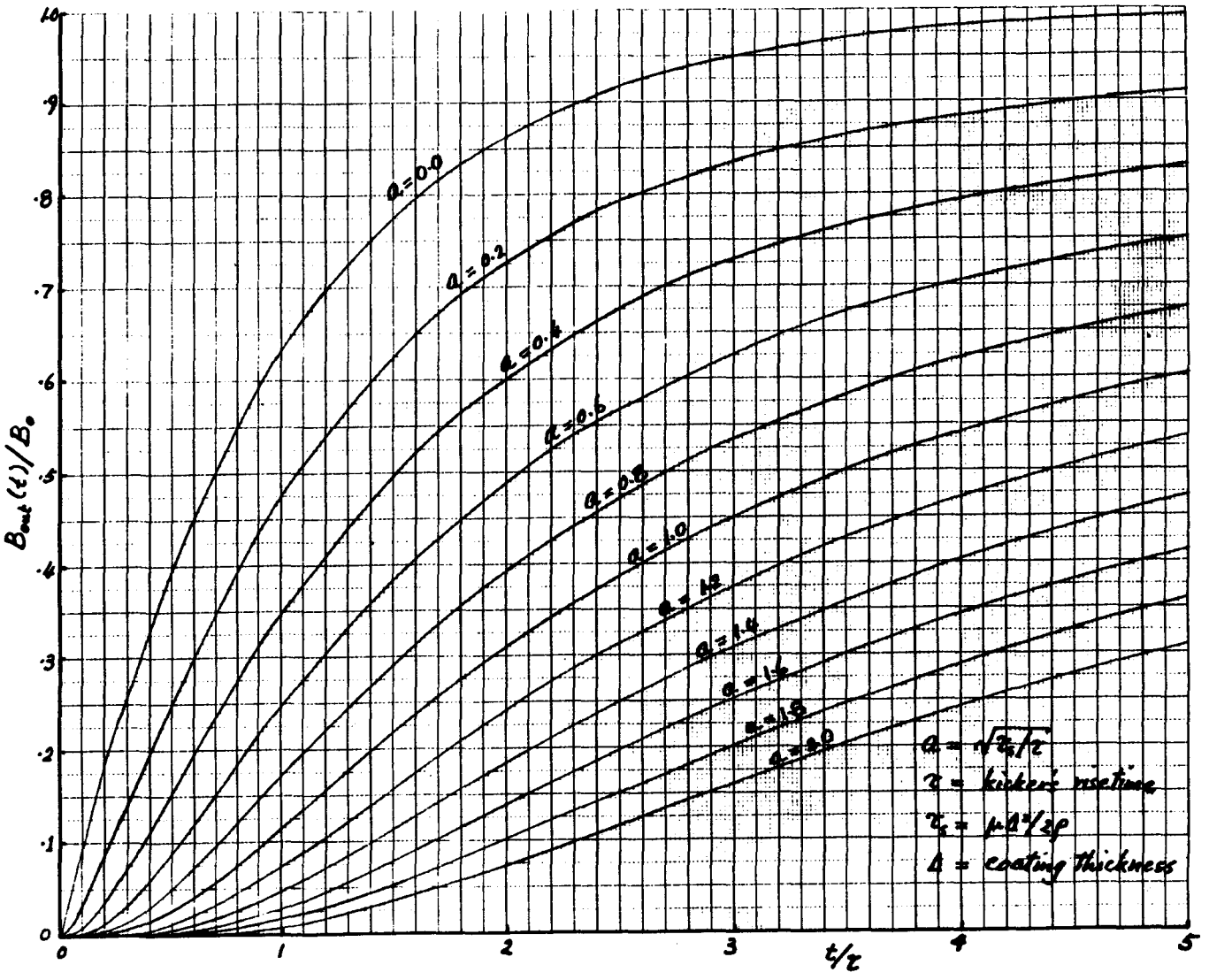

Fig. 2. Rise of magnetic field inside beam pipe as a function of t/τ.

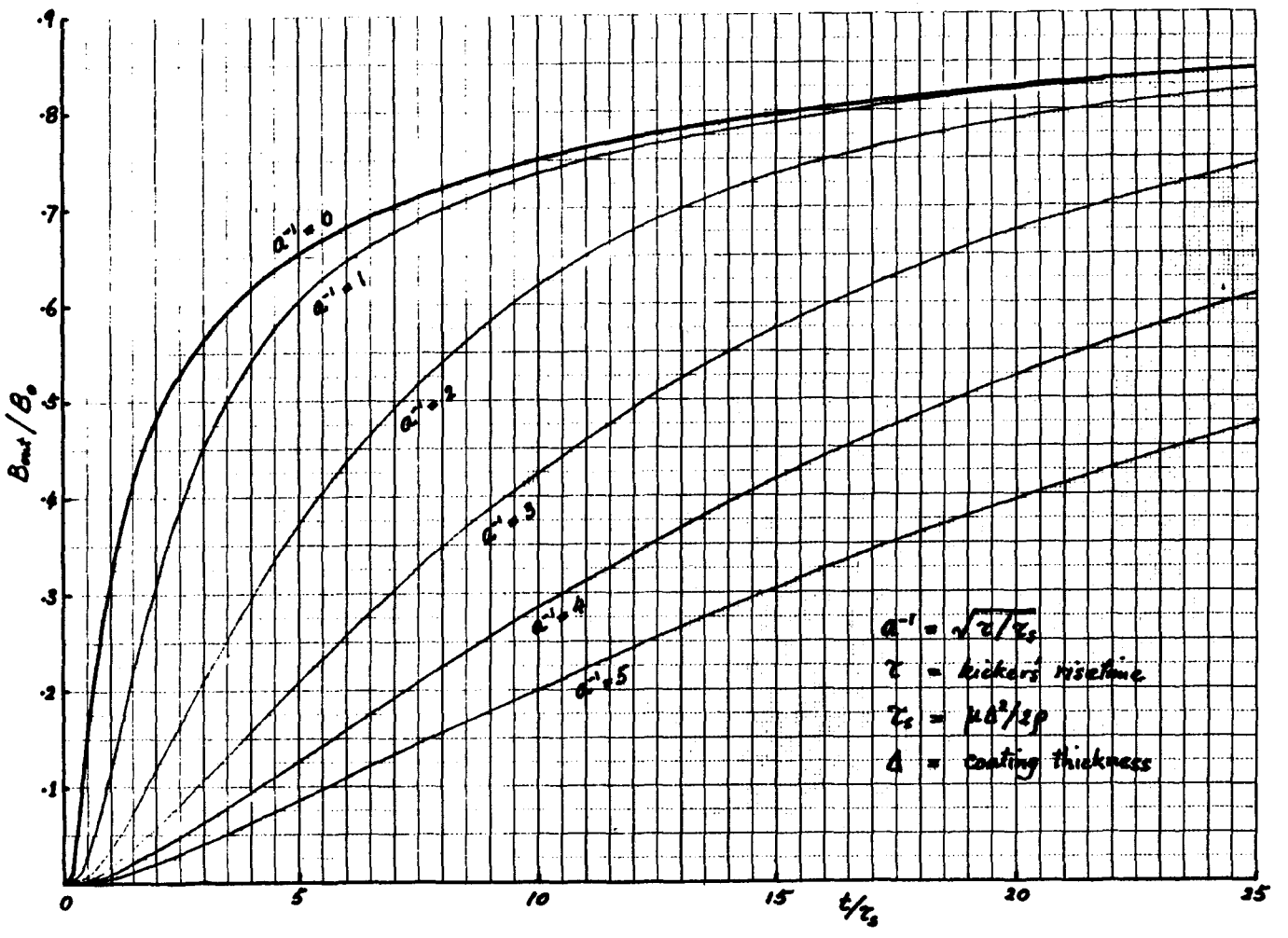

Fig. 3. Rise of magnetic field inside beam pipe as a function of t/τ_s.

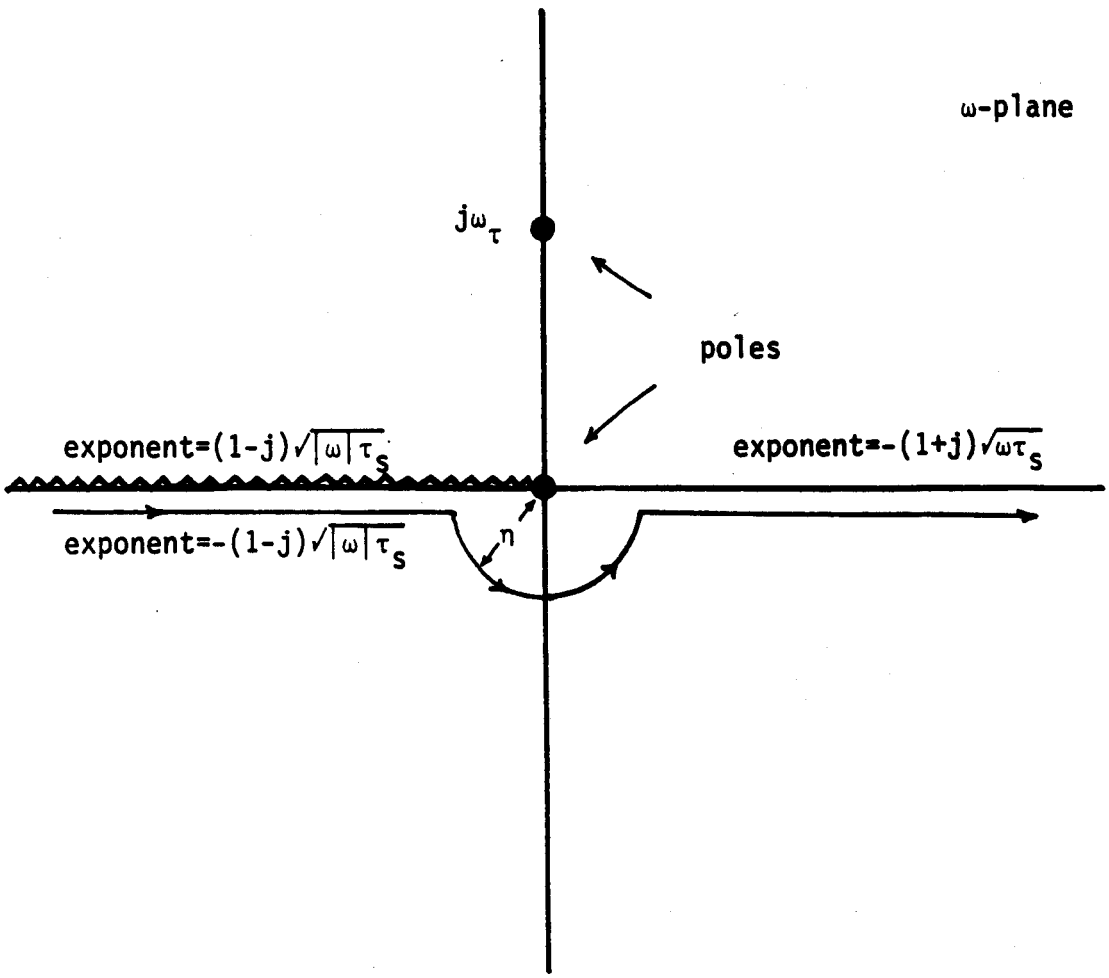

Fig. 4 The ω-plane and path of integration.

Impedance Measurement Group Report

J. Simpson, Sal Giordino, Fred Voelker,
Jim Hinkson, and George Spalek

July 9, 1985

Impedance Measurements - Some Thoughts

The first indication of trouble was that each member of the group stated disclaimers - each was here to learn and was not well prepared. Fortunately, this was not totally the case, and some progress resulted.

Questions and issues were first identified as potential topics for discussion. These included:

1) What can be done with "wires" regarding-
   a) Useful frequency range
   b) Longitudinal vs transverse measurements
   c) Resolution and sensitivity

2) Where do beam and wire measurements differ? What are the corresponding limits for beam measurements?

Useful Frequency Limits for Wire Techniques

The low frequency limit is determined mostly by wall penetration of the fields, generally at a much lower frequency than is of interest for beam dynamics.

Measurement techniques to perhaps 1.5 GHZ are not too difficult if the individual impedances are $\ll \lambda$ in axial extent. The accuracy of the measurement decreases for distributed impedances, but the measurements can still be useful in providing relative improvement factors.

The useful high frequency limit for the technique is probably the beam pipe cut off -- when $\lambda \approx 2\pi r$. For 1.5 cm radius this is about 3 HGZ. Measurements at higher frequencies, where higher order modes can propagate, will require careful attention to differentiate between waveguide resonances and the impedance to be measured. One can think of special geometries which may permit waveguide mode damping and possibly higher useful frequencies for impedance measurement.

Sensitivity Resolution for Wires

It should be possible to measure impedance differences due to transverse position of 1/2 Ω on a 200 Ω wire transmission line. For a half cm displacement of the wires this corresponds to a transverse impedance of 100 Ω/m. It isn't clear whether perturbations caused by the wires (or probes) will be greater than this.

For Z_{11} (longitudinal), absolute values of ~ ±5% are resasonable. Differential sensitivity is somewhat better.

Transverse impedance is more difficult to measure, and the group had little experience with it. A proposal was made by Voelker that one might be able to use wire excitation plus a small "probe" to obtain information of $\frac{\partial E_z}{\partial x}$. The transverse gradient of E_z, $\frac{\partial E_z}{\partial x}$, is a measure of the transverse kick. Perhaps a discontinuity in the beam pipe can be excited by a wire, and $\frac{\partial E_z}{\partial x}$ measured by a suitable electric field probe moved transversely along a radius. This approach may be very model sensitive (multi-mode effects, etc)

Preliminary measurements with a two wire system have been tried and reported in the literature. The results indicate that such measurements are feasible, and it is strongly recommended that work on such a system start as soon as possible.

CW vs Pulses

We do not regard these two techniques as having significantly different limitations. Peters (DESY) is believed to be using the pulsed wire technique to about 3 GHZ. Wilson (SLAC) generally focuses on lower frequencies.

Beams vs Wires

The useful frequency limits for "beam" measurements are not limited at high frequencies end by guide modes in the pipe. Beam measurements can also accommodate simultaneous seriesed??? impedances. On the other hand, detailed sensitivity estimates haven't been made.

The use of actual beams to make impedance measurements, especially the use of a witness pulse as a probe of fields, is a new idea. Models of impedance sources must be developed to permit estimates of the usefulness of this method.

Impedance Source Models

Quite some time was spent in our group discussing possible models for transverse impedance producing geometry. To avoid embarrassment we will not detail the discussion. However, it is clear that experimentalists and theorists should establish better dialogue on this subject (at least our group of experimentalists). Joe Bisognano gave us a model to use for estimating transverse Z of a bellows:

$Z_\perp$ (low freq)	100 Ω/m/convolution
f_c	15 GHZ
Q	6

Sensitivity of Beam Method (Transverse)

Assuming a single "resonance" model, what can we do?

For

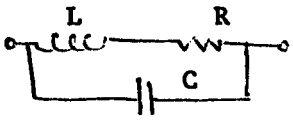

$$Z_{\perp}(s) = \frac{\frac{R}{LC} + \frac{S}{C}}{S^2 + \frac{R}{L} S + \frac{1}{LC}}$$

with poles at $-\frac{R}{2L} \pm \frac{1}{2}\sqrt{\left(\frac{R}{L}\right)^2 - \frac{4}{LC}}$

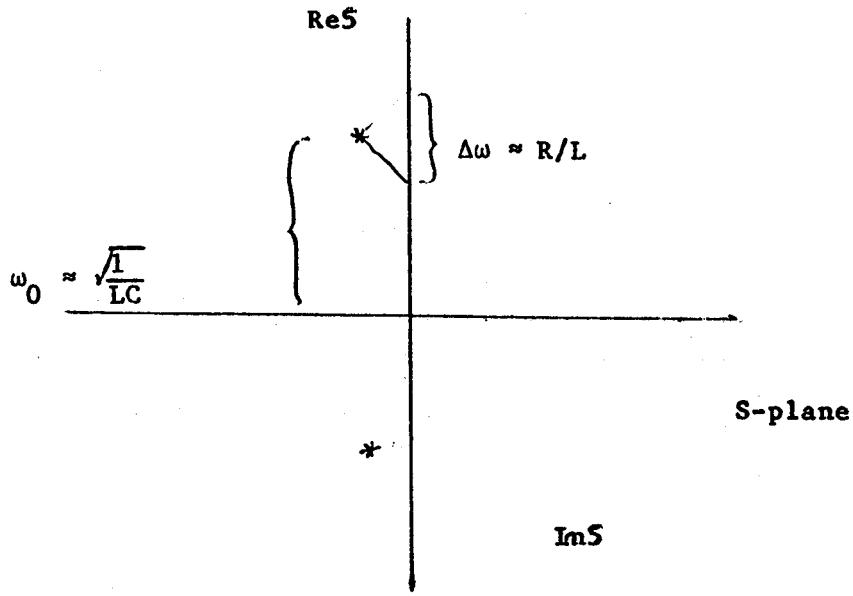

$$f_o \approx \frac{2\pi}{\sqrt{LC}}$$

$$Q = \frac{\omega_0}{\Delta\omega_{3\,db}} \approx \frac{\omega L}{R}$$

For Low Q systems $Z_{max} \approx QR$.

Because Z(s) is the delta-function response, we can estimate the "kick" seen by a witness pulse follow a driving pulse $q\delta(0)$.

$$L^{-1}Z(s) \approx qR\omega_0 e^{-\frac{R}{2L}t}(Q \cos\omega_0 t + \sin \omega_0 t)$$

if $q \simeq 5 \times 10^{-9}$ C (charge in driver pulse)

$\omega_0 \simeq 2\pi \times 15 \times 10^9$ HZ

$R \simeq 100\ \Omega$

$Q \simeq 6$

then

$$|L^{-1}Z(s)|_{t = 0+} \simeq 286 \text{ KeV/m}$$

For a 1 cm offset of the driver, this is 2.9 KeV. Θ_{kick} of witness is $\frac{2.9}{15} \approx 0.2$ mrad.

It would be difficult to accurately measure such a kick with the proposed ANL measurement system. On the other hand, several bellows convolutions could be simultaneously measured, yielding somewhat larger kicks.

To estimate sensitivity for Z_{11}/n measurements, let's assume the

following:

$$Z_{11}/n \approx 1\ \Omega$$

$$f_o \approx 2.5\text{KH}$$

$$f_{res} \approx 15\ \text{GHz}$$

$$Q \approx 6$$

$$n \approx 15 \times 10^9/2.5 \times 10^3 = 6 \times 10^6$$

If there are 10^4 such "bellows" in the SSC, each than would contribute $6 \times 10^6/10^4 = 600\Omega$. If ewach is modeled by the circuit above, $R \approx 100\Omega$, and the resulting energy kick available from a change of $q = 5 \times 10^9$C would be

$$\Delta E \approx qR\omega_{res}Q \approx 28\ \text{KeV}.$$

This is several times the resolution now being planned in the ANL facility. All of the above is, in a sense, a swindle. Better estimates must be made to properly assess the potential of the beam method. (Note - See the short note by Simpson when TBCI based estimates are made - J.S.)

The sensitivity of the facility could be increased by a factor of 50 or so by the addition of a short pulse, perhaps 300 KeV witness. Such a witness could be obtained from a photo cathode illuminated from a triggered laser or

from Cerenkov light produced by part of the main pulse. The corresponding low β would impose additional contraints on the length of test objects but for many experiments would not introduce serious problems.

Summary

Wire measurements are applicable to frequencies up to 1.5 GHz, maybe 3 or 4 with effort and in special cases. Beam measurements appear useful to perhaps 20 GHz provided the driving and witness pulses are < 10 ps. More investigation of this proposed method must be made.

Finally, we urge more open, frank, no embarrassment discussions between hardware and non-hardware people to better define the problems.

A Better Estimate of Expected Beam Wake Test Sensitivity

J. Simpson
Argonne National Labortory

In the Measurement Group summary report we indicated that the quick estimate of bellows wakes was in suspect. Consequently, I have done a couple of TBCI (Tom Wieland's code) runs to get a better number for the longitudinal and transverse kicks that one would obtain from a bellows convolution.

A single convolution, 5 mm radial by 3 mm longitudinal was modeled in a 3 cm diameter tube. A single pulse of gaussian shape, sigma=2 mm, beta=1.0, was the beam pulse. Figures 1 and 2 show the TBCI calculated wake potentials for beam both on and off axis (off axis by 1.0 cm).

From these results, I conclude that for a 5 nC drive pulse, the initial design value of the ANL test facility, the corresponding kicks felt by the witness pulse are 2.8 KeV and .04 mrad for the longitudinal and transverse cases respectively. The longitudinal number is in reasonable agreement with the preliminary estimate obtained at the workshop. The transverse kick is considerably smaller. The proposed ANL facility should still be capable of measuring the longitudinal wake produced by a single convolution but will probably not be able to measure the small angular kick without modification to the experiment or to the facility.

The expected angular resolution of the facility is a few tenths of a mrad. Several convolutions could be simultaneously measured. Another improvement could be modification of the first 90 deg bend from the linac to permit 15 nC drive pulses. A third possibility is that of generating a much lower energy witness pulse by using a photocathode triggered by either Cerenkov or laser light plus a small (few kV) column. The present design will have a 15 MeV witness to avoid phase slip in tests of long objects, but for short object tests a low energy beam would work well and yield much more sensitivity.

I will conclude by repeating a conclusions of the Measurement Group - R&D in this area must be done soon.

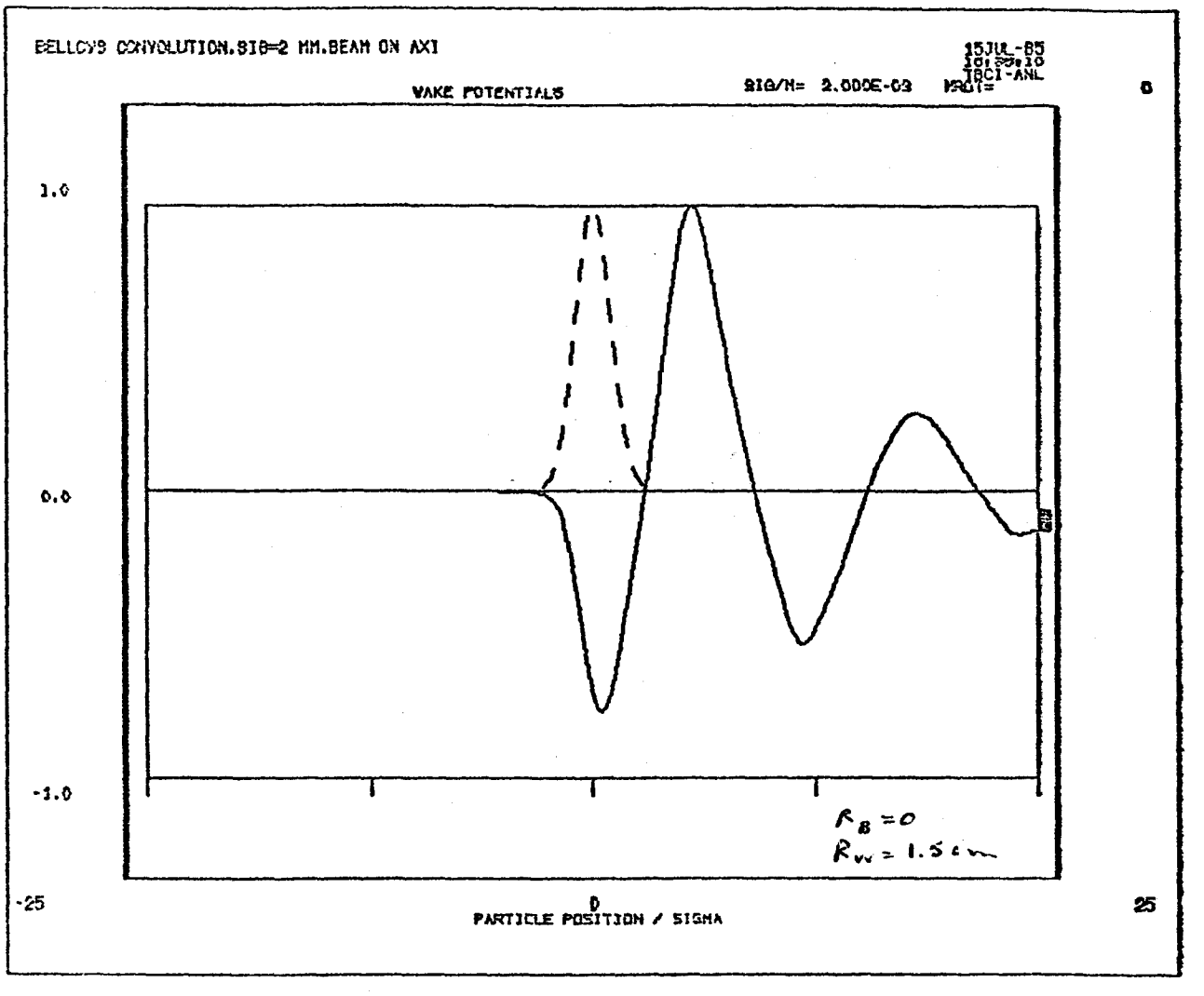

LINE CHARGE DENSITY MIN/MAX= 0.000E+00/ 1.995E+02AS/M, SCALE= 1.995E+02AS/M AT R= 0.000E+00M , OR 1.000E+00 AS TOTAL
LONGITUDINAL WAKE MIN/MAX=-4.319E+11/ 5.613E+11 V , SCALE= 5.613E+11 V AT R= 1.500E-02M , OR 5.613E+11 VAS/M**0

INTEGRATED LONGITUDINAL WAKE * CHARGE DENSITY = -3.113E+11VAS , OR -3.113E+11 VAS/M**0

Fig. 1. Long wake, beam on center, σ = 2 mm.

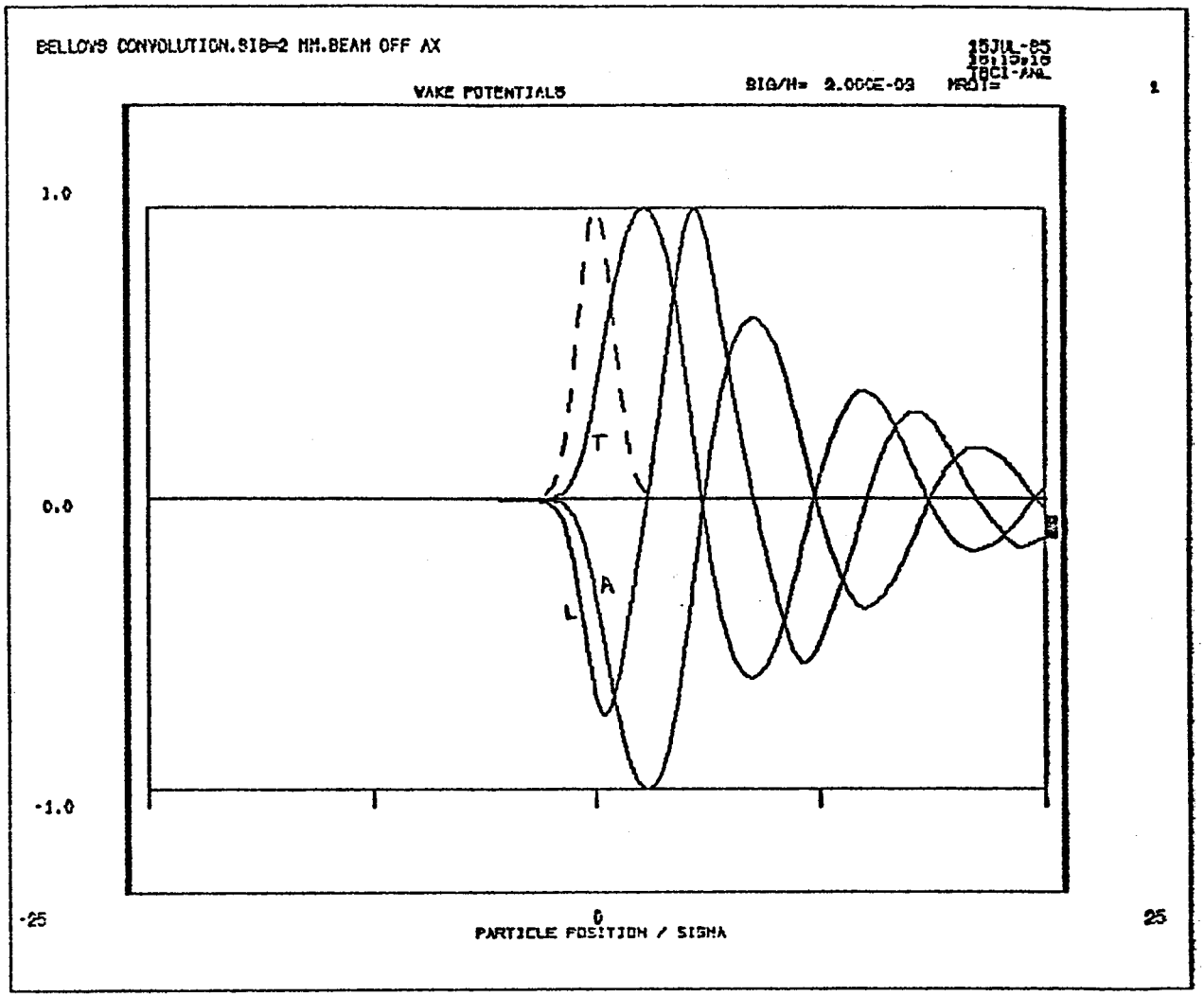

Beam Set at R=1.0 cm

```
LINE CHARGE DENSITY MINMAX= 0.000E+00/ 1.995E+02AS/M, SCALE= 1.995E+02AS/M AT R= 1.000E-02M , OR 1.000E+00 AS TOTAL
AZIMUTHAL    WAKE   MINMAX=-1.683E+11/ 1.041E+11 V  , SCALE= 1.683E+11 V   AT R= 1.500E-02M , OR 1.683E+13 VAS/M**1
TRANSVERSE   WAKE   MINMAX=-1.042E+11/ 1.685E+11 V  , SCALE= 1.685E+11 V   AT R= 1.500E-02M , OR 1.685E+13 VAS/M**1
LONGITUDINAL WAKE   MINMAX=-4.484E+11/ 6.017E+11 V  , SCALE= 6.017E+11 V   AT R= 1.500E-02M , OR 4.011E+15 VAS/M**2

INTEGRATED  AZIMUTHAL    WAKE * CHARGE DENSITY = -6.351E+10VAS  , OR -6.351E+12 VAS/M**1
INTEGRATED  TRANSVERSE   WAKE * CHARGE DENSITY =  6.883E+10VAS  , OR  6.883E+12 VAS/M**1
INTEGRATED  LONGITUDINAL WAKE * CHARGE DENSITY = -3.225E+11VAS  , OR -2.150E+15 VAS/M**2
```

Fig. 2. Pipe radius = 1.5 cm; wakes at pipe radius.

EXPERIENCE WITH WIRE IMPEDANCE MEASUREMENTS

S. Giordano

July 10, 1985

A transmission line test set up, that was constructed at BNL, is shown in Fig. 1. Figs 2 and 3 show the amplitude and phase variation as a function of $V = \frac{V_r}{V_o}$ (where V_r is the reference voltage and V_o is the test line voltage.) These variations are the result of physical differences between the two lines. No great care was taken in constructing this preliminary test set up, and a reduction of these variations can be achieved by improving the mechanical tolerances. These variations can be added or subtracted from the final measurements (to be made later), to cancel out their effect. The two coaxial lines from the power splitter must be of equal length as are the two output coaxial lines.

Once the system has been balanced (as above) the insertion section is removed and replaced with the particular piece of equipment to be tested. Figs. 4 and 5 show the amplitude and phase of V for a pick up and clearing electrode system (with no damping). It can be shown that the longitudinal impedance is given by

$$Z = 2Z_o\left(\frac{1}{V} - 1\right)$$

where Z_o is the characteristic impedance of the insertion section (in our case, for the Ø.012" wire, Z_o=340Ω).

(Please note that Figs. 4 and 5 cover the full frequency range - the actual measurements were made by expanding the frequency sweep, to obtain better resolution, as shown in Figs. 6 and 7.

To get some idea as to the resolution and accuracy of the system, we look at Figs. 8, 9 and 10, 11 where the voltage V (in db) is ploted as a function of z. Depending on the network analyzer used, if we take an absolute accuracy of .01db, we see that at low impedances (10Ω) we can have an error of ±10%. This error decreases as we go to higher impedances.

To the above errors we must add, as previously noted, to the errors resulting from the variations between the two lines, but as also noted these can be taken into account.

Another error that must be taken into account is the effect of the wire. Test were made, by comparing with bead measurements on cavities at 200, 400 and 800 MHz, errors at 200 MHz were negligible while at 800 MHz they were ≈5%. Calculations showed about the same effect.

Overall, an accuracy of ±10% can be achieved without too much difficulty.

Limitations

Waveguide modes limit the above system to frequencies below ≈2GHz.

With the 6 foot long tapered sections used in the above set up, severe mismatch below 80 MHz can lead to additional errors.

Below 80 MHz a straight through 50Ω system can be used (an inner pipe of ≈1" diameter). It can be shown that at very low frequencies the error of the pipe is small.

Results

The final result after damping (both external and internal) the pick up and clearing electrodes are shown in Fig .1 A comparison of the damped and undamped (Figs. 4 and 5) clearly demonstrate the usefulness of the instrumentation.

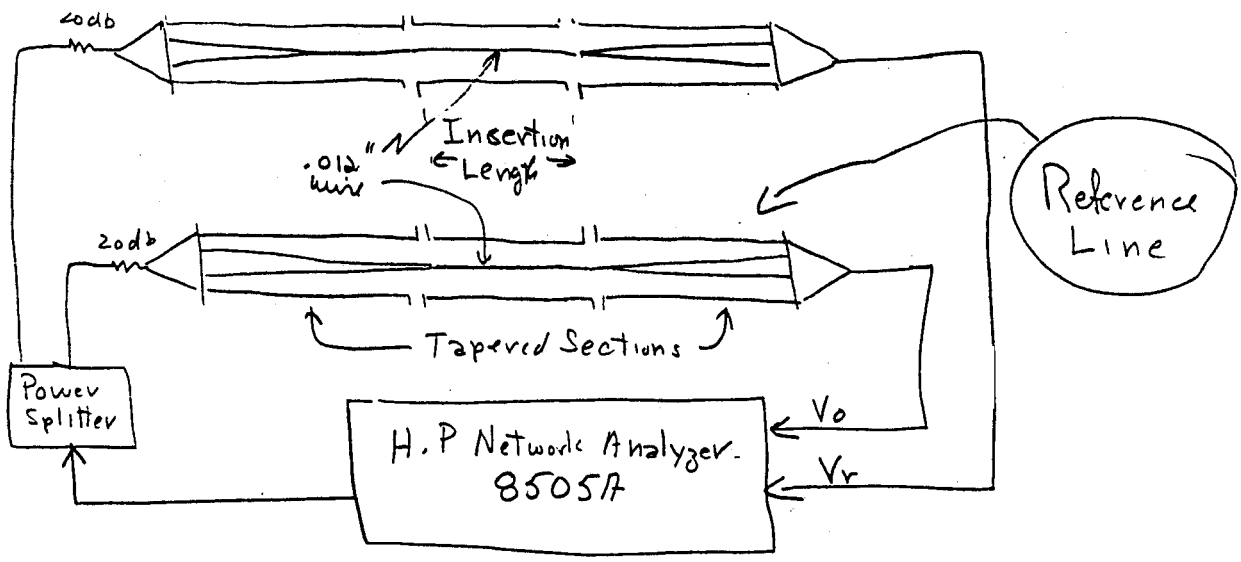

Fig. 1. Typical wire measurement set up.

Tapered sections

a) outer pipe ≈ 3 in. diam.
b) Length ≈ 6 ft
c) Inner pipe taper with triangular distribution--seemed at the time easiest to machine (Foundations for Microwave Engineering, Collins, p. 239)

Insertion Length

a) The length of the insertion line is made equal to the length of the piece of equipment to be tested.

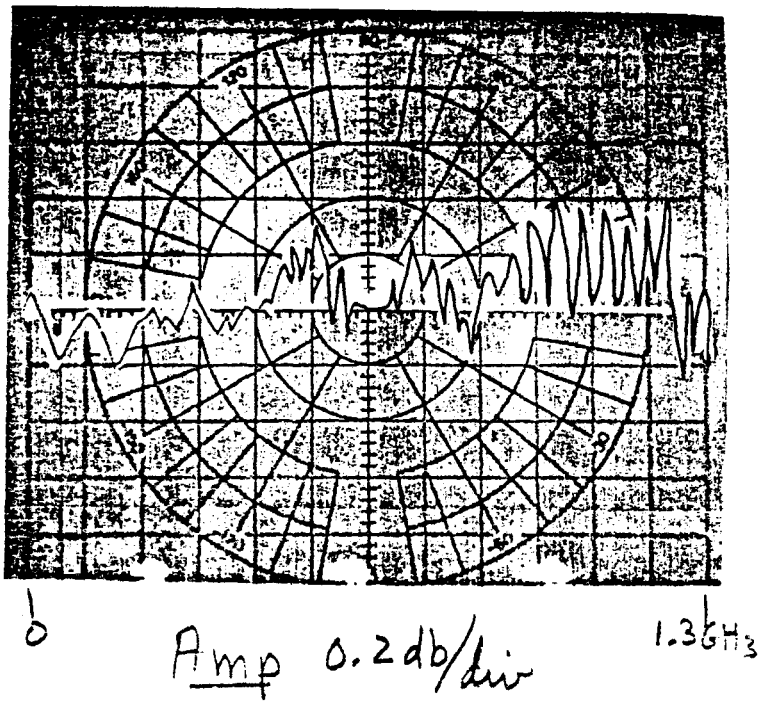

Fig. 2

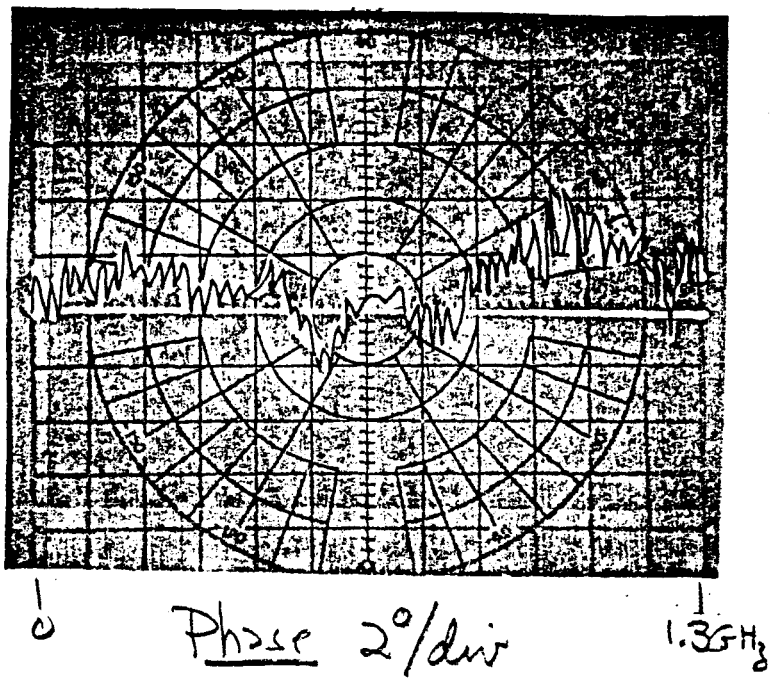

Fig. 3

No Load

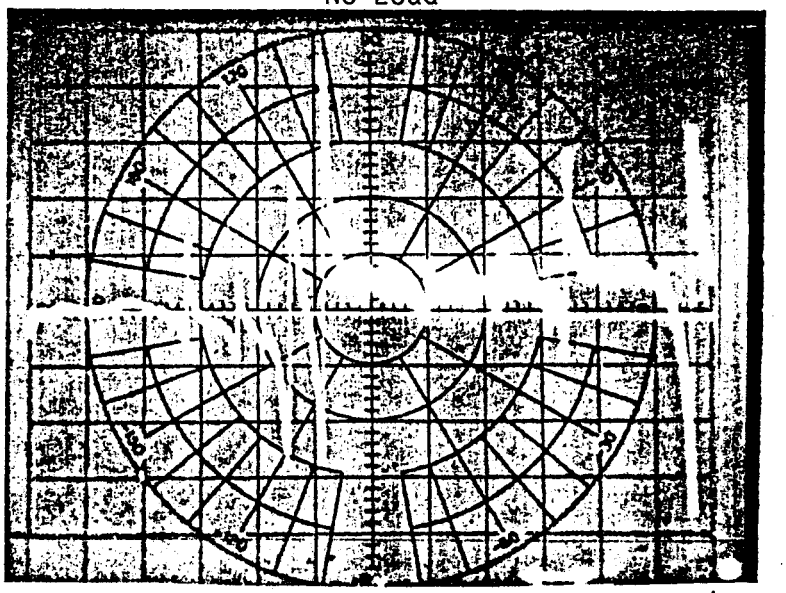

0 Phase 10°/div 1300 MHz

Fig. 4

No Load

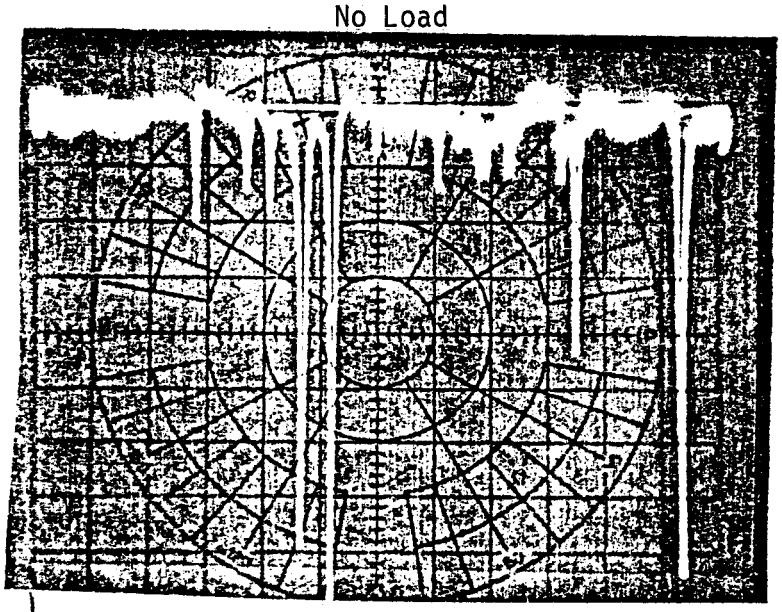

0 Amp 1 db/div 1300 MHz

Fig. 5

No Load at All

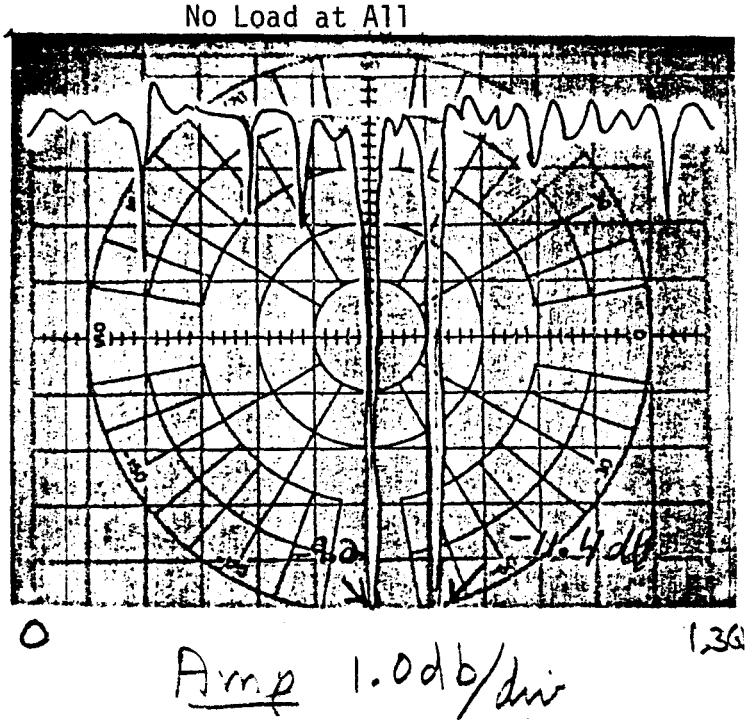

Fig. 6

No Load

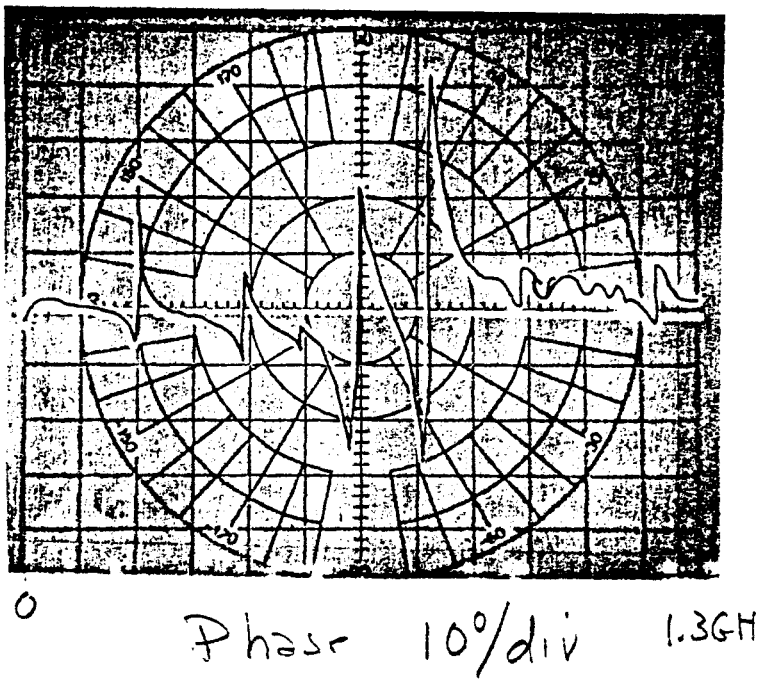

Fig. 7

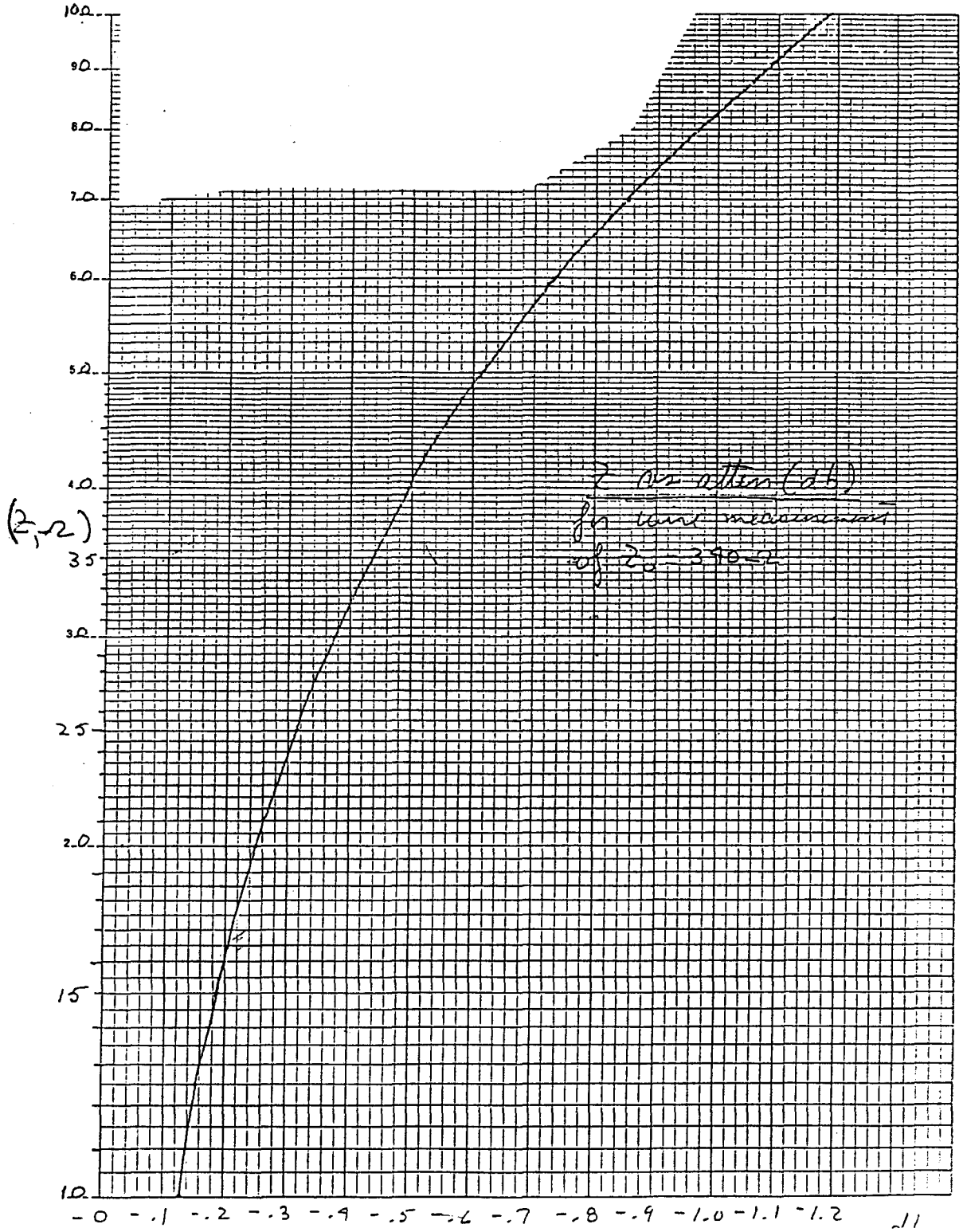

10.0
9.0
8.0
7.0
6.0
5.0
4.0
(Z, Ω)
3.5
3.0
2.5
2.0
1.5
1.0
-0 -.1 -.2 -.3 -.4 -.5 -.6 -.7 -.8 -.9 -1.0 -1.1 -1.2
Z as atten (db)
for wire measurement
of Z0 = 390 Ω

Fig. 8

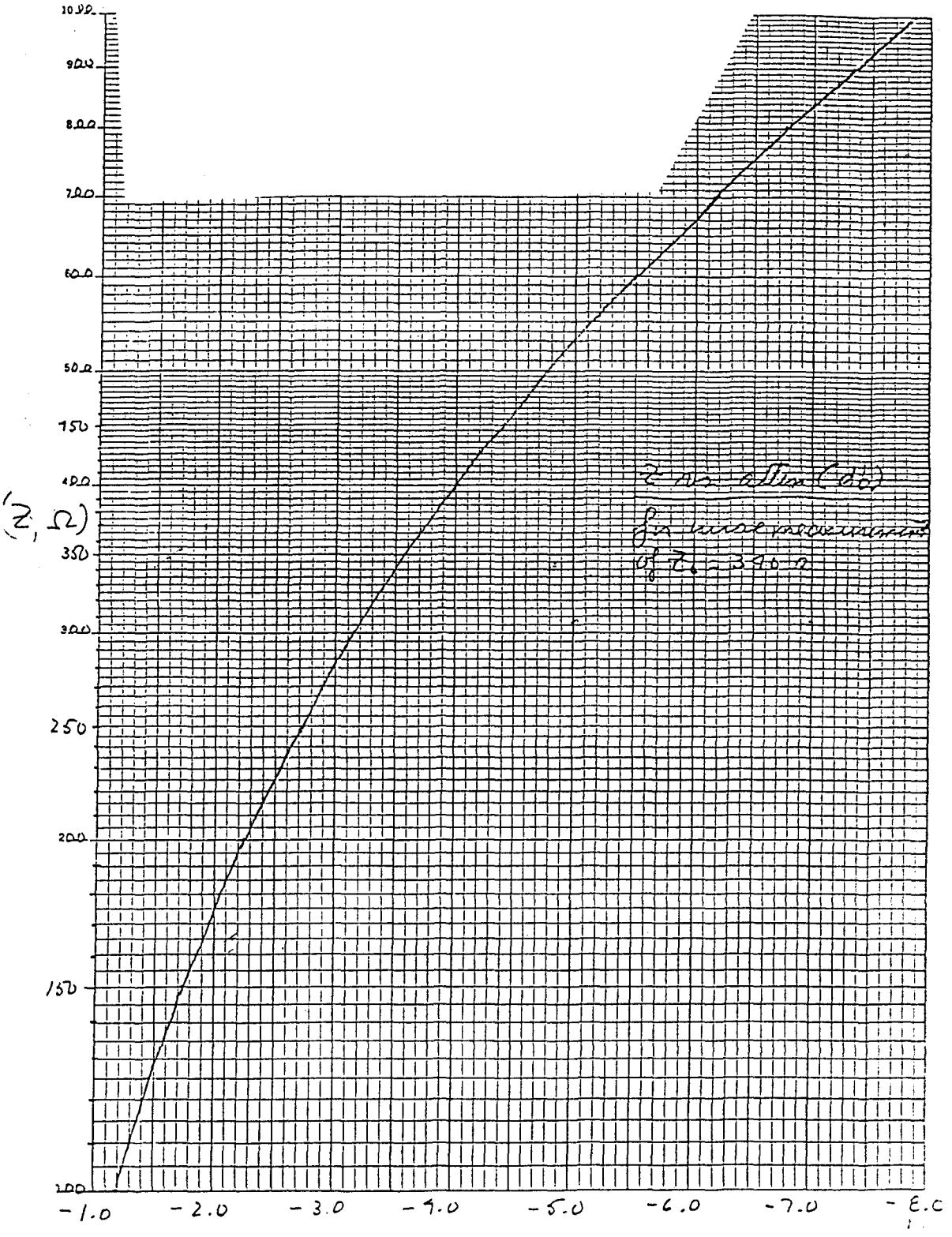
1000
900
800
700
600
500
450
400
350
300
250
200
150
100
(Z, Ω)
-1.0
-2.0
-3.0
-4.0
-5.0
-6.0
-7.0
-8.0

Fig. 9

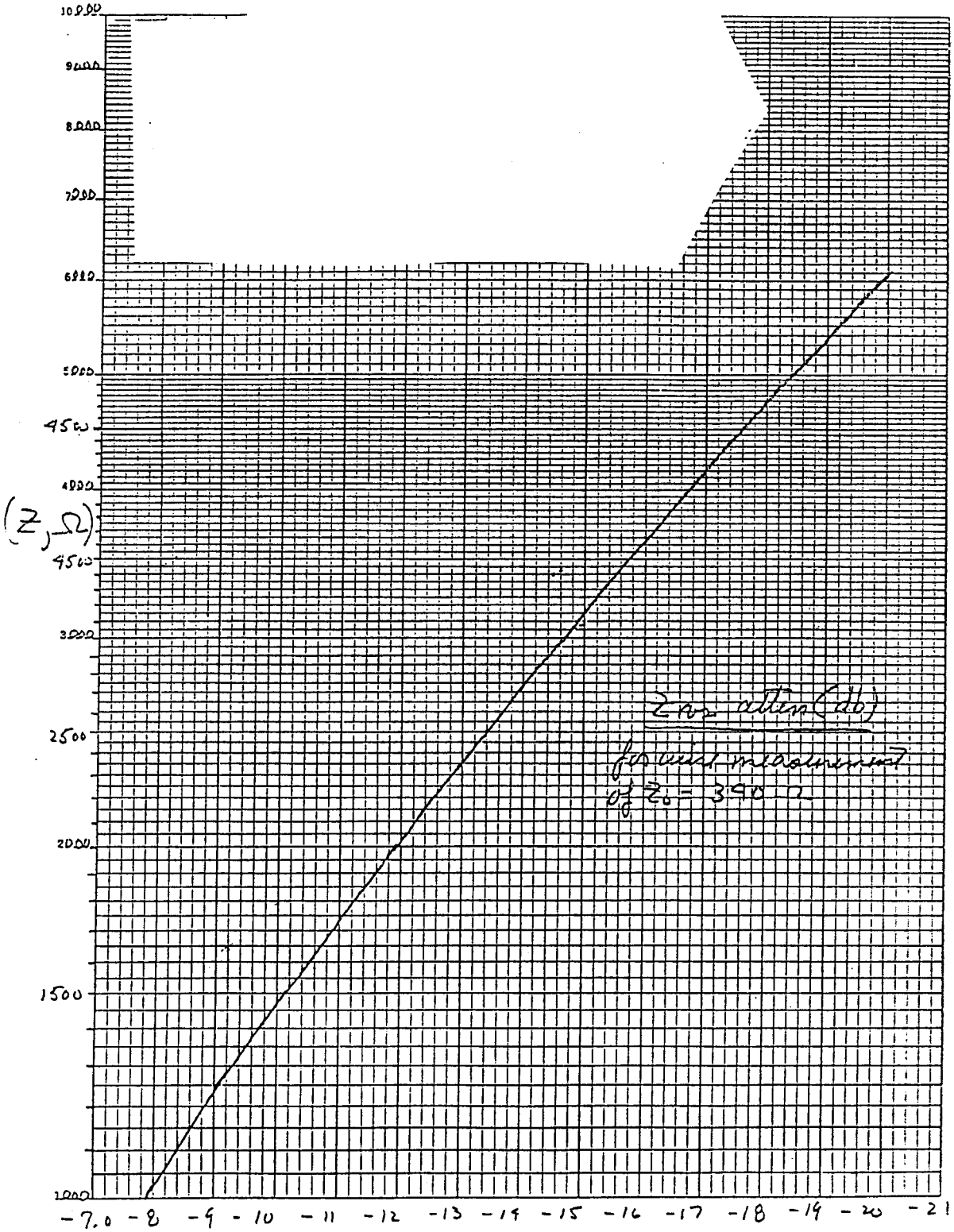
10000
9000
8000
7000
6000
5000
4500
4000
(Z, Ω)
4500
3000
2500
2000
1500
1000
-7.0 -8 -9 -10 -11 -12 -13 -14 -15 -16 -17 -18 -19 -20 -21
Z vs atten (db)
for wire measurement
of Z₀ = 390 Ω

Fig. 10

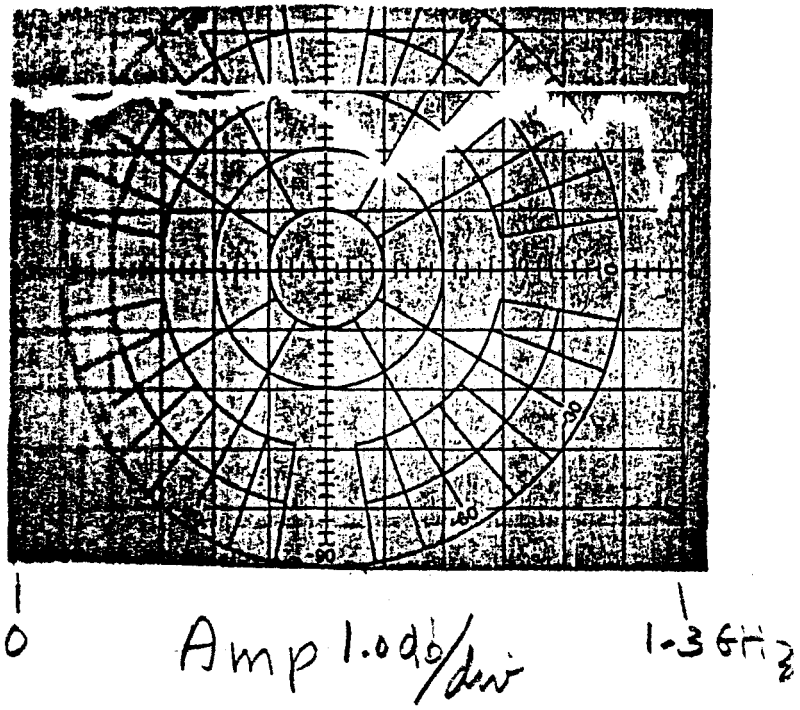

Fig. 11

SSC KICKER IMPEDANCES*

E. Colton and T. F. Wang, MS H829

Los Alamos National Laboratory
Los Alamos, NM 87545

We have calculated the longitudinal and transverse complex impedances Z_ℓ/n and Z_t, respectively, for both the SSC injection and abort kickers described in Reference Design Study (RDS) Appendix A. The calculations assumed that no attempt was made to shield the beam from the kickers. We took the injection and abort kickers to be as specified.[1] The injection kickers were ferrite with a single-turn design, and the abort kickers were of a "window-frame design" with tape wound cores. Table I lists the kicker characteristics relevant to the impedance calculations. The apertures for the injection kicker were estimated.

TABLE I. KICKER SPECIFICATIONS

	Injection Kickers	Abort Kickers
Type	C-magnet	Window-frame
Number of modules, N_K	6	9
Length of each module, ℓ	0.7 m	1.0 m
Core	Ferrite	Tape Wound
Half height, a	15 mm	27 mm
Half width, b	20 mm	30 mm

For a C-magnet kicker, the expressions for the complex impedance were obtained from Nassibian.[2] We write

* Work performed under the auspices of the US Dept. of Energy.

$$\mathrm{Re}\left(\frac{Z_\ell}{n}\right) = \frac{Z_o N_K}{4n}(1 - \cos k\ell)F \quad , \tag{1}$$

$$\mathrm{Im}\left(\frac{Z_\ell}{n}\right) = \frac{Z_o N_K}{4n}(k\ell - \sin k\ell)F \quad , \tag{2}$$

$$\mathrm{Re}(Z_t) = \frac{cZ_o N_K}{4\omega b^2}(1 - \cos k\ell)F \quad , \text{ and} \tag{3}$$

$$\mathrm{Im}(Z_t) = \frac{cZ_o N_K}{4\omega b^2}(k\ell - \sin k\ell)F \quad , \tag{4}$$

where Z_o is the characteristic impedance of the kicker (assume $Z_o = 25\ \Omega$), and the wave number $k = \omega\mu_o b/(Z_o a)$.[2] The frequency $f = \omega/2\pi = nf_r$, where f_r is the revolution frequency of particles. In the SSC, f_r is 3.3 kHz. The "F" factors appearing in Eqs.(1)-(4) describe ferrite losses at high frequency for the injection kickers; μ_o is the permeability of free space, $\mu_o = 4\pi \times 10^{-7}$ H/m.

In the case of the abort kickers, the right-hand sides of Eqs. (1) and (2) must be multiplied by $(x/b)^2$, where x is the beam displacement from center line.[3] For a well-centered beam, the longitudinal impedance is essentially zero. For the calculation we merely take $x/b = 0.1$.

Nassibian has stated[2] that the expressions in Eqs. (1)-(4) are valid strictly below the cut-off frequency of the structure. For higher frequencies, one should account for ferrite losses. This has been done by G. Schaffer et al.[4] in an internal note for the IKOR proposal. They obtain

$$F = e^{-2a/s} \Big/ \left(1 + \frac{R_F}{R_A}\right)^2 \quad , \tag{5}$$

where the skin depth s is given by

$$s = \frac{c}{\omega}\left(\frac{2}{\varepsilon\mu}\right)^{1/2} \left\{\left[1 + \left(\frac{c^2\mu_0}{\omega\rho\varepsilon}\right)^2\right]^{1/2} - 1\right\}^{-1/2} , \tag{6}$$

$$R_A = \frac{a}{\mu_0 b\ell} , \tag{7}$$

and

$$R_F = \frac{a + b}{\mu\mu_0 s\ell} . \tag{8}$$

In the calculations, we assume a constant permittivity $\varepsilon = 11$, a resistivity $\rho = 10^3$ Ω-m, and a constant relative permeability $\mu = 100$.

The impedances are presented in Figs. 1-2 for the injection kickers and in Figs. 3-4 for the abort kickers. We present the data up to 100 Mhz ($n = 3 \times 10^4$). For longitudinal stability, we observe $|Z_\ell/n|$ is about 0.04 Ω for the injection kickers and about 6×10^{-4} Ω for the abort kickers. The transverse impedance peaks at about 1.0-1.2 MΩ/m.

It should be noted that the impedances of the abort kicker were calculated here by using the resistivity, the relative permeability, and the permittivity of ferrite. If the loss factor were calculated according to the parameters of iron, then the impedances of the abort kicker should be lower than those shown.

Referring to the RDS,[1] it appears that these impedances are modest in comparison to those from other sources.

References

1. SSC Reference Designs Study, Appendix A, pp. A-194 to A-210.

2. G. Nassibian,"The Low Frequency Beam Impedance of Matched Travelling Wave Kickers," CERN/PS 84-25 (BR) 1984.

3. G. Nassibian and F. Sacherer, "Methods for Measuring Transverse Coupling Impedances in Circular Accelerators," Nucl. Inst. Meth., 159, 21(1979).

4. G. Schaffer, V. G. Vaccaro and G. Wüstefeld,"Ferrite Losses and Implications to Beam Stability in IKOR," KFA Julich internal note 2.5.GS/VV/GW.1 (1981), unpublished.

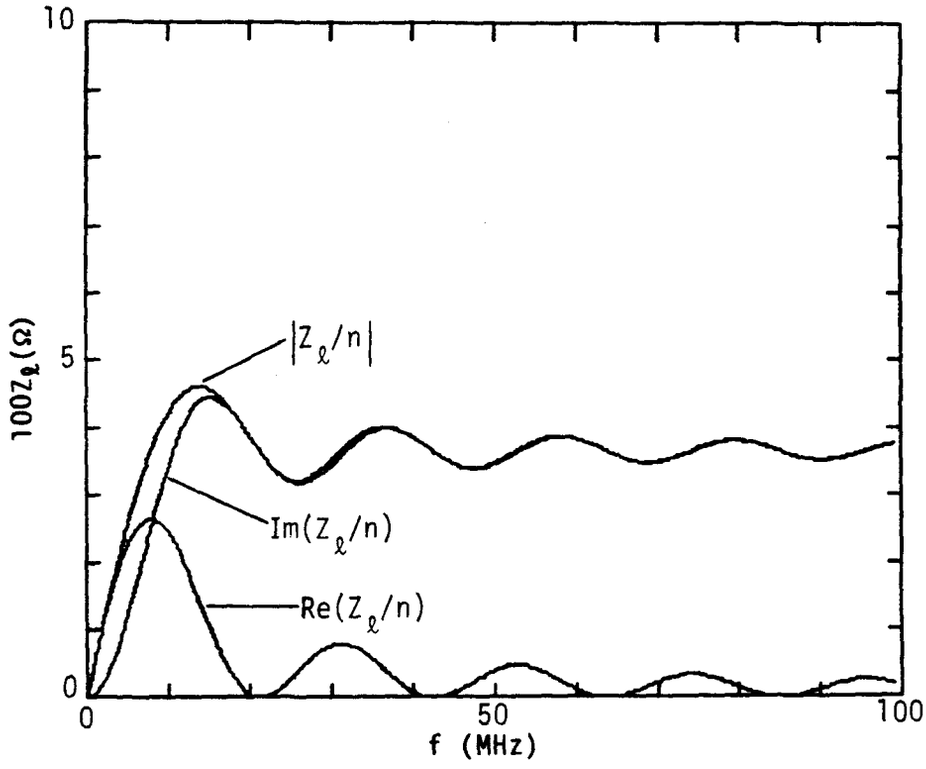

Fig. 1. Z_ℓ/n vs. frequency for the injection kickers.

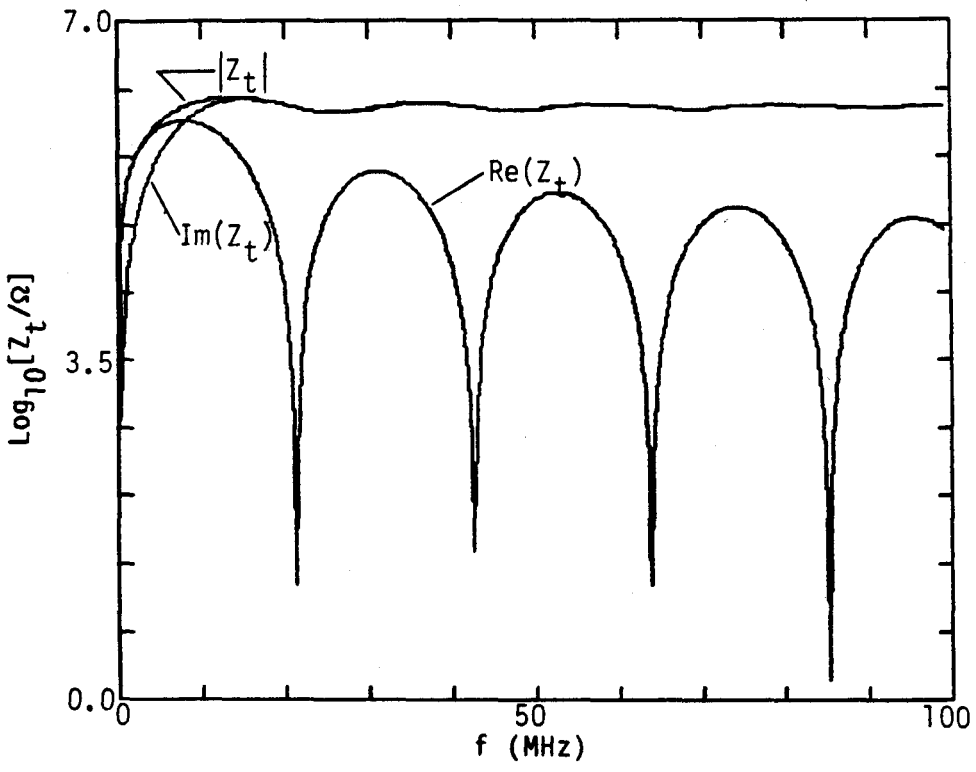

Fig. 2. $\mathrm{Log}_{10}[Z_t/\Omega]$ vs. frequency for the injection kickers.

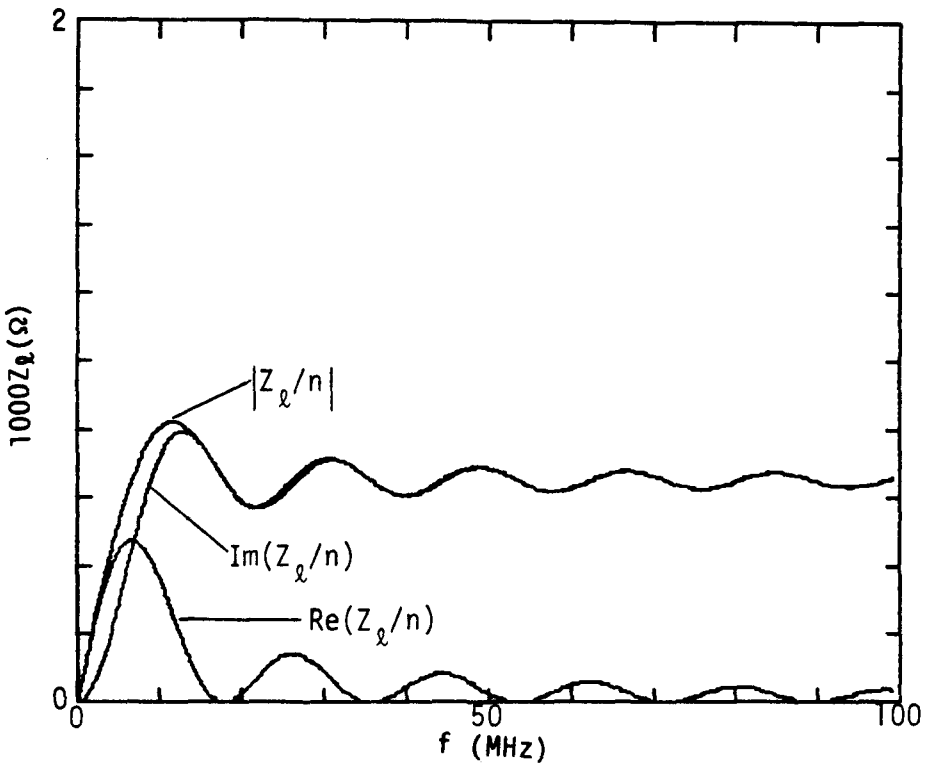

Fig. 3. Z_ℓ/n vs. frequency for the abort kickers.

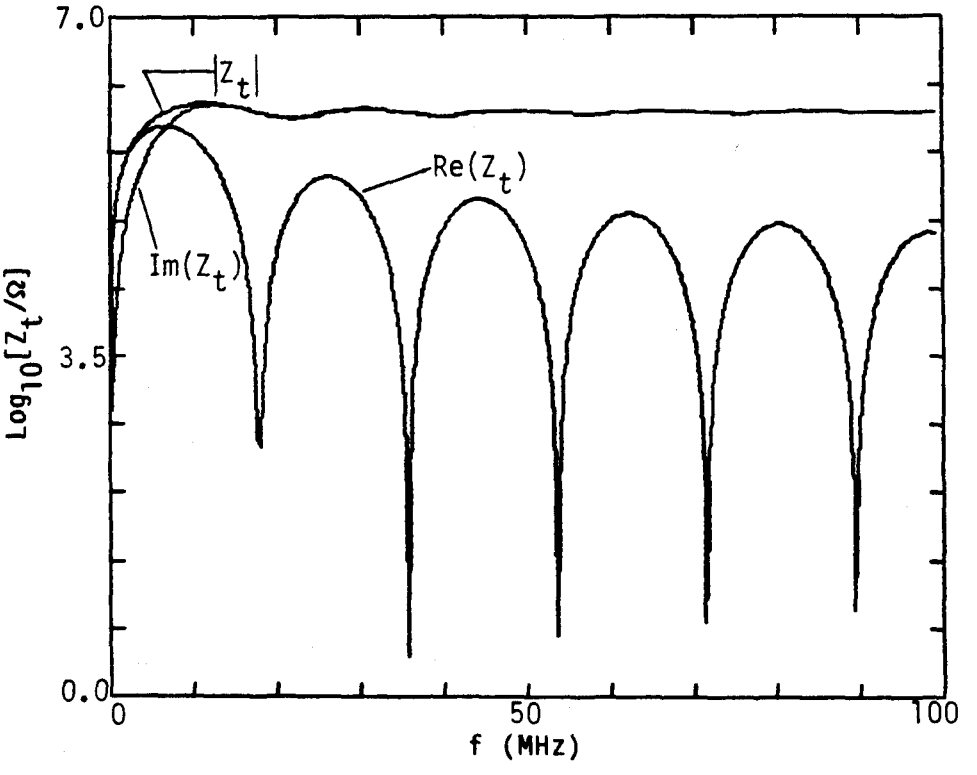

Fig. 4. $Log_{10}[Z_t/\Omega]$ vs. frequency for the abort kickers.

LONGITUDINAL AND TRANSVERSE COUPLING IMPEDANCES OF BEAM POSITION MONITORS

R. Shafer

Fermi National Accelerator Laboratory
P.O. Box 500
Batavia, Illinois 60510

1. Introduction

Beam position monitors by their very nature must absorb power from the beam. By definition, this implies the existance of the real part of a longitudinal coupling impedance. If the coupling impedance is frequency dependent, as it must be since there is no DC coupling, an imaginary component must also exist. Furthermore, if there is any transverse dependence of the coupled power, then there must also be a transverse coupling impedance.

The purpose of this note is to review the properties of both electrostatic and stripline type beam position monitors, and in particular to estimate the coupling impedances of the latter. The text is divided into the following sections:

2. Stripline vs. Electrostatic Pickups
3. Signal Response of Stripline Pickups
4. Longitudinal and Transverse Coupling Impedances
5. Application to SSC

2. Stripline vs. Electrostatic Pickups

If a metallic strip is placed inside the beam vacuum chamber in such a position that the passing beam bunches can induce image charges on the inside surface, then there must also be image currents induced on the outer surface (facing the vacuum chamber wall). These image currents on the outer surface must travel at the speed of light (as required by the wave equation in vacuum), unlike the image charges on the inner surface which must travel at the beam velocity. At certain frequencies where the strip is a multiple of half integer wavelengths long, it is highly resonant. The coupling impedance increases rapidly near resonance, and the phase switches from inductive (below resonance) to capacitive (above resonance). For a 20 cm strip, this would occur at harmonics of 750 MHz.

If this strip is tied to an external circuit, currents can flow to drain off the induced charge on the outside surface of the strip. If the connection to the external circuit is not impedance matched to the strip, or if the connection is not made at the end of the strip, the resonances are only damped but not eliminated. Although all the induced charge is eventually drained off in any case, it only drains off immediately (i.e., without standing waves) if:

a) the impedance of the external circuit is equal to the characteristic impedance of the strip (as defined by the inductance and capacitance per unit length), and

b) the connection is made at either one or both ends of the strip (i.e., not in the middle).

If one assumes that these sharp resonances are destructive to the beam, and should be avoided, then the beam position monitor electrodes should be of the stripline design. There are many variations of the stripline design, but they all share the two characteristics mentioned above.

3. Signal Response of Stripline Beam Position Monitors

The characteristics and signal response of stripline BPM's (beam position monitors) is reviewed elsewhere[1]. In particular, for a centered bunched beam the voltage output of a single electrode is, for the mth harmonic of the rf bunching frequency:

$$V_m = \frac{eN\omega_0 Z_0}{\pi}\left(\frac{\phi_0}{2\pi}\right)\sin\left(\frac{m\omega_0 \ell}{c}\right)\exp\left[\frac{-m^2\omega_0^2\sigma^2}{2}\right] \qquad (3.1)$$

where for a typical application (Tevatron BPM's)

e	electron charge	1.6×10^{-19} Coul
N	# particles in a single bunch	$\geq 10^{+8}$
ω_0	2π x bunching frequency	3.33×10^{8} sec^{-1}
Z_0	characteristic impedance of stripline	50 ohms
ϕ_0	subtended angle of stripline	120°
m	harmonic of bunching frequency	1
ℓ	length of stripline	20 cm
c	speed of light	3×10^{10}cm/sec
σ	RMS bunch length	1-2 nsec

the above stripline BPM, with a 70 mm aperture, was suitable to commission the Tevatron with about 3×10^{9} total circulating protons[2,3].

Figures 1 and 2 show the side view and end view of a typical two-electrode geometry stripline beam position monitor. The peak voltages seen at the outputs of the two striplines for a small beam centered at r_0, θ_0 are:

$$V_A(\omega) = \frac{Z_0\phi_0 I_0(\omega)}{2\pi}\sin\left(\frac{\omega\ell}{c}\right)\left[1+\frac{4}{\phi_0}\sum_{n=1}^{\infty}\frac{1}{n}\left(\frac{r_0}{b}\right)^n\cos n\theta_0\sin\left(\frac{n\phi_0}{2}\right)\right] \qquad (3.2)$$

and

$$V_B(\omega) = \frac{Z_0\phi_0 I_0(\omega)}{2\pi}\sin\left(\frac{\omega\ell}{c}\right)\left[1+\frac{4}{\phi_0}\sum_{n=1}^{\infty}\frac{1}{n}\left(\frac{r_0}{b}\right)^n\cos n\theta_0\sin\left[n\left(\pi+\frac{\phi_0}{2}\right)\right]\right] \qquad (3.3)$$

where $I_0(\omega)$ is the peak beam current at frequency ω. The total power output into a termination of impedance Z_0 is then

$$P(\omega) = \frac{1}{2Z_0}\left[V_A^2(\omega)+V_B^2(\omega)\right] = Z_0\left(\frac{\phi_0}{2\pi}\right)^2 G(x,y)\sin^2\left(\frac{\omega\ell}{c}\right)I_0^2(\omega) \qquad (3.4)$$

where
$$G(x,y) = 1 + \left[\left(\frac{y}{\phi_0}\right)^2 \sin^2\left(\frac{\phi_0}{2}\right) + \left(\frac{y}{\phi_0}\right)\sin\phi_0\right]\frac{x^2}{b^2} - \left[\left(\frac{y}{\phi_0}\right)\sin\phi_0\right]\frac{y^2}{b^2} \qquad (3.5)$$

4. Longitudinal and Transverse Coupling Impedances

The real part of the longitudinal coupling impedance must absorb the power output calculated in Section 3. Specifically for P electrode pairs

$$\frac{1}{2}\mathrm{Re}\left[Z_{\parallel}(\omega)\right] I_0^2(\omega) = P Z_0 \left(\frac{\phi_0}{2\pi}\right)^2 G(x,y) \sin^2\left(\frac{\omega \ell}{c}\right) I_0^2(\omega) \qquad (4.1)$$

This may be solved for $\mathrm{Re}[Z_{\parallel}(\omega)]$, and the imaginary part of $Z_{\parallel}(\omega)$ may be determined by using the Kramers-Kronig relations[4]:

$$Z_{\parallel}(\omega) = 2 P Z_0 \left(\frac{\phi_0}{2\pi}\right)^2 G(x,y)\left[\sin^2\left(\frac{\omega \ell}{c}\right) + j \sin\left(\frac{\omega \ell}{c}\right)\cos\left(\frac{\omega \ell}{c}\right)\right] \qquad (4.2)$$

Using $\omega = n\omega_0$ we may write the low frequency longitudinal coupling impedance (for a centered beam):

$$\frac{Z_{\parallel}}{n} = 2 P Z_0 \left(\frac{\phi_0}{2\pi}\right)^2 \frac{\ell}{R} \ \text{ohms} \qquad (4.3)$$

where R is the mean ring radius.

It is important to note that although the impedance (4.2) is inductive at low frequencies, it switches to capacitive when $\omega = \pi c/2\ell$. For a 20 cm long electrode, this occurs at 375 Mhz. This impedance function will oscillate between inductive and capacitive at higher frequencies as determined by eqn. 4.2.

The transverse impedance is given by[5]

$$Z_x(\omega) = \frac{+R}{b^2}\left[\left(\frac{y}{\phi_0}\right)^2 \sin^2\left(\frac{\phi_0}{2}\right) + \left(\frac{y}{\phi_0}\right)\sin\phi_0\right]\frac{Z_{\parallel}(\omega)}{n} \ \frac{\text{ohms}}{\text{m}} \qquad (4.4)$$

and

$$Z_y(\omega) = \frac{-R}{b^2}\left[\left(\frac{y}{\phi_0}\right)\sin\phi_0\right]\frac{Z_{\parallel}(\omega)}{n} \ \frac{\text{ohms}}{\text{m}} \qquad (4.5)$$

Note that since the beam coupling to the electrodes decreases as the beam is moved vertically (for horizontal beam position monitors) the y component of the transverse coupling impedance is negative. Because beam position monitoring electrodes are traditionally placed at locations where the betatron amplitude functions are a maximum, the values of the ring-average Z_T may be as much as twice the canonical resistive wall value:

$$Z_x(\omega) = Z_y(\omega) = Z_T(\omega) = \frac{2R}{b^2}\frac{Z_{\parallel}(\omega)}{n} \ \frac{\text{ohms}}{\text{m}} \qquad (4.6)$$

5. Application to SSC

In the SSC, the most demanding requirements for the beam position monitors is in the commissioning stage where very low beam currents must be used in order not to quench magnets. In the case of the Tevatron, each BPM pickup contained two electrodes with ϕ=110° and ℓ=20 cm. In the case of the SSC, it appears that both coordinates must be measured at every quadrupole (one per half cell) so the pickup must be a 4-electrode design. However, as the aperture of the SSC is smaller than the Tevatron (33 mm vs. 70 mm) the resolution requirements, measured as a percentage of the aperture, are probably not as great. Hence a 4 electrode geometry with ϕ_0=55° and ℓ=20 cm will be used in the following calculations. Using Q as the quantity of BPM's required, the longitudinal and transverse low frequency coupling impedances are:

$$\frac{Z_{\parallel}}{n} = 4Q Z_0 \left(\frac{\phi_0}{2\pi}\right)^2 \frac{\ell}{R} \qquad (5.1)$$

$$Z_T = \frac{R}{b^2}\left(\frac{4}{\phi_0}\right)^2 \sin^2\left(\frac{\phi_0}{2}\right) \frac{Z_{\parallel}}{n} = \frac{16Q}{\pi^2 b^2} Z_0 \ell \sin^2\left(\frac{\phi_0}{2}\right) \qquad (5.2)$$

When a 4 electrode BPM is used, one pair is at a minimum of the betatron amplitude function when the other is at a maximum. Hence when this geometry is used, the two tranverse coupling impedances are equal.

Parameter	Ref. Design A	Ref. Design B	Ref. Design C
Peak field B (tesla)	6.5 T	5 T	3 T
Tune ν	97.76	115.26	121.26
Radius R (meters)	14,324m	17,985m	26,165m
Phase advance per cell	80°	80°	80°
Aperture (2b)(mm)	33	33	25
Q (# BPMs)	880	1037	1096
ϕ_0 (degrees)	55°	55°	55°
ℓ (cm)	20 cm	20 cm	20 cm
Z_0 (ohms)	50Ω	50Ω	50Ω
$Z_{\parallel}/n$ (ohms)	0.057	0.054	0.039
Z''_T (ohms/m)	11.2×10^6	13.2×10^6	24.2×10^6

References

1. R.E. Shafer, IEEE NS-32 #5, page 1933 (1985).

2. R.E. Shafer and R.E. Gerig, Proc. 12th Int. Conf. on High Energy Accelerators, page 609 (Fermilab, 1983).

3. R.E. Shafer and R.C. Webber, IEEE NS-28 #3, page 2290 (1981).

4. See Reference 1, equation 10.5.

5. See Reference 1, equation 11.2.

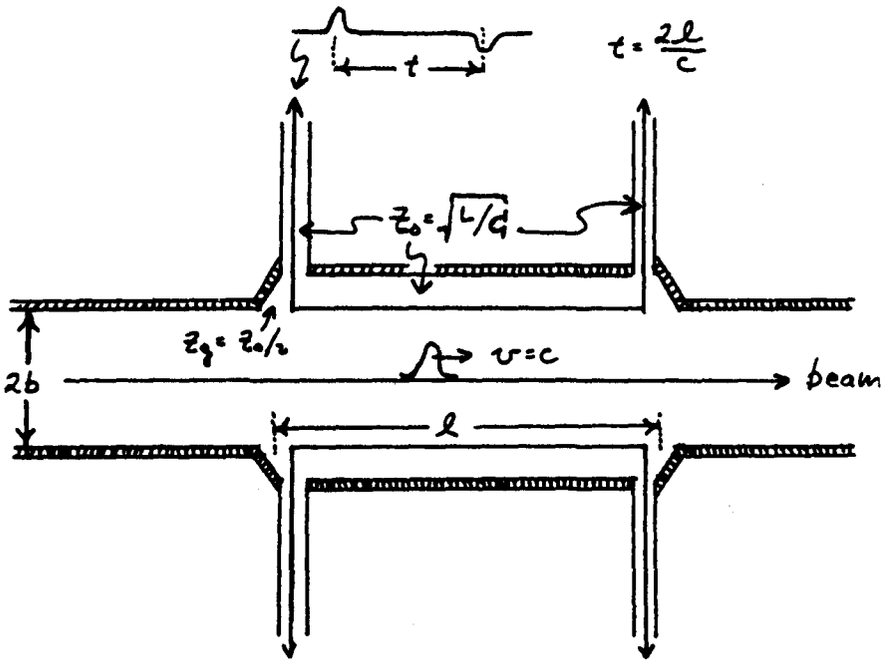

Figure 1. Side view of stripline beam position monitor.

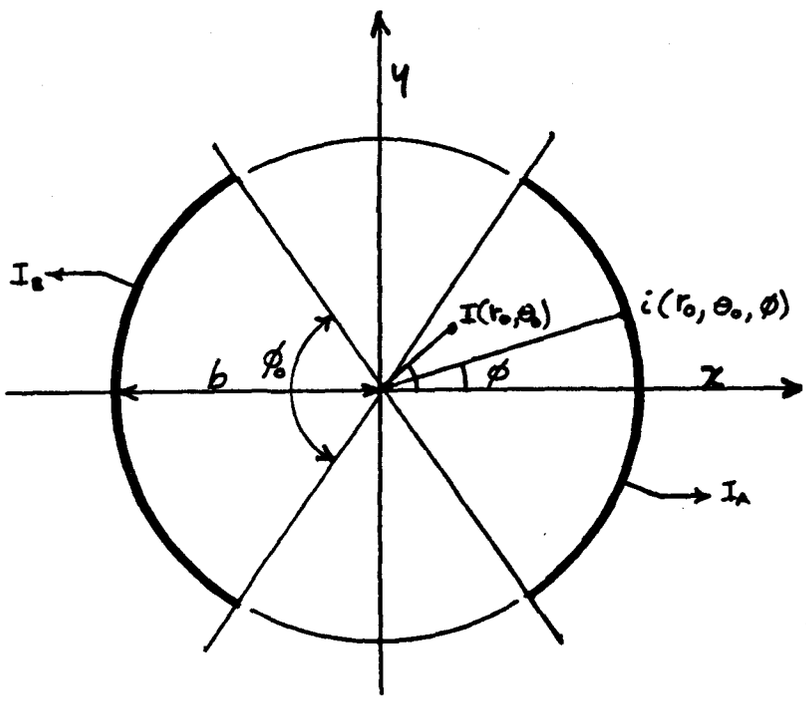

Figure 2. End view of stripline electrode geametry for calculating the equations in Section 3.

ON SHIELDING THE BEAM FROM KICKER MAGNETS AT HIGH FREQUENCIES

R. Shafer

Fermi National Accelerator Laboratory
P.O. Box 500
Batavia, Illinois 60510

1. Introduction

Kicker magnets contain a considerable amount of ferromagnetic material and introduce a large coupling impedance at high frequencies if not properly shielded. As kicker magnets are inherently low frequency devices, their performance will not be affected by shielding them from the beam at high frequencies. Specifically for the SSC, the kicker risetimes are:

Injection and injection abort kickers	10's of nsec
Main abort kicker	≥1 μsec

This note discusses the shielding properties of thin conducting tubes inside the kicker magnets. It is divided into the following sections:

2. Shielding Properties of Conducting Tubes in the Frequency Domain
3. Shielding properties of Conducting Tubes in the Time Domain
4. Relation to Skin Depth
5. Application to the SSC Abort Kicker

2. Shielding Properties of Conducting Tubes in the Frequency Domain

If a thin conducting tube of radius a, thickness b, and volume resistivity ρ is placed with its axis perpendicular to an oscillating dipole magnetic field given by:

$$B(\omega) = B_0 \sin \omega t \tag{2.1}$$

The magnetic field inside the tube is given by[1]

$$B_s(\omega) = \frac{B_0}{(1+\omega^2\tau^2)^{1/2}} \sin(\omega t - \epsilon) \tag{2.2}$$

where

$$\tau = \frac{\mu_0 a b}{2\rho} \tag{2.3}$$

and

$$\epsilon = \tan^{-1}(\omega\tau) \tag{2.4}$$

Hence we may define a 3 db bandwidth as

$$(1+\omega_c^2\tau^2)^{1/2} = \sqrt{2} \quad \text{or} \quad \omega_c = \frac{1}{\tau} = \frac{2\rho}{\mu_0 ab} \tag{2.5}$$

The attenuation of the dipole field inside the tube is the result of induced currents in the tube wall, which by necessity also produce a dipole moment outside the tube. For this reason, the kicker circuit impedance depends on the geometry and physical properties of the conducting tube.

It is assumed that reciprocity holds. If the conducting tube attenuates dipole fields from penetrating into the interior volume, it also prevents dipole moments produced by the beam from penetrating into the exterior volume (i.e., the kicker circuit). The induced currents in the tube walls by necessity also produce dipole fields in the interior volume which give rise to the transverse space charge impedance.

3. Shielding Properties of Conducting Tube in Time Domain

Equation (2.2) may be rewritten as:

$$B_s(\omega) = \left[\frac{1-j\omega\tau}{1+\omega^2\tau^2}\right] B_0 \sin \omega t \tag{3.1}$$

Using s=jω we can rewrite the part in brackets

$$\frac{1-j\omega\tau}{1+\omega^2\tau^2} = \frac{1-s\tau}{1-s^2\tau^2} = \frac{1}{1+s\tau} \tag{3.2}$$

If we impose a step function field at t=0

$$\begin{aligned} B(t) &= 0 \qquad t<0 \\ &= B_0 \qquad t \geq 0 \end{aligned} \tag{3.3}$$

then the Laplace transform is

$$B(s) = \frac{B_0}{s} \tag{3.4}$$

and the inverse transform of the product of eqns. 3.2 and 3.4 gives the time dependence of the field inside the tube:

$$B_s(t) = \mathcal{L}^{-1}\left\{\frac{B_0}{s}\,\frac{1}{1+s\tau}\right\} = B_0\left[1-e^{-t/\tau}\right] \tag{3.5}$$

where τ is given by eqn. 2.3.

4. Relationship to Skin Depth

The skin depth is defined as the thickness of a conductor to attenuate a normally incident plane wave to 1/e of its incident amplitude

$$\delta = \sqrt{\frac{2\rho}{\mu_0 \omega}} \tag{4.1}$$

Hence for a conducting tube with thickness b we can define the skin depth cutoff frequency as

$$\omega_{sc} = \frac{2\rho}{\mu_0 b^2} = \frac{a}{b}\omega_c \tag{4.2}$$

where ω_c was defined in eqn. 2.5. This skin depth cutoff frequency represents the frequency below which the longitudinal harmonics of the revolution frequency can penetrate the conducting tube and interact with the kicker magnet.

Using eqn. 2.5 we may rewrite 4.2 in the form

$$\omega_{sc} = \frac{\mu_0 a^2}{2\rho\tau^2} \tag{4.3}$$

which indicates that for a required aperture 2a and risetime τ, a high resistivity material is preferred to minimize the coupling of the longitudinal harmonics.

5. Application to the SSC Abort Kicker

Consider a stainless steel bore tube with the following properties:

$\rho = 72\times10^{-8}$ ohm-m	(resistivity at 20°C)	
$a = 0.02$ m	(4 cm aperture)	(5.1)
$b = 25.4\times10^{-6}$ m	(1 mil)	

then

$\tau = 0.44\,\mu\text{sec}$	(risetime)	
$f_c = \frac{\omega_c}{2\pi} = 0.36$ MHz	(cutoff frequency-transverse dipole)	
$f_{sc} = \frac{\omega_{sc}}{2\pi} = 280$ MHz	(cutoff frequency-longitudinal)	(5.2)

This has adequate risetime to be used in the SSC main abort kicker. There are a few materials with slightly higher resistivity than stainless steel (e.g. nichrome, about 100×10^{-8} ohm-m), but none with substantially higher resistivities that I am aware of.

References

1. Fermilab TM-991 (unpublished), R. Shafer (9/22/80). See eqns. 10, 12, and 17.